Aspects of the Li-SOCl2 cell

ASPECTS

OF THE

Li-$SOCl_2$ CELL

by

Alexander J. Hills

Supervisor: Professor N. A. Hampson

A Doctoral Thesis submitted in partial fulfilment of the requirement for the award of Doctor of Philosophy of the Loughborough University of Technology, September, 1987.

The work described in this thesis has not been submitted in full or in part, to this or any other institution for a higher degree.

SYNOPSIS

This thesis describes an investigation of some of the factors which govern the operation of the commercially important Li-$SOCl_2$ cell.

Electrode processes at lithium anodes and C-$SOCl_2$ cathodes have been studied using the technique of Faradaic impedance. A kinetic interpretation of the results has been advanced. Additionally some aspects of the formation and nature of LiCl films, which frequently cover the anode surface have been revealed from the decomposition of the numerical data. The impedance study further yielded kinetic data relating to the lithium dissolution process. Complementary, preliminary studies of the impedance of glassy carbon-$SOCl_2$ cathodes have shown that the cathode process is complicated.

A fundamental study of the relationship between carbon cathode thickness, the active reaction time and current density was undertaken for the reduction of $SOCl_2$ on uncatalysed carbon. For a given cathode thickness, current density and reaction time were related - approximately the Sand equation - an optimum limiting thickness at high current density was determined revealing a well defined penentration depth. The diffusion control of this cathode reaction was demonstrated from this and also from work using a glassy carbon cathode which clearly showed de facto dissolution of passivating phases.

Improvements in cell performance (duration and voltage) achievable by the addition of the free Lewis acid $AlCl_3$ to the electrolyte have been identified. This was done by studying the increased active life of cathodes which arises from the suppression of 'active surface cover passivity' by the complexing Lewis acid. Free Lewis effects on other types of carbon electrodes with different surface areas were also studied.

The profiles of blocking LiCl deposits throughout the entire thickness of porous carbon cathodes have been obtained by using a microtome. This tedious approach, the only feasible one for systems of commercial dimensions produced profiles which have been interpreted in terms of current density and electrolyte composition. This investigation confirmed the results of the electrometric experiments and provided complementary data concerning porous electrode utilisation. Interesting observations on a phthalocyanine catalysed carbon have additionally been made.

ACKNOWLEDGEMENTS

I wish to thank Professor Noel Hampson for his supervision and encouragement during my work. I am very grateful for the way in which he has given me the confidence to use my initiative, yet remains approachable and willing to advise in spite of many other commitments.

I also wish to thank my fellow research workers for their friendship and advice, particularly Dr. W. P. Hagan for useful discussions relating to my experiments and Dr. S.A.G.R. Karunathilaka (now at Chloride Research) for assistance with computing software.

Dr. M. Hayes and other (former) members of the Battery Group at the GEC (Hirst) Research Centre are thanked for their assistance with the project. I should like to acknowledge financial support by G.E.C. Research and S.E.R.C.

The technical and secretarial staff of this department are thanked for their efforts on my behalf.

Finally my deepest thanks go to Margaret Critchlow for her excellent typing of this thesis.

DEDICATION

To my wife, Ruth and my children, Naomi and Benjamin,
who I can rely on being behind me in all I undertake.

CONTENTS

LIST OF SYMBOLS

A	Electrode area
a	Tafel intercept or electrode separation
a_o, a_R	Activity of oxidised and reduced species
b	Tafel slope
C_{dl}	Double layer capacitance
C_O^b, C_R^b	Bulk concentration of oxidised and reduced species
C_O^S, C_R^S	Surface concentration of oxidised and reduced species
D	Diffusion coefficient
E	Electrode potential or residual error
Ee	Equilibrium potential
$E^\ominus$	Standard electrode potential
F	Faradays constant
f	Frequency of alternating current
ΔG	Gibbs free energy
$\Delta G^\ominus$	Standard Gibbs free energy
I	Alternating current
I_{max}	Amplitude of alternating current
i	Current density or current
i_o	Exchange current density
i_f, i_b	Cathodic and anodic partial current density
j	Complex number $(-1)^{\frac{1}{2}}$
k	Reaction rate constant
k_f, k_b	Cathodic, anodic reaction rate constant
$k^\ominus$	Standard rate constant
N	Number of data points
n	Number of electrons, number of parameters in the equivalent circuit

O	Oxidised species
Pi	Parameter i of the equivalent circuit
q	Flux of diffusing species
R	Reduced species, gas constant or resistance
R_{Ω}	Solution resistance
t	Time
T	Temperature
V	Voltage
V_{max}	Amplitude of alternating voltage
W	Warburg impedance
x	Distance from electrode
Z	Complex cell impedance
Z'	Real impedance component
Z''	Imaginary impedance component
$\|Z\|$	Absolute value of impedance
α	Charge transfer coefficient
γ	Roughness factor
η	Overpotential
θ	Charge transfer coefficient
ν	Velocity of reaction
σ	Warburg coefficient
τ	Transition time
ϕ	Galvani potential or phase angle
ω	Angular frequency

CHAPTER 1

INTRODUCTION

Lithium batteries have become increasingly important electrochemical power sources during the last 20 years. The need for light weight, high performance battery systems for many military and commercial applications has led to the emergence of a range of cells based on lithium anodes [1]. Such requirements include high energy density for military and space programs, as well as requirements of long shelf life and miniaturization for electronic devices.

Lithium anode cell configurations may be grouped according to the nature of the cathode material.

(1) Cells with solid cathode materials employ transition metal oxides, sulphides and chromates, or carbon-halogen compounds such as CFx. The working voltage of the cell is determined by the nature of the cathode, some cells with voltages of about 1.5 V may find applications as direct replacements for the widely used MnO_2/Zn cell e.g. Li/CuO, Li/FeS_2. Others have a higher cell potential of around 3 V e.g. Li/MnO_2, Li/CFx. Electrolytes for such solid cathode cells usually contain a lithium salt in an organic solvent, however solid electrolytes do exist. The obvious advantages that solid electrolytes have over liquid electrolytes include an improved power to weight ratio and wider temperature range. The most widely used solid electrolyte today is lithium iodide, as used in the Li/LiI/PbI_2 cell, although solid polymer electrolytes have recently been proposed.

(2) In liquid cathode systems the active cathode reactant also serves as a solvent or part of the electrolyte, the cathodic reduction occuring at an inert current collector electrode. This electrode is often referred to as a cathode for reasons of simplicity, although strictly speaking this is incorrect. These cells operate at around 3 V and can sustain higher currents than solid cathode couples, although they do have associated safety problems. Liquid cathode systems include the lithium sulphur dioxide cell and lithium oxyhalide

systems, the most developed of these being the Li-$SOCl_2$ cell. The other major oxyhalide systems include the Li-SO_2Cl_2 and Li-$POCl_3$ cells.

Fig. 1.1 shows the discharge characteristics for some lithium primary systems, along with some conventional systems for comparison. All the cells were AA* sized and all discharged at 20 mA [2].

The development of lithium secondary systems has been slower than for primary batteries. This is mainly due to difficulties in efficiently recycling lithium. The most promising systems contain solid state cathodes which undergo intercalation reactions with lithium, e.g. TiS_2 using 2Me-THF/$LiAsF_6$ as the electrolyte.

The work described in this thesis relates to a study of the Li-$SOCl_2$ cell, which consists of a lithium anode isolated from a porous carbon cathode by a separator. An electrolyte such as $LiAlCl_4$ is added to the $SOCl_2$ in order to increase the conductivity and facilitate Li^+ ion transport. This work includes a study of electrode processes at the anode and cathode as well as an investigation of various electrolyte compositions. The work is orientated towards high rate cells, which until 1986 were being developed by G.E.C. research.

*Footnote
"AA" represents an American National Standard size specification for a cylindrical cell whose height is 48.8mm and whose diameter is 14.3mm. Other standard specifications include "C" which is for a cell of height 46.4mm and diameter 26.2mm and "D" whose height is 57.9mm and whose diameter is 34.1mm.

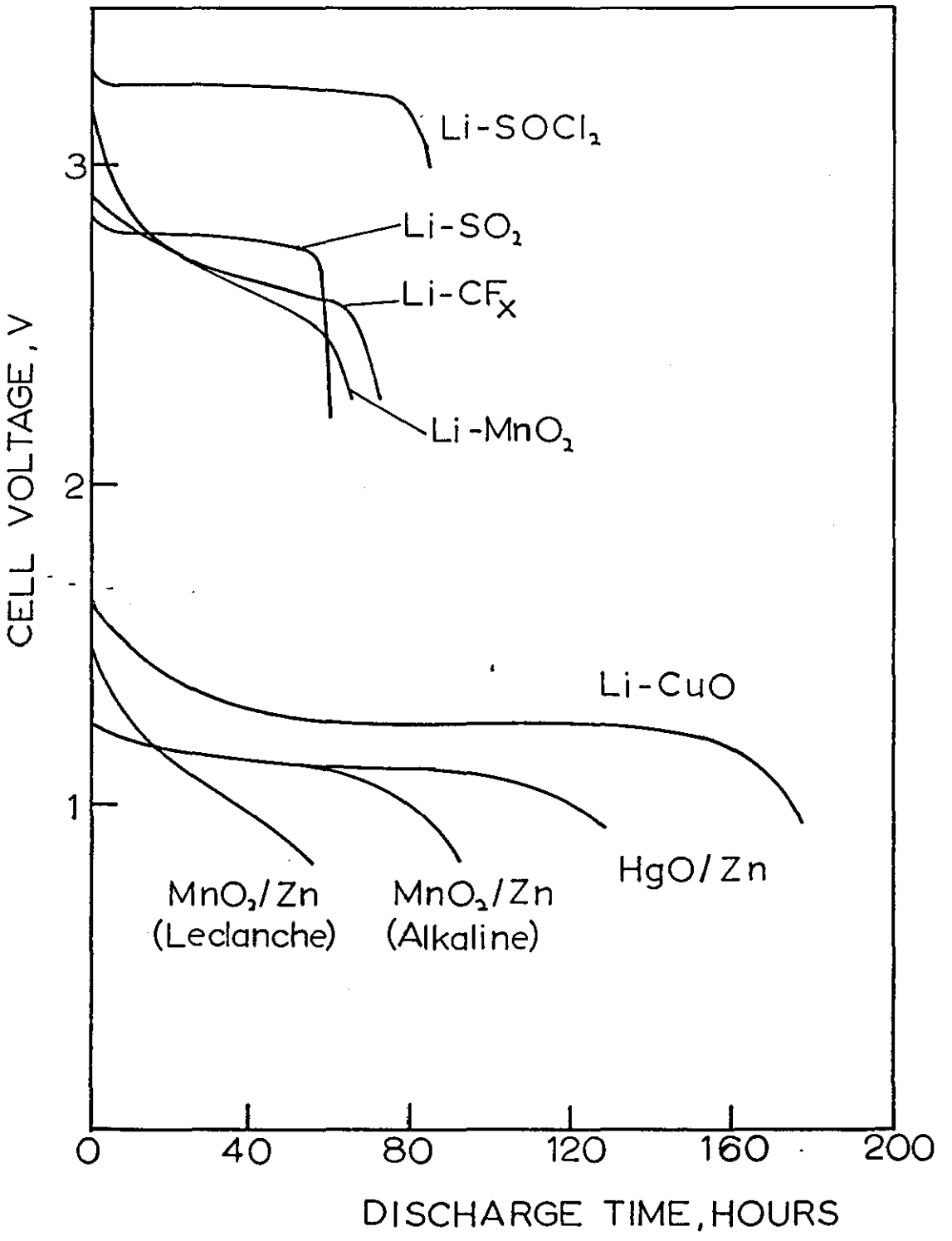

FIG 1.1 DISCHARGE CHARACTARISTICS OF VARIOUS AA SIZED PRIMARY BATTERY SYSTEMS CURRENT=20mA.

CHAPTER 2

THE $Li-SOCl_2$ CELL - A REVIEW

2.1 History

In 1969 J.P. Gabano [3] patented the use of $SOCl_2$ as a solvent for chlorine or bromine in a rechargable lithium cell, 1.0 M $LiAlCl_4$ being added as an electrolyte. He mentioned that important supplementary capacity could be obtained from the thionyl chloride and that the products of reaction would be sulphur, sulphur dioxide and lithium chloride. It was noted that at lower rates such cells delivered almost twice the expected capacity based on the bromine present.

It was soon realised that $SOCl_2$ could perform well by itself as a depolariser in a primary lithium cell. In 1972 a German patent [4] described such a cell in which the $SOCl_2$ was reduced at a porous carbon surface, $LiAlCl_4$ being added to the solvent.

By 1973, the $Li-SOCl_2$-C cell was truly born, Auborn [5] and Behl [6] in separate communications describing such a cell, along with other suitable oxyhalide depolarisers.

2.2 Cell Reaction Mechanisms

Previous to the development of the $Li-SOCl_2$ cell, Spandau and co-workers [7] studied the reduction of $SOCl_2$ solutions. They found that the electrolysis was not possible in the poorly conducting pure solvent, but could be carried out with the addition of 0.25 M $(C_2H_5)_3NCl$. The following scheme was proposed for the overall electrolytic reduction:

$$4\ SOCl_2 + 4e^- \rightarrow 2SO_2 + 2Cl_2 + 4Cl^- \qquad (2.2.1)$$

The formation of chlorine was not confirmed by later experiments.

The cell reaction usually cited today for the $Li-SOCl_2$ cell discharge reaction is as follows:-

$$4Li + 2SOCl_2 \rightarrow 4LiCl + SO_2 + S \qquad (2.2.2)$$

This reaction was originally proposed by Gabano [3]. The reaction

mechanism is thought to be rather more complex than this, various intermediates have been proposed. Other reaction stoichiometries have also been put forward.

Early work by Auborn [5] led to the following reaction being proposed:-

$$8Li + 3SOCl_2 \rightarrow 2S + Li_2SO_3 + 6LiCl \qquad (2.2.3)$$

Li_2SO_3 was detected by x-ray analysis and was thought to form rather than SO_2, whose presence could not be confirmed.

At the same time Behl [6] put forward a similar scheme, he believed that the SO_2 was reduced to $Li_2S_2O_4$ and S_2Cl_2.

$$8Li + 4SOCl_2 \rightarrow Li_2S_2O_4 + 6LiCl + S_2Cl_2 \qquad (2.2.4)$$

Later however the presence of SO_2 neglected by the previous two reaction schemes was positively confirmed. Quantitative analysis [8] showed the presence of LiCl, SO_2 and elemental sulphur in discharged cells, but in relative quantities which corresponded to no known reaction stoichiometry. Dey and Schlaikjer [9] noted internal pressure build up in discharged C sized cells, which were found by infra-red spectroscopy to contain SO_2. They also confirmed the existence of sulphur crystals in the cells and the absence of sulphur oxy-acid salts in the cathode. Beketaeva [10] after examining dried cathodes confirmed that no $S_2O_3^{2-}$, SO_3^{2-}, SO_4^{2-} or S^{2-} was present.

Dey [11] proposed that reaction (2.2.2) represents the cell reaction which occurs via an unstable biradical SO which disproportionates to form SO_2 and elemental S. Marincic [12] however maintained that there was insufficient SO_2 pressure in balanced Li-$SOCl_2$ cells to justify such a reaction. Schlaikjer and co-workers [13] confirmed that only a fraction of the SO_2 predicted from equation (2.2.2) is actually produced during the discharge. However Deys [11] proposed reaction was essentially upheld, slow decomposition of the unstable SO radical, thought to undergo polymerisation, occurred at the end of the discharge. The following two stage reaction was proposed.

$$2nLi + nSOCl_2 \rightarrow 2nLiCl + (SO)n$$

$$(SO)n \rightarrow (^n/_2)S + (^n/_2)SO_2 \qquad (2.2.5)$$

At least one sulphur oxyacid salt, thought to be Li_2SO_3 was identified in cathodes from cells discharged at -20°C. At this low temperature a reaction such as (2.2.3) proposed by Auborn [5] and since discounted, was suggested.

Results of a comprehensive qualitative analysis of discharged cells were reported by Bailey and Kohut [14]. The studies were carried out on 1.3 Ah cells, discharged at three different rates and at temperatures ranging from -50°C to 71°C. From their results these workers were confident that equation (2.2.2) summarized the overall cell discharge reaction at all temperatures, depths and rates of discharge investigated.

Behl [15] carried out a study of the electrochemical $SOCl_2$ reduction by cyclic voltammetry at a glassy carbon surface. A large reduction peak, thought to correspond to equation (2.2.2) was identified with no corresponding anodic peak, indicating an irreversible reaction. If any SO radical species existed, he concluded that it was unstable and quickly disproportionates. No evidence for further reduction of SO_2 was found. Venkatasetty [16] however identified three reduction peaks, thought to be due to a two stage $SOCl_2$ reduction process via an $SOCl^-$ radical followed by SO_2 reduction. Unlike Behl [15] however who used only $SOCl_2$ as the solvent, Venkatasetty carried out the analysis in solutions of $SOCl_2$ in dimethyl formamide and dimethyl sulphoxide, with added electrolyte.

Bowden and Dey [17] from another cyclic voltammetric study of $SOCl_2$ reduction in various organic solvents and supporting electrolytes also proposed the following two, one electron steps

$$SOCl_2 + e^- \rightarrow SOCl^{\cdot} + Cl^-$$

$$SOCl + e^- \rightarrow SO^{\cdot} + Cl^- \qquad (2.2.6)$$

Again as discussed previously the SO radical subsequently decomposes. Towards the end of the reaction, dimerisation and polymerisation of SO is likely, as proposed by Schlaikjer [13]. Immediate polymerisation of the SO radical is further substantiated by little experimental evidence for the existence of this intermediate, although the presence of $SO^{\cdot}$ and S_2O have been indicated by infra-red analysis [18], the stability of both however is thought to be low.

Analyses of cyclic voltammograms show a substantial dependence of peak potential on scan rate, indicative of the irreversible character of $SOCl_2$ reduction. A plot of peak height versus the square

root of scan speed was linear passing through the origin, indicating a diffusion controlled process [19, 20]. At lower overpotentials however [20], the reduction is thought to be kinetically controlled, a transition to diffusion control occurring with increasing overpotential. At potentials more negative than +2.7 V mass transport processes were thought to govern all cell reactions occurring, the controlling factor being the nature of the LiCl film on the electrode.

All things considered, equation (2.2.2) is still regarded as the most acceptable overall equation for the cell reaction, although it is likely that this occurs via an SO radical. However other species thought to take part in the reaction at some stage have been proposed. Venkatasetty and Saathoff[21] using cyclic voltammetry to study the reduction of a $SOCl_2$ -1.8 M $LiAlCl_4$ solution at a glassy carbon surface, found peaks corresponding to chlorine and sulphur dioxide. The chlorine was thought to form by the dissociation of SCl_2. Intermediates such as SCl_2, Cl_2 and OClS [22-24] have been identified in cells, which have led to more complex cell reaction mechanisms [24,25] being suggested.

2.3 The Anode

Lithium has many advantages as a battery anode material, it is mechanically strong, has a low equivalent weight and the highest equilibrium potential of any metal. In Li-$SOCl_2$ cells the negative electrode consists of lithium foil pressed onto an expanded nickel screen, or cold bonded with stainless steel, aluminium or zinc, which acts as a current collector. The anode is closely packed in a cell facing a porous carbon cathode from which it is isolated by a piece of separator material. Under such conditions anodic oxidation proceeds uniformly over the surface even at high current density (>200 mA/cm^2) according to the following process:

$$Li \rightarrow Li^+ + e^- \qquad (2.3.1)$$

The theoretical capacity based on weight of the anode is never actually achieved [26]. This is thought to be due to lithium corrosion at low rates with some sort of mechanical erosion at higher rates. The anode is not usually regarded as the performance limiting electrode since passivation of the carbon cathode by insulating LiCl is generally the reason for cell failure [27, 28]. However under certain conditions, lithium is anodically passivated in $SOCl_2$ solutions at room temperature [29, 30]. Anode passivation

is associated with the accumulation of anodic dissolution products in the pores on the surface layer of the metal, and has been found to limit the utilisation of the lithium electrode at high current densities. Abraham and co-workers [31] also concluded that anode polarization may terminate the end of discharge and that anode limited cells were not necessarily the same as lithium limited.

2.3.1 Film formation

The kinetic stability of lithium in many organic solvents has been known since the 1960's. This is due to a film which forms on the lithium surface, preventing further lithium dissolution which would result from its thermodynamic instability, e.g. for lithium thionyl chloride:

$$4Li + 2SOCl_2 \rightarrow 4LiCl + SO_2 + S, \quad \Delta G = 1432.35 \text{ kJ mol}^{-1}$$

This film has been extensively studied for a number of battery electrolytes [32-47] its growth mechanism and effect on battery performance have been evaluated. The film forms immediately the electrode and electrolyte are in contact and grows continually with storage time and temperature. A variety of methods exist for monitoring the film thickness and growth rate. An obvious way of determining the film thickness is by examining cross sections of lithium electrodes from SEM photographs [32, 36]. Film growth on the lithium electrode can be monitored by measuring the weight gain on storage in the electrolyte solution [34]. Micropolarization measurements on a lithium electrode enable determination of the interfacial capacity, from which the film thickness can be calculated using a parallel plate capacitor equation [38, 39]. A.C. impedance measurements on lithium electrodes have led to an easy, reproducible method for monitoring the surface film in $SOCl_2$ based electrolyte solutions [42, 43].

Peled [38, 44] described this film as a solid electrolyte interphase (SEI), since it acts as an interphase between the electrode and solution, having the properties of a solid electrolyte. Ideally, SEI's should not allow electron transfer, however a large number of Schottky lattice defects allow Li^+ ion transfer through the film. Growth of the film has been shown to occur by ionic migration and diffusion in the film, [32, 34, 35] the rate of increase of this SEI can be approximated to a parabolic growth law. The rate of film

growth on a lithium electrode in $SOCl_2$ is greater for more concentrated $LiAlCl_4$ solutions and increases with temperature [32, 36]. The size of the LiCl crystals [36] have also been demonstrated to increase with temperature. This may however only be true up to 130°C after which the crystal size decreases, possibly due to a greater quantity of SO_2 present in the electrolyte [45].

It is widely believed that this LiCl film consists of two layers [33-35, 45, 46], the first is a thin compact film which forms immediately the electrode and electrolyte make contact. On top of this is a thicker layer of porous non-insulating LiCl film which grows continually with time. It has also been suggested that there may be three films [47].

2.3.2 Voltage delay and its alleviation

The voltage delay phenomenon occurs when a lithium cell is discharged after a prolonged period of storage. Cell voltage at the start of the discharge is lower than expected, and increases slowly with time. This effect is caused by a passivating film which forms on the anode [33]. Dey [36] demonstrated that this was an anode effect by measuring the potential-time behaviour for several lithium specimens after storage for various times in an electrolyte solution. The voltage against a lithium reference electrode after galvanostatic anodic polarization was measured and found to slowly rise from an initially low value. As the electrode is polarized the film breaks up due to slow mechanical disruption caused by dissolution of lithium from underneath the film.

Purity of the anode and electrolyte solution have been shown to be an important factor in controlling the voltage delay problem [8, 48]. For example iron present in the electrolyte has been shown to increase the rate of film growth causing a much thicker film to form with more associated voltage delay [48]. Driscoll [8] found that storing the electrolyte solution over lithium metal at 71°C removed Fe, Cu, HCl and hydroxyaluminium compounds which are reactive to lithium. Cells using electrolyte purified in this manner showed no voltage delay until after 208 hours of storage.

Alloying lithium with other metals such as silver (1%) and magnesium has been carried out in an attempt to alleviate voltage delay [8]. Calcium was found to be the best alloying agent [49], it is thought to act by plating the anode surface, making it more resistant to passivation than lithium.

Dey [32] showed that the presence of SO_2 in the electrolyte causes the passive film to acquire a more orderly appearance as well as reducing corrosion. Chua and Merz [50] after finding that voltage delay was less for partially discharged cells showed that a significant reduction in voltage delay could be achieved by doping the electrolyte with around 5% SO_2. Additions of greater than 10% however aggrevated the problem. Other inorganic additives may also help reduce voltage delay [51].

Additions of PVC to the electrolyte have also had the effect of reducing voltage delay [48, 52]. PVC is thought to act by coating the lithium surface thereby creating a different crystal morphology with larger pores and tunnels, facilitating Li^+ ion transport.

Cyanoacrylate coatings on lithium [53] improve voltage delay in Li-$SOCl_2$ cells, although it is not certain whether they merely provide a physical barrier to LiCl film formation, produce a slowly formed film of different morphology or control crystal growth from the electrolyte.

Schlaikjer [54, 55] proposed the use of thionyl chloride electrolytes containing $B_{10}Cl_{10}^{2-}$ and $B_{12}Cl_{12}^{2-}$ as replacements for the commonly used $LiAlCl_4$. He showed that using such electrolytes the voltage delay problem was lessened [56], probably due to the smooth structure of the passivating layer on the lithium electrode in the polyhedral borane electrolyte. Dey showed that relatively small quantities of closoborane anions in the electrolyte significantly reduce voltage delay [57, 58]. SEM pictures showed the anode film consisting of uniformly grown small crystals. Gabano [59, 60] claims that an electrolyte made by dissolving either Li_2O or Li_2S in an $AlCl_3$-$SOCl_2$ solution, has superior voltage delay characteristics, although capacity is somewhat reduced.

2.4 The Cathode

The cathode substrate in Li-$SOCl_2$ cells provides a conductive surface on which $SOCl_2$ is depolarized. This inert electrode is usually made from amorphous carbon powder with a PTFE binder, the filamentary nature of which minimises blockage of the active carbon surface [61]. The most commonly used carbon is acetylene black, which consists of submicron sized particles produced by thermal or oxidative vapour phase decomposition of hydrocarbons [62]. Cathodes are usually prepared by pasting a Carbon/PTFE mix onto an expanded nickel current collector and pressing [6, 62]. Auborn used hot pressing at 200 psi for three minutes [5]. Another procedure entails

rolling the carbon/PTFE mix onto the current collector [11, 63].

During cell discharge $SOCl_2$ reduction takes place at such a cathode resulting in the precipitation of reaction products mainly LiCl, within the pores of the substrate. This leads to eventual passivation of the cathode surface and hence cell failure. Much of the Li-$SOCl_2$ cell research undertaken is in connection with improving the performance of this positive electrode.

Optimisation of cathode performance

(1) Type of carbon

Properties of manufactured carbons vary according to the carbon source or pre-cursor, as well as the manufacturing procedure. Shawinigan Acetylene Black (SAB) is the most widely used carbon black powder for Li-$SOCl_2$ cathodes, this carbon was initially found to give the highest coulombic capacity [6, 64]. Dey after examining twelve carbon types found that particle size BET surface area and density did not greatly affect cell performance, most performing as well as SAB [61]. Wade and co-workers in a later study found two other carbons, namely Cabot CSX-179B and United Carbon XC-6310, both having high surface areas, displayed less cathode polarization and much greater capacity than SAB [65, 66] in Li-SO_2Cl_2 cells.

In a recent study by Klinedinst [67], nine different carbon blacks were compared. He considered their ability to accommodate solid discharge products with minimum resistance losses and their ability to behave as heterogeneous catalysts for the cathodic half cell reaction. Of the commercially available carbon blacks examined Ketchenblack EC (surface area 1000 m^2/g) and Black Pearls 2000 (surface area 1050 m^2/g) displayed high capacity and load voltages. They gave almost twice the capacity of SAB (surface area 60 m^2/g).

It is possible to use materials other than carbon as current collector cathodes, e.g. nickel [68] has been proposed as an alternative to carbon for low rate cells.

(2) Cathode Structure

Klinedinst concluded that the porosity of the carbon black material has an important bearing on the Li-$SOCl_2$ cell capacity [67]. The porosity is in turn more directly related to the dibutyl phthalate absorption of the cathodes ($cm^3/100$ g), than the surface area as defined by iodine absorption (m^2/g). Other workers have also found

that the cell capacity is related to the pore volume of the cathode [64, 69]. Danel and co-workers [70] concluded that the pore-size distribution in carbon cathodes was very important since small pores are quickly blocked and give little capacity. This distribution results from carbon black manufacturing processes and characteristics. Addition of pore-formers has been successfully used to improve the pore size distribution within the cathode [67]. Finely divided $(NH_4)_2CO_3$ and NH_4HCO_3 were added to the cathode and subsequently removed by thermal decomposition.

Pre-treatment of carbon cathodes with acetone has led to an increase in cell voltage and capacity for Li-SO_2Cl_2 cells [65, 66] and Li-$SOCl_2$ cells [71]. This treatment is thought to work by removing impurities from the carbon and increasing the total pore volume and average pore diameters.

Provision should be made in the cell for electrode swelling during discharge since this has been shown to increase electrode capacity by up to 33%, due to an increase in cathode porosity [64, 72-74].

PTFE is used as an inert binder in the cathode giving mechanical stability. Dey [11] found a 10% $^{w}/_{w}$ PTFE addition was necessary to bind the carbon particles together, more than this reduced the capacity by physically restricting the active surface. Other workers however concluded that up to 50% PTFE may be used without unduly affecting the cathode efficiency [70], since the pore size distribution is not greatly affected by the PTFE content. Binders other than PTFE have been used, for example chlorinated hydrocarbons have been identified as an alternative, these have low contact angles and good chemical stability in the electrolyte [75]. These elastomer bonded carbon electrodes contained a different pore structure and were found to have 100% greater capacity than PTFE bound electrodes at high current density.

The thickness of the cathode is also critical, cathodes which are too thick are under utilized at high current density, as demonstrated by Dey and Bro [27,76] using depth profile analysis. In terms of capacity per unit mass or volume of cathode material, thinner cathodes have a greater rate capability [77, 78]. A mathematical study by Pollard and co-workers [79, 80] confirms that the reaction distribution in porous carbon cathodes is predominantly towards the front face of the electrode, nearest to the anode. EDAX analysis of discharged cathodes has also shown this [73].

(3) Electrocatalysts

The use of carbon in commercial cells arises from its availability and cheapness. The performance of carbon cathodes can however be further enhanced by the addition of other materials which have a catalytic effect on the cell performance. Substantial increases in cell operating voltage and discharge capacity have been achieved by using finely divided platinum in the cathodes [78] as little as 1% $^{w}/_{w}$ addition of platinum is sufficient to greatly increase cell performance. Such small quantities were thought to be economically viable. Copper powder additions to the cathode have been found to increase the performance and safety of Li-$SOCl_2$ cells [81]. The increase in safety was thought to be due to copper reacting with sulphur produced in the cell reaction which would otherwise react explosively with lithium. Behl [82] showed that in $SOCl_2$, copper is oxidised to copper(II) chloride, which during the cell reaction is reduced to copper(I) chloride, before susbsequent re-oxidation. Other pure metals have been found to have a catalytic effect on Li-$SOCl_2$ cell performance including iron [83], silver and palladium [84].

Transition metal phthalocyanines, successfully employed as catalysts for fuel cell cathodes, also increase the performance of Li-$SOCl_2$ cells. Doddapaneni after comparing eight organometallic complexes as possible catalysts found cobalt and iron phthalocyanine to be the most effective [85]. Other workers have since confirmed this [74], although these catalysts have been found less effective at higher temperature [71]. The way in which these catalysts function is complex and not fully understood, but in many instances they are thought to alter the reaction mechanism [86, 87]. Halogens have also been used as electrocatalysts [88, 89], although strictly speaking they do not directly affect the cathode structure, since they are added to the electrolyte solution.

(4) Temperature

As the temperature is increased, the capacity of the Li-$SOCl_2$ cell increases, due to greater cathode utilisation [77]. This is attributed to an increased solubility of reactants and products, improved efficiency of LiCl depostion and increased electrolyte conductivity. Although most workers agree with this, some found a decrease in cathode efficiency beyond 23.9°C, thought to be due to a parasitic reaction between $SOCl_2$ and S [90].

The low freezing point of $SOCl_2$ (-104.5°C) has favourable implications for Li-$SOCl_2$ cells with low temperature applications. However at sub-zero temperatures there is a loss in capacity [91, 92] and a higher cell polarization [67, 91]. This has been attributed to an increase in the precipitation of elemental sulphur which is less soluble than at ambient temperature [66]. Some of the capacity is however recovered on warming. It is likely that two temperature regions exist each with different thermodynamic characteristics [19].

2.5 The Electrolyte Solution

Addition of a suitable electrolyte to $SOCl_2$ is necessary in order to increase its conductivity and to facilitate Li^+ ion transport. $LiAlCl_4$ is the electrolyte usually employed, probably because of its reasonable solubility in $SOCl_2$ and relative cheapness. Dey [11] found that the intrinsic capacity of Li-$SOCl_2$ cells increased as the electrolyte concentration decreased, 1.0 M $LiAlCl_4$ being the optimum concentration. He later suggested that for high rate cells, higher concentrations of electrolyte were preferable 1.8 M being the optimum [27, 93], this is still generally regarded as so today [94].

The presence of free $AlCl_3$ in the electrolyte solution can result in higher cell voltages and increased capacity [77, 95-97]. The $AlCl_3$, a Lewis acid is thought to react with the chloride ions formed as a result of $SOCl_2$ reduction, and therefore delay LiCl precipitation. 3.0 M $AlCl_3$ was found to be an optimum concentration for cells employing thick carbon cathodes, 4.5 M $AlCl_3$ being more effective for thinner ones (37 μm) [77, 95]. Such an electrolyte solution however is restricted to reserve cells which shall be considered further in a subsequent section.

As discussed previously, alternative electrolyte salts with closoborane anions reduce the voltage delay problem in Li-$SOCl_2$ cells [54-58], as do salts containing Li_2O and Li_2S [60, 98].

Auborn [98] reported that other than BCl_3 solutions, group 3b chlorides in $SOCl_2$ dissolve LiCl. $LiGaCl_4$ and $Li_2O.2GaCl_3$ when used as electrolyte solutions in Li-$SOCl_2$ solutions, have shown similar conductivity and solubility to $LiAlCl_4$ but yield 60% greater capacities [100].

Electrolyte purity is important [11, 57], better battery performance has been obtained from laboratory prepared electrolyte. Purification methods include refluxing with lithium metal after distillation [101], and distillation after pre-treatment with triphenyl phosphate to remove sulphur containing impurities [5, 13].

Szpak and Venkatasetty [102-105] have undertaken an extensive study into the properties of $SOCl_2$ electrolytes containing $AlCl_3$ and LiCl. Conductance, viscosity and density data for these solutions has been obtained and analysed for a range of temperatures and compositions. Effects of dissolved SO_2 have also been investigated. The results are interpreted in terms of ion-solvent and ion-ion interactions, and should be of interest to battery technologists.

2.6 Battery Design, Performance and Applications

Li-$SOCl_2$ cells have one of the highest energy densities of all commercial battery systems (~500 Wh/kg), as well as high cell voltage, long shelf life and good low temperature performance. This has led to many proposed and existing applications ranging from low rate cells for medical implants to super high rate batteries for military use. For convenience in the ensuing discussion the systems shall be classified according to their rate capability.

2.6.1 Cells for low rate applications

These are usually AA size, ½ AA size or small D shaped cells, and are used for implantable cardiac pacemakers [106, 107] where they have shown an excellent record of reliability during clinical evaluation. Recently Li-$SOCl_2$ cells have also found applications in micro-electronics for CMOS memory preservation [52].

The "bobbin", or concentric electrode structure is a simple, popular design. This structure comprises of a cylindrical cell in which one electrode is attached to the wall of the container and completely surrounds the other. One such design allows a central hollow volume for additional electrolyte, since there is insufficient space within the cathode pores to accommodate all of the electrolyte solution [12, 108]. The rate capability of a bobbin cell is enhanced by using two concentric cylindrical anodes with a carbon cathode in between them [26]. Fig. 2.6.1 shows a range of electrode structures.

2.6.2 Intermediate cells

Attempts to scale bobbin construction to any cell larger than a D size results in a poor performance [109]. The rate capability can however be greatly enhanced using a spirally wound structure which increases the surface area of the electrodes. Cell construction involves winding a pair of flat strip electrodes, with separators, around a mandril and placing in a cylindrical cell container, which

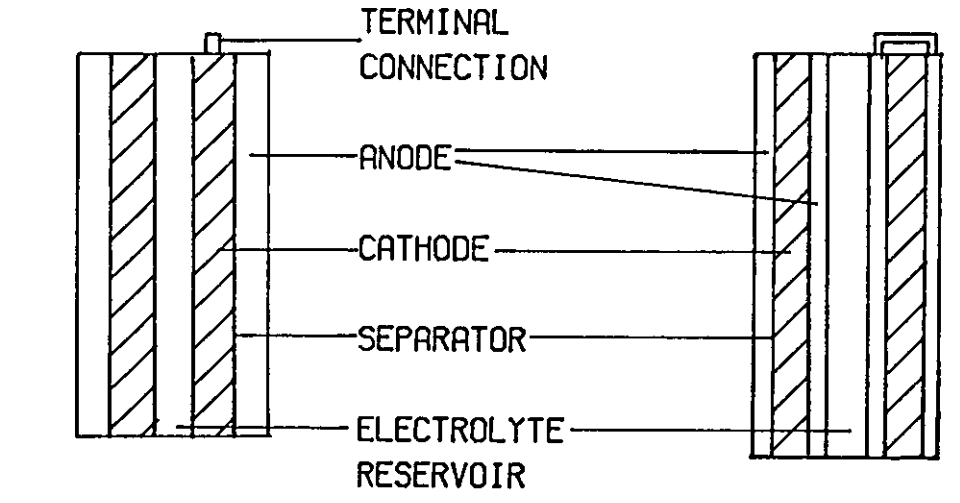

a) CONCENTRIC (BOBBIN)

b) DOUBLE ANODE

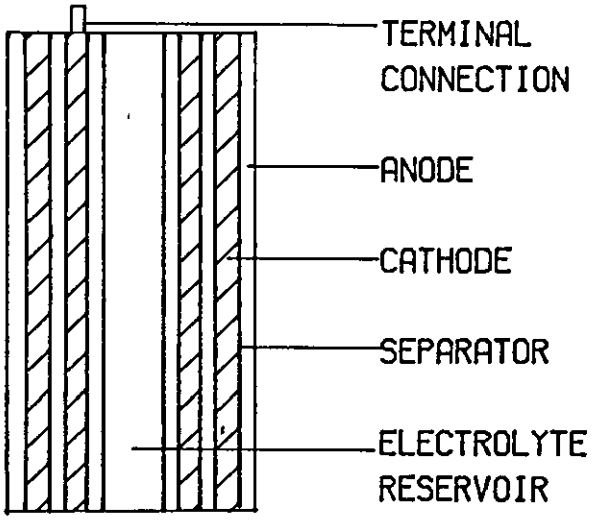

c) SPIRALLY WOUND

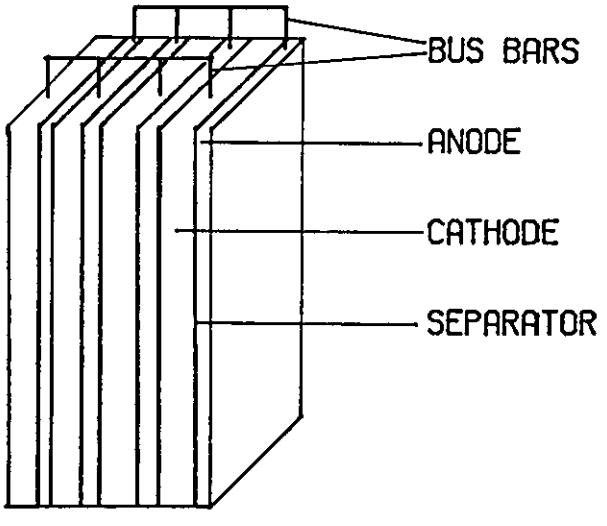

d) PRISMATIC

FIG 2.6.1 SCHEMATIC REPRESENTATIONS OF ELECTRODE STRUCTURES.

acts as one terminal. The other terminal is provided by a contact, fed through the glass-to-metal seal incorporated as a part of the cover assembly in hermetically sealed cells. Optimum design of such cells has been achieved through computer modelling [109, 110]. Dey has carried out a number of studies on C and D sized wound structures [11, 27, 28, 76]. Using an empirical approach, it was shown that about 3.3 Ah/g of carbon, was the maximum possible capacity which could be obtained using a wound geometry. It was also demonstrated that most of the reaction at high currents is localised near the cathode tab, making the cell wall the hottest part on shorting.

A flat, cylindrical cell has been described consisting of 35 disc shaped anodes and cathodes with glass separators, stacked in parallel. This arrangement was able to provide high power in pulsed and continuous mode [111].

2.6.3 High capacity cells

Large Li-$SOCl_2$ cells usually employ prismatic structures with parallel electrodes (Fig. 2.6.1), [110]. Partly because of safety hazards associated with such a high powered system, commercial applications are limited, the major uses of high rate cells being military [112].

10,000 Ah batteries are currently installed in minuteman missile silos, in parallel with lead acid batteries [113]. Load sharing between the two batteries allows for a smooth transition between the two systems with no voltage delay effects, the lead acid system initially taking most of the load. Very high rate batteries have been developed, even a 16,500 Ah system [114]. Many other examples of high capacity batteries are cited in the literature.

High rate cells are used for many naval and undersea applications such as mines, aids to navigation, submersed sonobouys, portable communications, missiles and torpedoes [115].

2.6.4 Reserve cells

A reserve cell is one in which the electrolyte is maintained in a separate compartment from the main electrode stack and is only admitted as power is required. Such cells avoid problems with voltage delay which may be critical for high rate applications where the overall discharge time is a few minutes. Reserve cells also give an almost indefinite shelf life, which make them ideal for standby power applications. Many reserve cells use free Lewis acid in the electrolyte,

in order to increase cell discharge times [77]. Actual concentrations of aluminium chloride are rarely quoted, although an electrolyte based on 3.0 M $AlCl_3$ has been found to give good performances [77, 116].

A major design problem, which exists with reserve batteries involves activation. Small low rate reserve cells have been designed in which the central reservoir of electrolyte is held in a glass ampoule which could be broken by striking the bottom of the cell [117, 118]. In some instances activation can take advantage of the application. For example a reserve cell used to power an artillery delivered communications device is activated by the high spin rate encountered as the device is fired [116]. More usually a more cumbersome means of activation is employed, the electrolyte being forced into the electrode stack by means of a gas generator as power is required [97, 119].

2.7 Safety of Li-$SOCl_2$ Cells

In spite of the many performance advantages of Li-$SOCl_2$ cells, there still remain questions relating to the hazardous nature of the cell. A few widely publicised incidents of cells exploding under abuse conditions, or venting to evolve noxious gasses have led to a general wariness. The major safety hazards of these cells are over-heating during and after discharge, pressure build-up, abuse and hazards during cell reversal. The reasons for each of these shall briefly be examined.

2.7.1 Heat generation

As previously discussed an increase in temperature can improve the performance of Li-$SOCl_2$ cells, however excessive heat production in the cell is a safety hazard. Much of the heat generated arises from chemical reactions both during and after the cell reaction as SO radical species are converted to SO_2 and S [120, 121].

Ohmic heat losses are considerable during cell discharge, and in one example were calculated to account for 37.3 kW of heat generated out of 120 kW of total electrical output [122].

Additional heat generation is likely with cells containing an excess of $AlCl_3$ in the electrolyte [123]. This is due to the anode corrosion reaction and an entropy increase during the transition from the acidic reaction, producing $LiAlCl_4$, to the reaction in neutral electrolyte [124].

As the temperature increases several safety hazards have been identified, the electrolyte boils, the sulphur melts and if the

temperature is raised sufficiently the lithium melts. Marincic [122] calculated that for a 90 kg, high rate Li-$SOCl_2$ battery that unless external cooling of the battery is provided, all of the safety hazards would be encountered, although the power source should be exhausted before the lithium melts. Excessive heat generation causing the cell temperature to approach the melting point of lithium results in what is known as thermal runaway conditions [125]. It is likely that a critical size of cylindrical high rate Li-$SOCl_2$ battery exists, below which external cooling is not necessary, although other factors such as cell geometry and materials of construction are important [126]. Mathematical predictions show that a high rate torpedo battery can only be stable under certain limiting conditions and with flowing electrolyte [127]. Improved designs should improve heat dissipation in cylindrical batteries [128].

2.7.2 Internal pressure build-up

This is likely to occur directly as a result of a build up of SO_2 within the cell, due to the solubility of SO_2 in the electrolyte decreasing with temperature [122]. This internal pressure may become critical [90] therefore most cells require a safety vent. Dey showed that such a vent needs to respond to relatively low pressures in order to prevent explosion [28], so developed a truly hermetic, reliable low pressure vent, resistant to external abuse [129].

2.7.3 Abuse

The major 'accidental' abuse conditions likely to occur in Li-$SOCl_2$ cells are short-circuiting and charging. The former may result in thermal runaway conditions or explosions [125]. Short circuiting can usually be prevented by the use of fuses, semi-conductor devices or relays [130]. Charging although thought not to be a major safety hazard [131] can usually be eliminated by incorporation of a safety diode [130].

The results of numerous electrical and mechanical abuse tests on Li-$SOCl_2$ cells are to be found in the literature, as attempts to improve safety are carried out. Small low rate cells are generally regarded as reasonably abuse resistant [132,133].

2.7.4 Hazards during cell reversal

After the discharge has finished, cell voltage reversal is a likely condition in high rate battery stacks and is potenitally explosive. This may occur in anode limited cells when depletion of

lithium from the negative electrode forces other oxidation reactions to occur at this electrode, or in cathode limited cells in which polarization of the $SOCl_2$ reduction process causes lithium deposition on the positive electrode [134]. There is much debate concerning the relative safety of anode and cathode limited cells. Some claim that cathode limited cells are safer, since in anode limited cells explosions are possible due to sensitive substances produced by oxidation of materials present in the cell [31, 133]. Others however maintain that anode limited cells in which the lithium is exhausted just prior to cathode failure are safer, since heating may cause any remaining lithium to melt, in cathode limited cells. Less heat is evolved in anode limited cells, since cathode polarization is lower [135]. Also in such cells there is less potential for a hazardous reaction between lithium and sulphur [90]. It must be borne in mind that anode limited and lithium limited may not be the same since under certain circumstances anode polarization may cause the end of cell life [29-31]. A 'balanced' cell composition in which cell reactants are exhausted simultaneously, is thought to show good safety characteristics on voltage reversal [136].

A ceramic separator when employed in place of a porous alumina/silica based one has been demonstrated to reduce hazards on voltage reversal [137]. Internal and external switching devices have also been proposed to overcome this hazard [138].

CHAPTER 3

THEORETICAL PRINCIPLES

3.1 Thionyl Chloride as a Solvent

Thionyl chloride although providing a reasonable ionising medium for chemical reactions, has a high chemical reactivity and is unable to dissolve many salts, which limits it as a useful non-aqueous solvent. Thionyl chloride is a colourless liquid, it melts at -104°C and boils at 75.6°C, it has a density of 1.629 gcm^{-3} (at 25°C) and has a dipole moment of 1.58D [139]. The low dielectric constant (9.05 at 22°C) and high viscosity hinder its effectiveness as a charge transfer medium.

Thionyl chloride is a highly reactive substance, when added to metals and metal oxides, it produces the corresponding chloride. Other metal compounds when treated with $SOCl_2$ also form anhydrous chlorides [139].

The low specific conductance ($3.5 \times 10^{-9} ohm^{-1}cm^{-1}$) is usually enhanced by the addition of a compound such as $SbCl_3$, $SbCl_5$, $FeCl_3$, $SnCl_4$ or $AlCl_3$. These behave as Lewis acid electrolytes (see Section 3.3) by increasing the relative concentration of $SOCl_2^+$ ions.

Organic bases such as triethylamine, pyridine, quinoline and acetone behave as Lewis bases by increasing the concentration of chloride ions present. Potentiometric titrations between acids and bases in $SOCl_2$ are possible [139].

3.2 The Structure of the Electrode/Electrolyte Interphase

This is the region close to the electrode surface where electrode reactions take place, making it a region of great importance.

A simple model of this interface was first put forward by Helmholtz [140]. He showed that any excess charge situated on the surface of a metallic phase in solution, was balanced by an equal, opposite layer of charge in the solution immediately adjacent to the electrode surface. The term "double layer" arose from this treatment, the two layers of charge behaving as a parallel plate capacitor.

Gouy and Chapman [141, 142] realized that not all of the charge in the solution could be confined to the surface layer.

since thermal motion of the solution particles resists the chemical and electrostatic attraction of the electrode. It was therefore proposed that a further diffuse layer of charge existed beyond the Helmholtz double layer. This Gouy-Chapman model however treated ions as point charges rather than particles of finite size, which led to much greater values of double layer capacitance being predicted than have been obtained experimentally. Stern [143] later made corrections to this model by considering an adsorbed layer of ions with finite size approaching within a critical distance of the electrode surface. The remainder of the ions were distributed in a diffuse layer extending from the plane of closest approach into the bulk solution. The development of theories relating to the electrode/electrolyte interphase are summarized in Figs. 3.2.1 to 3.2.3, which also show the variation of Galvani potential, ϕ, with distance from the electrode surface.

These models have since been further refined to consider the behaviour of water molecules, which hydrate the cations and electrode surface. However less is known about the precise structure of the interphase for non-aqueous solvents such as thionyl chloride. Precise data relating to transference numbers of lithium salts in aprotic solvents are not available. This makes it impossible to obtain accurate values of ionic mobilities which are required in order to understand ion-solvent and ion-ion interactions for electrolyte solutions, particularly at the electrode-electrolyte interphase. It is therefore inappropriate to assume that further refinements of this model developed for aqueous systems can be applied to non-aqueous media.

3.3 Lewis Acids

A widely accepted definition of acids and bases was put forward by J. N. Bronsted and T. M. Lowry (1923). An acid is normally definedas a substance with a tendency to lose a proton, and a base as one with a tendency to gain a proton.

This concept has been extended to consider solvents other than water which exhibit self-ionisation. This wider solvent theory considers any substance which increases the concentration of solvent cations to be an acid, and any substance increasing the number of solvent anions to be a base.

G. N. Lewis developed a different concept of acids and bases, sometimes referred to as the electronic theory [144]. This classification considers as acid-base reactions any in which an unshared electron pair in the base molecule is accepted by the acid

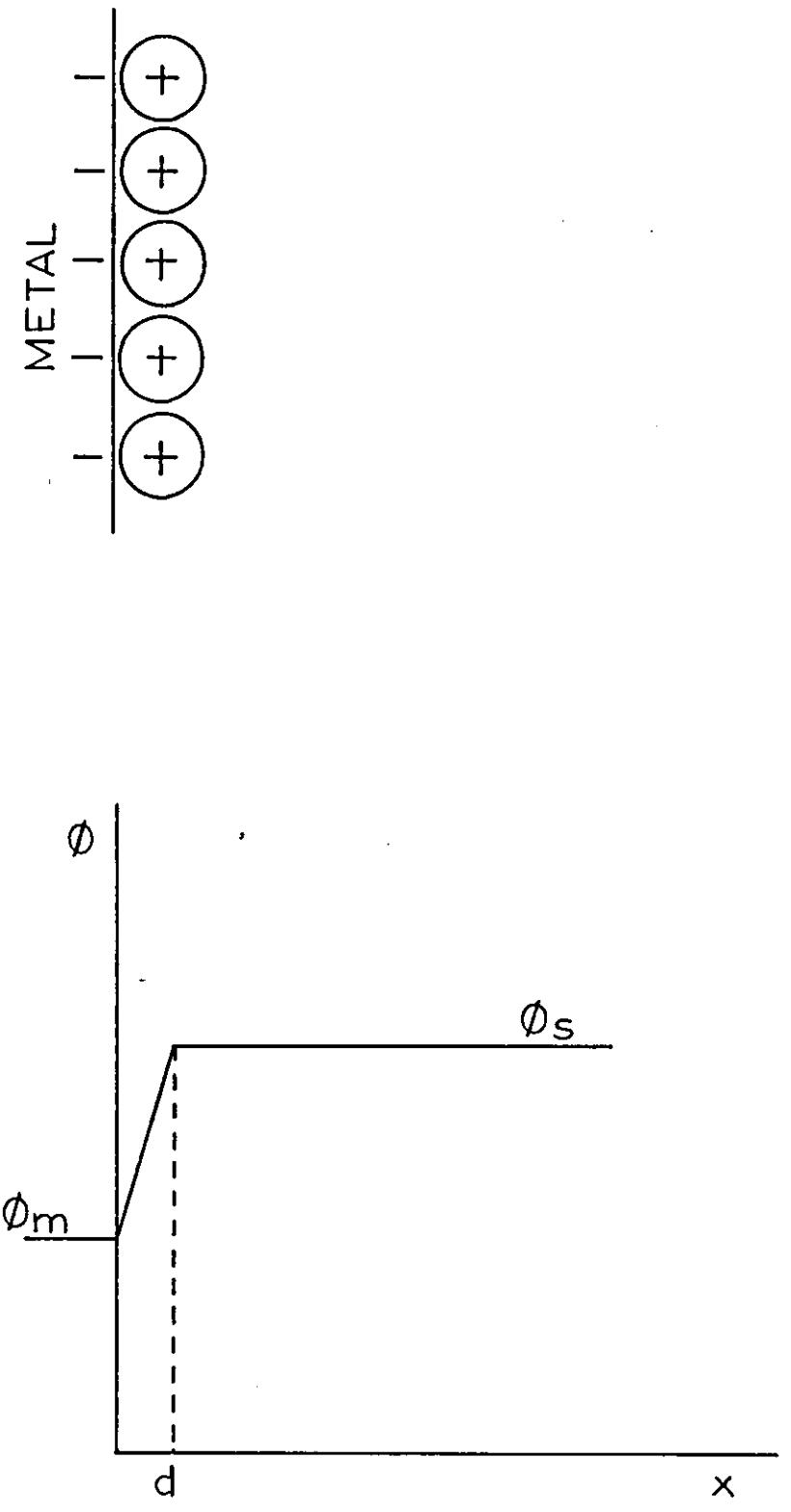

FIG 3.2.1 HELMHOLTZ MODEL OF THE DOUBLE LAYER, WITH CORRESPONDING POTENTIAL DISTRIBUTION.

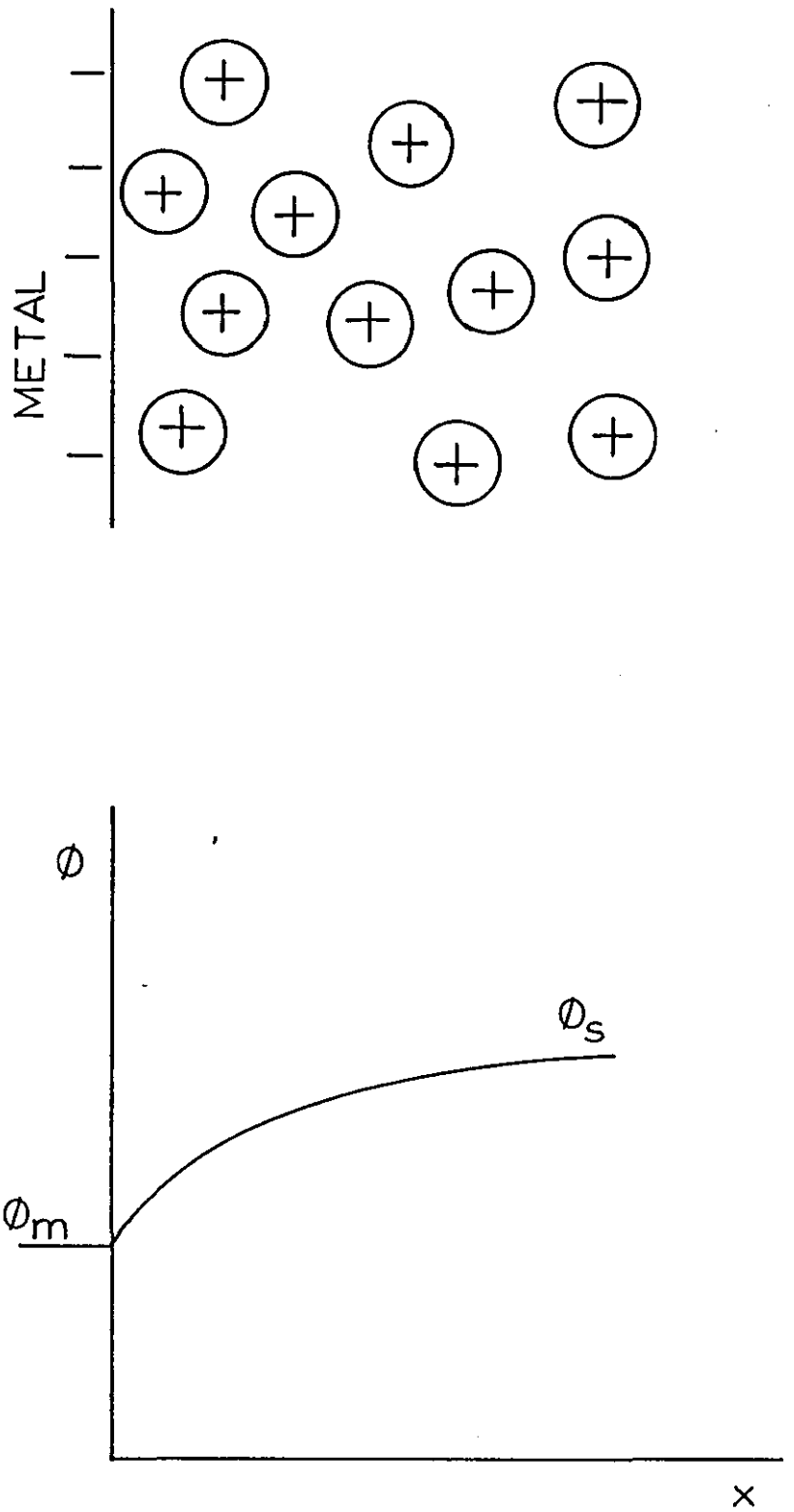

FIG 3.2.2 GOUY-CHAPMAN MODEL OF THE DOUBLE LAYER, WITH CORRESPONDING POTENTIAL DISTRIBUTION.

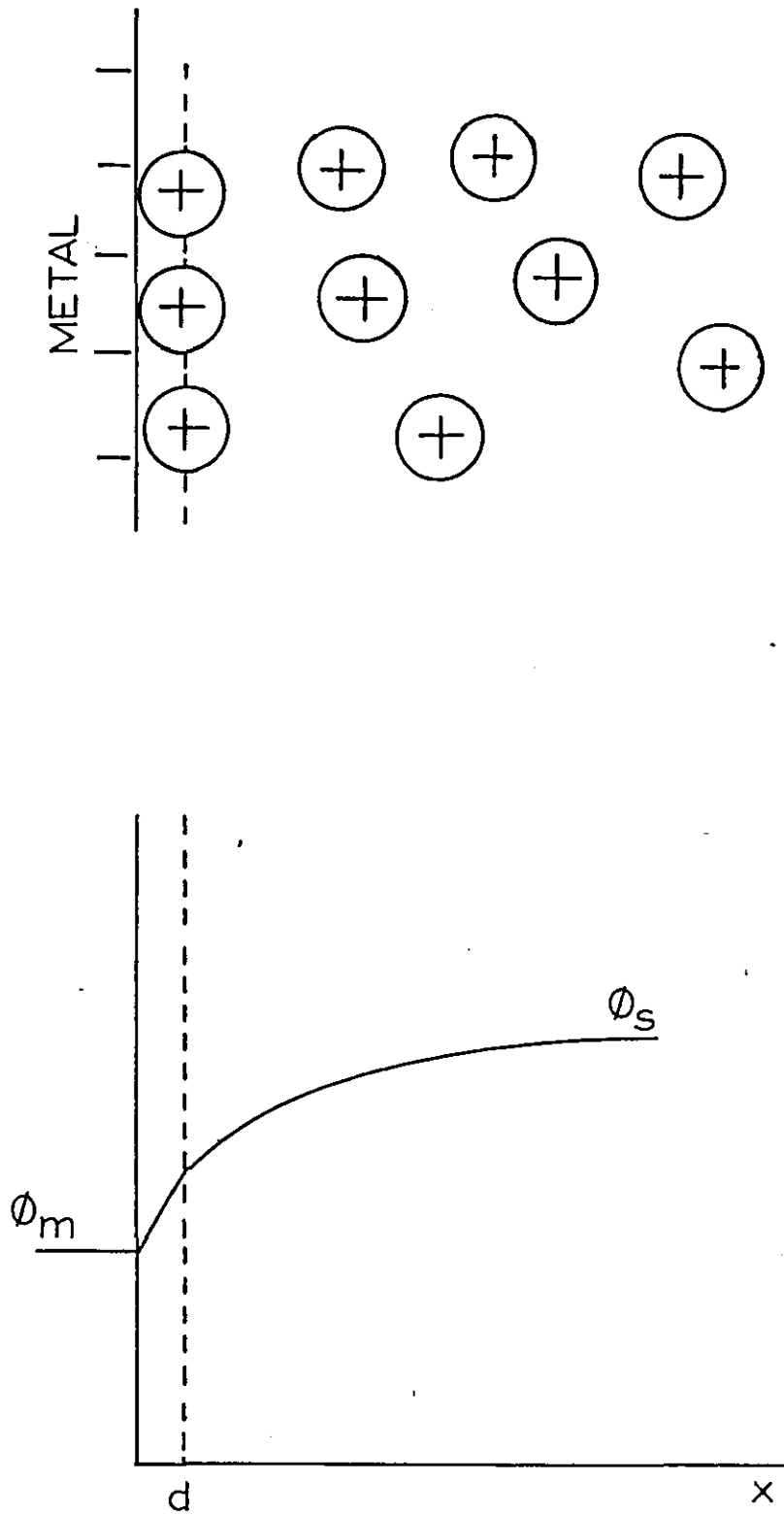

FIG 3.2.3 STERN MODEL OF THE DOUBLE LAYER, WITH CORRESPONDING POTENTIAL DISTRIBUTION.

molecule to form a covalent link. Thus an acid can be defined as a substance which accepts a lone pair of electrons, and a base as one which donates a lone pair. Lewis even encompassed classical proton acid-base reactions in his definition. This he did indirectly by supposing that the reaction below is initiated by a hydrogen bond.

In this instance the hydrogen accepts extra electrons from the base, justifying the inclusion of XH as an electron acceptor. Classical proton acids are sometimes referred to by the Lewis school as secondary acids. Clearly one must be cautious in not extending the concept to include too many substances, since this will devalue its meaning.

Classification of Lewis acids is not so straight forward as for simple proton acids, since relative acid strengths may vary in different solvents. One method of classification considers the polarizability of the base. This guiding principle was introduced by R. G. Pearson [145] who defined as "soft" bases, those for which the donor atom is of high polarizability, low electro-negativity and easily oxidised, e.g. I^-, SCN^-, S^{2-}. Conversely hard bases have the opposite properties and include OH^- and F^-. Hard and soft acids are defined as groups which respectively form stable complexes with hard and soft bases. Hard acids include small non-polarizable metal cations with high oxidation numbers and inert gas structures; soft acids include larger metal ions such as Cu^+, Ag^+ and Hg^{2+}.

Solvents such as thionyl chloride and phosphoryl chloride have very low conductivity due to a slight self ionisation.

$$SOCl_2 \rightleftharpoons SOCl^+ + Cl^-$$

$$POCl_3 \rightleftharpoons POCl_2^+ + Cl^-$$

This degree of self ionisation is not sufficient to serve as a foundation for the formation and reactions of acids and bases. In such solvents the acid-base act is initiated by the solvation of dissolved compounds. For example addition of aluminium chloride, a Lewis acid to thionyl chloride results in the transfer of chloride ions from the solvent to the solute. It is by this formation of complex anions that the relative concentration of $SOCl^+$ is increased:

$$AlCl_3 + SOCl_2 \rightleftharpoons [SOCl][AlCl_4] \rightleftharpoons SOCl^+ + AlCl_4^-$$

3.4 The Charge-Transfer Process

Reactions occurring at an electrode in an electrolyte solution, essentially involve the transfer of electrons from one substance to another. The following general redox process describes this:

$$O + ne \underset{k_b}{\overset{k_f}{\rightleftharpoons}} R \qquad (3.4.1)$$

where O and R are oxidised and reduced species, k_f and k_b are forward and backward rate constants, and n is the number of electrons transferred.

The rate or velocity of each process (ν_f and ν_b) is related to the rate constant by the concentration of reacting species. The rate may also be expressed in terms of forward (cathodic) or backward (anodic) current densities i_c and i_b, thus:

$$\nu_f = k_f C_O^S = \frac{i_f}{nF} \qquad (3.4.2)$$

$$\nu_b = k_b C_R^S = \frac{i_b}{nF} \qquad (3.4.3)$$

C_O^S and C_R^S refer to the concentrations of oxidised and reduced species near to the electrode surface, although not actually inside the diffuse layer (Fig. 3.2.3). This assumption simplifies the subsequent mathematical treatment.

The half cell reaction depicted by equation (3.4.1) will adopt a potential E, which is a function of its equilibrium position*. When the components of the half cell are in their standard states of activity the electrode adopts a standard electrode potential $E^\ominus$, which is characteristic of that system. The equilibrium potential of an electrode is related to this standard potential by the Nernst equation.

$$E_e = E^\ominus + \frac{RT}{nF} \ln (a_o/a_R) \qquad (3.4.4)$$

---

*Footnote

The potential is known as the Galvani potential difference between the metal and solution ($\Delta\phi$). However it is impossible to directly measure this quantity, we can only measure potential (E) with respect to a given reference electrode.

Any theory of electrode kinetics must predict this expression for corresponding conditions. The Nernst equation is derived from the Van't Hoff reaction isotherm which expresses the free energy change for a chemical reaction as:

$$\Delta G = \Delta G^{\ominus} + RT \ln (a_o/a_R) \qquad (3.4.5)$$

The Gibbs free energy change and the cell EMF are related as follows:

$$\Delta G = -nFE \qquad (3.4.6)$$

or in standard state:

$$\Delta G^{\ominus} = -nFE^{\ominus} \qquad (3.4.7)$$

$\Delta G^{\ominus}$ represents the standard free energy change and nF is a quantity of electricity.

Fig. 3.4.1 shows the free energy profiles for the species in equation (3.4.1). The solid curves correspond to an electrode potential of zero volts, $\Delta G^{\ddagger}_{oc}$ and $\Delta G^{\ddagger}_{oa}$ are the cathodic and anodic activation energies. As an external potential is applied a movement of electrons takes place resulting in the establishment of a new equilibrium potential. If a positive potential is applied the concentration of species O increases relative to R, thus favouring the backward or anodic reaction. The dashed line of Fig. 3.4.1 shows such a potential shift, to a value E volts. This change occurs by a decrease in the barrier for the anodic reaction and an increase in the barrier for the cathodic reaction. The overall free energy change is therefore split, a fraction (1-α) assists the anodic process, the remaining fraction, α, hindering the cathodic process. The term α is a symmetry factor which depends on the shape of the energy diagram. For simple electrode processes this is equivalent to the charge transfer coefficient and may range from zero to unity. The activation energies at this new potential now become:

$$\Delta G^{\ddagger}_{c} = \Delta G^{\ddagger}_{oc} + \alpha nFE \qquad (3.4.8)$$

$$\Delta G^{\ddagger}_{a} = \Delta G^{\ddagger}_{oa} - (1-\alpha)nFE \qquad (3.4.9)$$

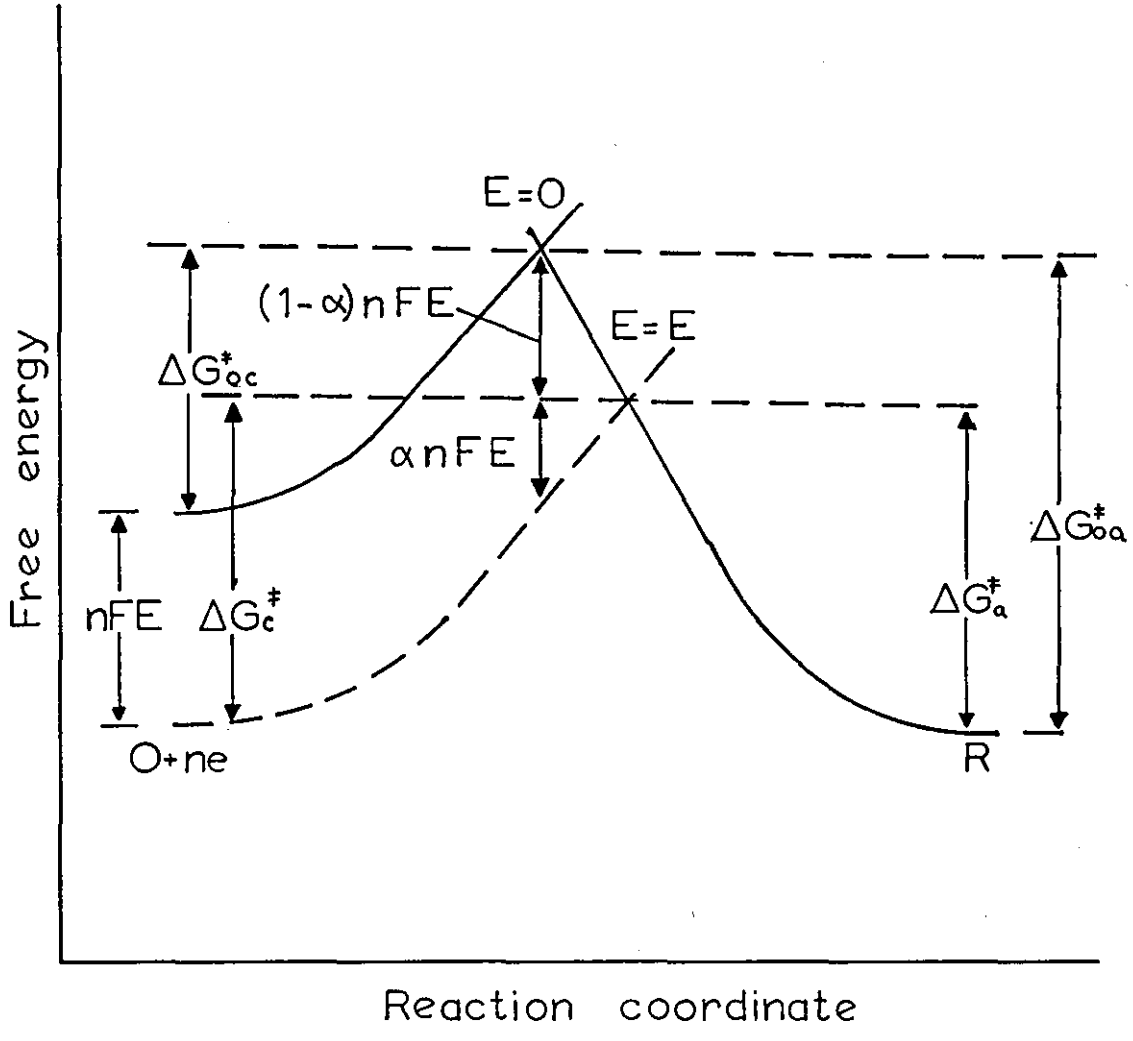

FIG. 3.4.1 A DIAGRAM SHOWING THE EFFECTS OF A POTENTIAL CHANGE ON THE FREE ENERGIES OF ACTIVATION FOR OXIDATION AND REDUCTION.

The forward and backward rate constants can be written in Arrhenius form:

$$k_f = A_f \exp\left[-\frac{\Delta G_c^{\ddagger}}{RT}\right] \qquad (3.4.10)$$

$$k_b = A_b \exp\left[-\frac{\Delta G_a^{\ddagger}}{RT}\right] \qquad (3.4.11)$$

where A_f and A_b are frequency factors. In terms of (3.4.8) and (3.4.9), the above equations become:

$$k_f = A_f \exp\left[\frac{-\Delta G_{oc}^{\ddagger}}{RT}\right] \exp\left[\frac{-\alpha nFE}{RT}\right] \qquad (3.4.12)$$

and

$$k_b = A_b \exp\left[\frac{-\Delta G_{oa}^{\ddagger}}{RT}\right] \exp\left[\frac{(1-\alpha)nFE}{RT}\right] \qquad (3.4.13)$$

The potential independent terms in the above expressions can be replaced by $k_c^{\ominus}$ and $k_b^{\ominus}$ at E=0 volts. Hence:

$$k_f = k_f^{\ominus} \exp\left[\frac{-\alpha nFE}{RT}\right] \qquad (3.4.14)$$

$$k_b = k_b^{\ominus} \exp\left[\frac{(1-\alpha)nFE}{RT}\right] \qquad (3.4.15)$$

At the standard electrode potential $E^{\ominus}$, C_O^S and C_R^S become equal and the rate constants k_f and k_b are considered equal to a standard rate constant $k^{\ominus}$. Thus:

$$k^{\ominus} = k_f^{\ominus} \exp\left[\frac{-\alpha nFE^{\ominus}}{RT}\right] \qquad (3.4.16)$$

$$k^{\ominus} = k_b^{\ominus} \exp\left[\frac{(1-\alpha)nFE^{\ominus}}{RT}\right] \qquad (3.4.17)$$

The forward and backward reaction rate constants can now be written in terms of this, standard rate constant:

$$k_f = k^{\ominus} \exp\left[\frac{-\alpha nF(E-E^{\ominus})}{RT}\right] \qquad (3.4.18)$$

$$k_b = k^{\ominus} \exp \left[\frac{(1-\alpha)nF(E-E^{\ominus})}{RT}\right] \qquad (3.4.19)$$

From (3.4.2) and (3.4.3) the current densities are given by:

$$i_f = nF\, k_f\, C_O^S \qquad (3.4.20)$$

$$i_b = nF\, k_b\, C_R^S \qquad (3.4.21)$$

These currents cannot be measured separately, since it is only possible to measure the net current density of a redox process:

$$i_{net} = i_f - i_b \qquad (3.4.22)$$

Expanding equations (3.4.20) and (3.4.21) in terms of (3.4.18) and (3.4.19) then substituting in (3.4.22), we obtain the following current-potential characteristic known as the Butler-Volmer equation [146]:

$$i = nF\, k^{\ominus} \left[\exp \left[\frac{-\alpha nF(E-E^{\ominus})}{RT}\right] C_O^S - \exp \left[\frac{(1-\alpha)nF(E-E^{\ominus})}{RT}\right] C_R^S\right] \qquad (3.4.23)$$

At equilibrium no net current flows, however the situation is dynamic, electron transfer occurs equally in both directions. The exchange current, i_o is a measure of the extent of electron transfer and can be expressed as follows:

$$i_o = nF\, k_f^{\ominus}\, C_O^b \exp \left[\frac{-\alpha nFEe}{RT}\right] \qquad (3.4.24)$$

$$i_o = nF\, k_b^{\ominus}\, C_R^b \exp \left[\frac{(1-\alpha)nFEe}{RT}\right] \qquad (3.4.25)$$

E_e is the equilibrium potential, C_O^b and C_R^b represent the bulk concentrations of species O and R, which at equilibrium should equal C_O^S and C_R^S. From the above expressions it follows that:

$$\frac{C_O^b\, k_f^{\ominus}}{C_R^b\, k_b^{\ominus}} = \exp \left[\frac{nFEe}{RT}\right] \qquad (3.4.26)$$

and

$$Ee = \frac{RT}{nF} \ln \left[\frac{k_f^{\ominus}}{k_b^{\ominus}}\right] + \frac{RT}{nF} \ln \left[\frac{C_O^b}{C_R^b}\right] \qquad (3.4.27)$$

The following expression is obtained from equations (3.4.16) and (3.4.17):

$$\frac{k_f^{\ominus}}{k_b^{\ominus}} = \exp\left[\frac{nFE^{\ominus}}{RT}\right] \qquad (3.4.28)$$

hence

$$E^{\ominus} = \frac{RT}{nF} \ln\left[\frac{k^{\ominus}f}{k^{\ominus}b}\right] \qquad (3.4.29)$$

Thus, equation (3.4.27) is simplified as follows:

$$Ee = E^{\ominus} + \frac{RT}{nF} \ln\left[\frac{C_O}{C_R}\right] \qquad (3.4.30)$$

This expression is the Nernst equation in terms of concentrations. From such a derivation, the kinetic treatment is shown to be consistent with the thermodynamic treatment.

Combining equations (3.4.26) and (3.4.28) and raising the result to the power -α yields:

$$\exp\left[\frac{-\alpha nF(Ee-E^{\ominus})}{RT}\right] = \left[\frac{C_O^b}{C_R^b}\right]^{-\alpha} \qquad (3.4.31)$$

Rewriting (3.4.24) in terms of $k^{\ominus}$ we obtain:

$$i_o = nF\, k^{\ominus}\, C_O^b \exp\left[\frac{-\alpha nF(Ee-E^{\ominus})}{RT}\right] \qquad (3.4.32)$$

Using the previous two equations we can now express the exchange current in terms of the standard rate constant $k^{\ominus}$ and concentrations of active species. $k^{\ominus}$ is a measure of the kinetic capability of a redox couple.

$$i_o = nF\, k^{\ominus}\, C_O^{b(1-\alpha)} C_R^{b\alpha} \qquad (3.4.33)$$

The net current density at a potential E is expressed as follows:

$$i = nF\, k_f^{\ominus}\, C_O^b \exp\left[\frac{-\alpha nFE}{RT}\right] - nF\, k_b^{\ominus}\, C_R^b \exp\left[\frac{(1-\alpha)nFE}{RT}\right] \qquad (3.4.34)$$

An assumption is made at this stage that in the electrolyte solution surface concentrations of species do not differ appreciably from bulk concentrations.

We are now able to express the current density at a potential E in terms of the exchange current density at any equilibrium potential E_e. Dividing equation (3.4.34) by (3.4.24) and (3.4.25) yields:

$$i = i_o \left[\exp \left[\frac{-\alpha n F \eta}{RT} \right] - \exp \left[\frac{(1-\alpha) n F \eta}{RT} \right] \right] \qquad (3.4.35)$$

The overpotential, η, is the difference between the equilibrium potential and the potential after polarization, thus:

$$\eta = E - E_e \qquad (3.4.36)$$

Equation (3.4.35) is the Erdey-Gruz and Volmer equation [147], and in practice is usually modified in one of two ways.

(a) At low overpotentials, where the electrode behaviour approaches reversibility the exponentials are expanded using only the first two terms of the series, i.e. $e^x = 1 + x$; thus:

$$i = i_o \left[\left(\frac{1-\alpha n F \eta}{RT} \right) - \left(\frac{1+(1-\alpha) n F \eta}{RT} \right) \right] \qquad (3.4.37)$$

$$= - \frac{i_o n F \eta}{RT} \qquad (3.4.38)$$

Under these conditions, near the equilibrium potential, the current is a linear function of potential. The exchange current density becomes:

$$i_o = - \frac{RT}{nF} \frac{i}{\eta} \qquad (3.4.39)$$

The ratio η/i is a resistance, often known as the charge transfer resistance θ, therefore:

$$\theta = \frac{RT}{nF\, i_o} \qquad (3.4.40)$$

(b) At high over potentials a large net current flows. In this situation one of the exponentials in the Erdy Gruz and Volmer expression may be neglected.

For high cathodic overpotentials:

$$i = i_o \exp\left[\frac{\alpha n F \eta}{RT}\right] \qquad (3.4.41)$$

and high anodic overpotentials:

$$i = -i_o \exp\left[\frac{(1-\alpha) n F \eta}{RT}\right] \qquad (3.4.42)$$

Taking natural logs and rearranging yields the following expressions for overpotential:

$$\eta = \frac{RT}{\alpha n F} \ln i_o - \frac{RT}{\alpha n F} \ln i \qquad (3.4.43)$$

$$\eta = \frac{RT}{(1-\alpha) n F} \ln i_o + \frac{RT}{(1-\alpha) n F} \ln i \qquad (3.4.44)$$

These equations reduce to a single expresion first put forward by Tafel [148]:

$$\eta = a + b \log i \qquad (3.4.45)$$

A plot of η vs log i should be linear with a slope

$$b = \frac{+2.303\ RT}{\alpha n F} \qquad (3.4.46)$$

for cathodic overpotentials, and

$$b = \frac{-2.303\ RT}{(1-\alpha) n F} \qquad (3.4.47)$$

for anodic overpotentials. From such a plot kinetic data may be obtained, α the charge transfer coefficient from the slope and i_o from the intercept.

3.5 Mass Transport

So far the rate of an electrode process has been considered in terms of charge transfer. The supply of reactants to an electrode surface, or removal of products from that surface may also limit the rate of an electrochemical process. These considerations are known as mass transport processes and may limit overall electrode reactions if they represent the slowest rate determining step. Such reactions are transport controlled, whereas a reaction limited only by the actual rate of electron transfer is charge-transfer or activation controlled. Both processes may contribute to the overall rate and any study of electrode kinetics must consider mass transport processes. There are three main modes of mass transfer.

(i) Migration

This involves the movement of charged particles under the influence of an electrostatic field. This is usually prevented by the addition of a large excess of supporting electrolyte.

(ii) Diffusion

This is the mass transport process which is normally of most significance. As charge is passed across an electrode interphase the concentration of ions next to the electrode changes, resulting in the establishment of a concentration gradient. This will lead to diffusion of ions in one direction or another depending on the sign of the applied potential, it can only be neglected for infinitely concentrated solutions, and becomes increasingly important as the concentration of electroactive species is reduced.

The diffusion process is controlled by Ficks Laws. Ficks first law states that the concentration gradient is proportional to the number of moles of oxidised species, O, crossing a given cross-sectional area, A, in a time, t, i.e.

$$q = \frac{\partial N}{\partial t}\,\frac{1}{A} = D_o \frac{\partial C_o(x,t)}{\partial x} \qquad (3.5.1)$$

where

N = number of moles of oxidised species O,

q = flux of material,

x = distance from the electrode surface of the plane under consideration,

D_o = diffusion coefficient,

C_o = the concentration of oxidised species.

This equation applies for steady state conditions, i.e. if the concentration of a substance in any given volume element is independent of time, where non-steady state conditions apply the change in concentration of active species with time must be determined.

Let us consider two planes separated by a distance, dx, the nearest plane located a distance x from the electrode surface. The change in C_O per unit area with time between the two planes is given by:

$$\frac{\partial C_{o(x,t)}}{\partial t} = q(x + dx) - qx = \frac{\partial q}{\partial x}, \text{ as } dx \to 0 \qquad (3.5.2)$$

From Fick's first law

$$\frac{\partial q}{\partial x} = D_o \frac{\partial^2 C_{o(x,t)}}{\partial x^2} \qquad (3.5.3)$$

This leads to Fick's second law:

$$\frac{\partial C_{o(x,t)}}{\partial t} = D_o \frac{\partial^2 C_{o(x,t)}}{\partial x^2} \qquad (3.5.4)$$

This equation is often solved in electrochemistry; its solution depends on the boundary conditions used.

Experimental data on diffusion coefficients are useful in evaluating mass transport limitations of electrochemical power sources for high power applications. Maximum discharge capabilities of battery systems are often diffusion limited. At the present time however there is little experimental data relating to diffusion coefficients of lithium battery electrolytes.

(iii) Convection

This develops in any solution undergoing electrolysis. Convection is due to density changes in the region of the electrode, which may be due to thermal or mechanical disturbances. External turbulence causes what is known as forced convection. Natural convection is usually avoided where the time of measurement is short.

3.6 Faradaic Impedance Measurements

3.6.1 Introduction

The study of the electrode interphase by the technique of a.c. impedance is employed successfully for the determination of kinetic parameters. The technique has been developed for some time and can now be used to examine complex reactions involving specific adsorption of reactants and products on the electrode surface.

In simple terms this method can be described as the application of a small sinusoidal perturbation to an electrode, superimposed onto a d.c. polarization. The frequency of this a.c. signal is varied, and the way in which the system responds to this perturbation is measured. Using this technique the electrode can be maintained at close to the equilibrium potential, thus disturbing the system as little as possible. This is in contrast to other electrochemical methods such as the potential step technique which involve much larger disturbances.

3.6.2 Some A.C. Theory

At this stage it is worthwhile surveying the laws which govern alternating currents and voltages [149]. The alternating voltage at a given time t may be expressed:

$$V = V_{max} \sin(\omega t) \qquad (3.6.1)$$

From Ohms law the resulting current will be

$$I = \left(\frac{V_{max}}{R}\right) \sin(\omega t) \qquad (3.6.2)$$

where V_{max} is the amplitude of the alternating voltage, R is the resistance and ω is the angular frequency ($2\pi F$). Expressing the resulting current in terms of I_{max} the amplitude of the alternating current, we obtain:

$$I = I_{max} \sin(\omega t') \qquad (3.6.3)$$

t and t' in the above equations represent the time elapsed since the voltage and current respectively passed zero in a positive direction. If we term ϕ as the phase angle between the current and voltage, then

$$\phi = \omega t' - \omega t \qquad (3.6.4)$$

and

$$I = I_{max} \sin (\omega t - \phi) \qquad (3.6.5)$$

Z, the impedance of a cell may be written in vector form:

$$Z = \frac{V_{max}}{I_{max}} \arg \phi \qquad (3.6.6)$$

$$= |Z| \arg \phi$$

i.e. the impedance may be defined as a vector of modulus $|Z|$ and arguement ϕ, the phase angle. This can be represented in a complex plane plot (Fig. 3.6.1) as Z' the resistance (or real component) and Z'' the reactance (or imaginary component). The complex impedance may thus be written in cartesian form:

$$Z = Z' + jZ'' \qquad (3.6.7)$$

where:

$$Z' = |Z| \cos \phi \qquad (3.6.8)$$

$$Z'' = |Z| \sin \phi \qquad (3.6.9)$$

and $j = \sqrt{-1}$

If the phase angle is negative, the current leads the voltage and the reactance can be represented by capacitors. If the phase angle is positive however the voltage leads the current and the reactance is inductive.

For electrode impedance, the former is the most common, thus in electrochemistry it is usual to represent capacitative reactances in the first quadrant of a complex plane plot, and the inductive component beneath the axis.

As ω, the angular frequency of the applied waveform varies, the magnitude of the phase angle ϕ, will vary, thus the values of Z' and Z'' are frequency dependent.

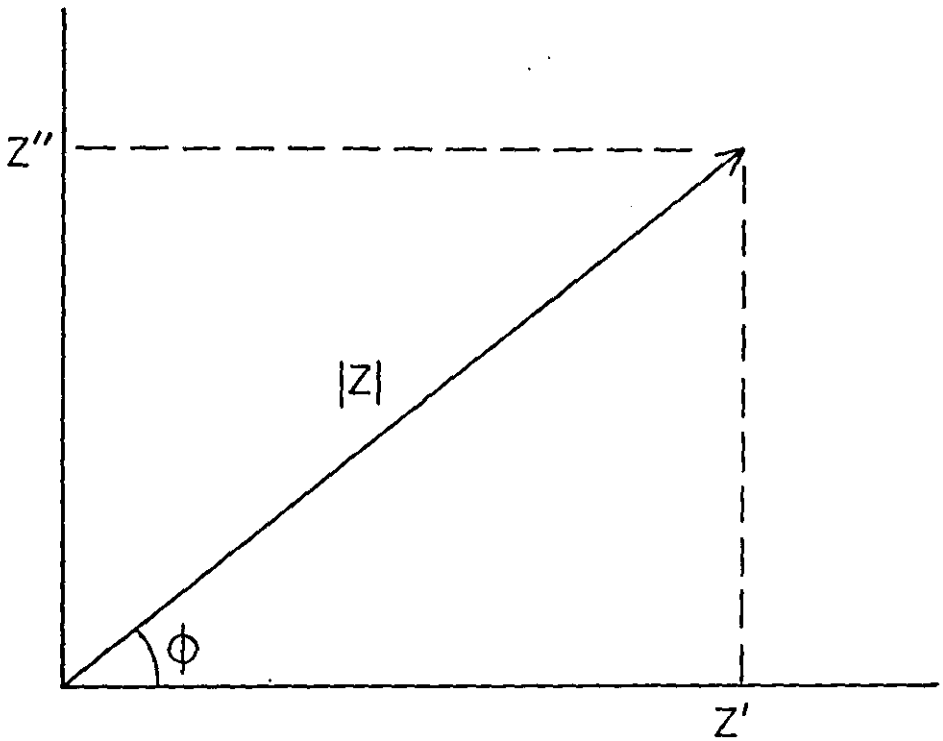

FIG 3.6.1 COMPLEX REPRESENTATION OF IMPEDANCE.

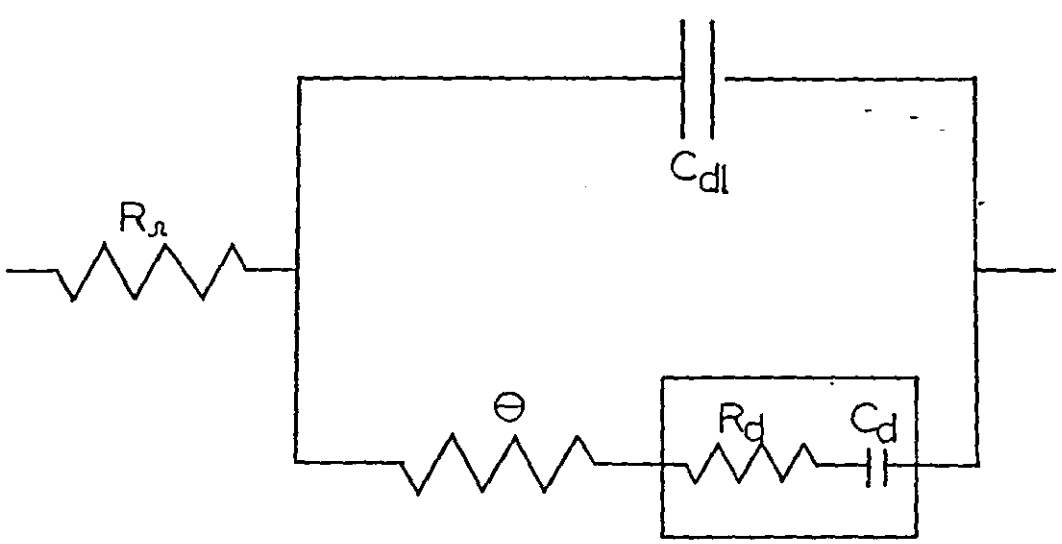

$R_d + C_d = W$

FIG. 3.6.2 RANDLES EQUIVALENT CIRCUIT.

3.6.3 Cell Impedance

Warburg first attempted the measurement of cell impedance [150] although he did not allow for the capacitance effect of the electrical double layer.

Randles [151] calculated the Faradaic impedance for fast electrode reactions. In his study he approximated the impedance of the working electrode to the total cell impedance, since the counter electrode had a much greater surface area than the working electrode. He was therefore able to neglect the contribution of the counter electrode to the total cell impedance. Randles assumed that the rate of the reaction was controlled solely by charge transfer and diffusional mass transfer.

It was found that the impedance behaviour of a cell could be represented by an equivalent circuit [151-153], consisting of resistors and capacitors. Such a circuit is a Randles equivalent circuit (see Fig. 3.6.2), comprising four elements. R_Ω represents the ohmic resistance of the electrolyte solution, including the metal leads to the electrodes. C_{dl} is the double-layer capacitance which varies with d.c. potential and is dependent upon the nature of the electrolyte. θ is the charge-transfer resistance, this represents the activation polarization of the electrode reaction. Finally there is a component known as the Warburg impedance (W) from which diffusion polarization arises, i.e. the a.c. impedance due to charged species diffusing to or from the electrode. Solution of Fick's second law of diffusion, taking into account suitable boundary conditions, yields the Warburg impedance:

$$W = \sigma\omega^{-\frac{1}{2}} - j\sigma\omega^{-\frac{1}{2}} \qquad (3.6.10)$$

where σ is the Warburg coefficient given by:

$$\sigma = \frac{RT}{n^2F^2A^2}\left[\frac{1}{C_O^b D_O^{\frac{1}{2}}} + \frac{1}{C_R^b D_R^{\frac{1}{2}}}\right] \qquad (3.6.11)$$

Randles [151] used vector methods for the determination of θ and σ. Sluyters [154] with Sluyters-Rehbach [149] interpreted the cell impedance in terms of R_Ω, C_{dl}, θ and σ. From the Randles circuit (Fig. 3.6.2), the overall impedance can be expressed in terms of the individual components using circuit theory.

$$Z = R_\Omega + \frac{1}{j\omega C_{dl} + \left[\frac{1}{\theta + \sigma\omega^{-\frac{1}{2}} - j\omega^{-\frac{1}{2}}}\right]} \qquad (3.6.12)$$

The real and imaginary parts which make up the total impedance can be separated.

$$Z' = R_\Omega + \frac{\theta + \sigma\omega^{-\frac{1}{2}}}{(\sigma\omega^{\frac{1}{2}}C_{dl} + 1)^2 + \omega^2 C_{dl}^2 (\theta + \sigma\omega^{-\frac{1}{2}})^2} \qquad (3.6.13)$$

$$Z'' = \frac{\omega C_{dl}(\theta + \sigma\omega^{-\frac{1}{2}})^2 + \sigma\omega^{-\frac{1}{2}}(\sigma\omega^{\frac{1}{2}}C_{dl} + 1)}{(\sigma\omega^{\frac{1}{2}}C_{dl} + 1)^2 + \omega^2 C_{dl}^2 (\theta + \sigma\omega^{-\frac{1}{2}})^2} \qquad (3.6.14)$$

This expression can be simplified for two limiting cases.

(1) At low frequency the effects of the double layer capacitance may be neglected, the impedance reduces to:

$$Z = R_\Omega + \theta + \sigma\omega^{-\frac{1}{2}} - j[\sigma\omega^{-\frac{1}{2}} + 2\sigma^2 C_{dl}] \qquad (3.6.15)$$

In this case a complex plane or Sluyters [154] plot of Z' versus Z'' produces a straight line of slope 45°. Such a linear correlation is characteristic of a diffusion controlled process.

The intercept of this line on the Z' axis is given by

$$R_\Omega + \theta - 2\sigma^2 C_{dl} \qquad (3.6.16)$$

A completely diffusion controlled process will consist only of this characteristic. Usually however as the frequency increases θ, the charge transfer resistance and C_{dl} the double layer capacitance increasingly contribute to the impedance causing a departure from this relationship.

(2) At higher frequencies for a fairly irreversible reaction, the concentration polarization can be neglected. In this instance the reaction is kinetically controlled and the equation becomes

$$Z = R_\Omega + \frac{\theta}{1 + \omega^2 C_{dl}^2 \theta^2} - \frac{\omega C_{dl} \theta^2}{1 + \omega^2 C_{dl}^2 \theta^2} \qquad (3.6.17)$$

From this equation a Sluyters plot describes a semi-circle, which has a radius equal to $\theta/2$. The frequency at the top of the semi-circle is given by:

$$\omega_{max} = \frac{1}{C_{dl}\,\theta} \qquad (3.6.18)$$

The semicircle usually originates some distance from the origin of the graph. This semicircle origin corresponds to the high frequency limit, where the cell impedance is determined only by the solution resistance, R_Ω, which represents the distances of this 'shunt'.

In reality we would expect to see a combination of these two effects, a semicircle at the high frequency end of the spectrum which distorts at intermediate frequencies, until a constant 45° low frequency 'tail' results [Fig. 3.6.3].

From such a plot all of the components of the Randles circuit can be calculated, i.e. θ from the diameter of the semicircle, R_Ω from the origin of the semicircle, C_{dl} from the frequency at the highest point, then knowing the other parameters, σ can be determined from the intercept of the extrapolated 45° line.

An alternative method of displaying this data can be employed and is known as a Randles plot. J.E.B. Randles first plotted R and $\frac{1}{\omega\, C_{dl}}$ against $\omega^{\frac{1}{2}}$. Such a plot yields two parallel lines [151] separated by a distance equal to θ.

3.6.4 Impedance at potentials other than the equilibrium potential

When the reaction is driven away from the equilibrium potential the impedance may be expressed as below:

$$Z = R_\Omega + \frac{1}{j\omega C_{dl} + \dfrac{1}{\theta' + \sigma'\omega^{-\frac{1}{2}} - j\sigma'\omega^{-\frac{1}{2}}}} \qquad (3.6.19)$$

θ', σ' representing the charge transfer resistance and Warburg coefficient at this new potential. From equation(3.4.40), θ' is related to the interfacial current i_o', by

$$\theta' = \frac{RT}{nf}\,\frac{1}{i_o'} \qquad (3.6.20)$$

Thus i_o' may be easily determined from the semicircle.

From a series of impedance spectra, produced from cells having certain potentials applied to them, it should be possible to produce a Tafel type relationship between log θ and E.

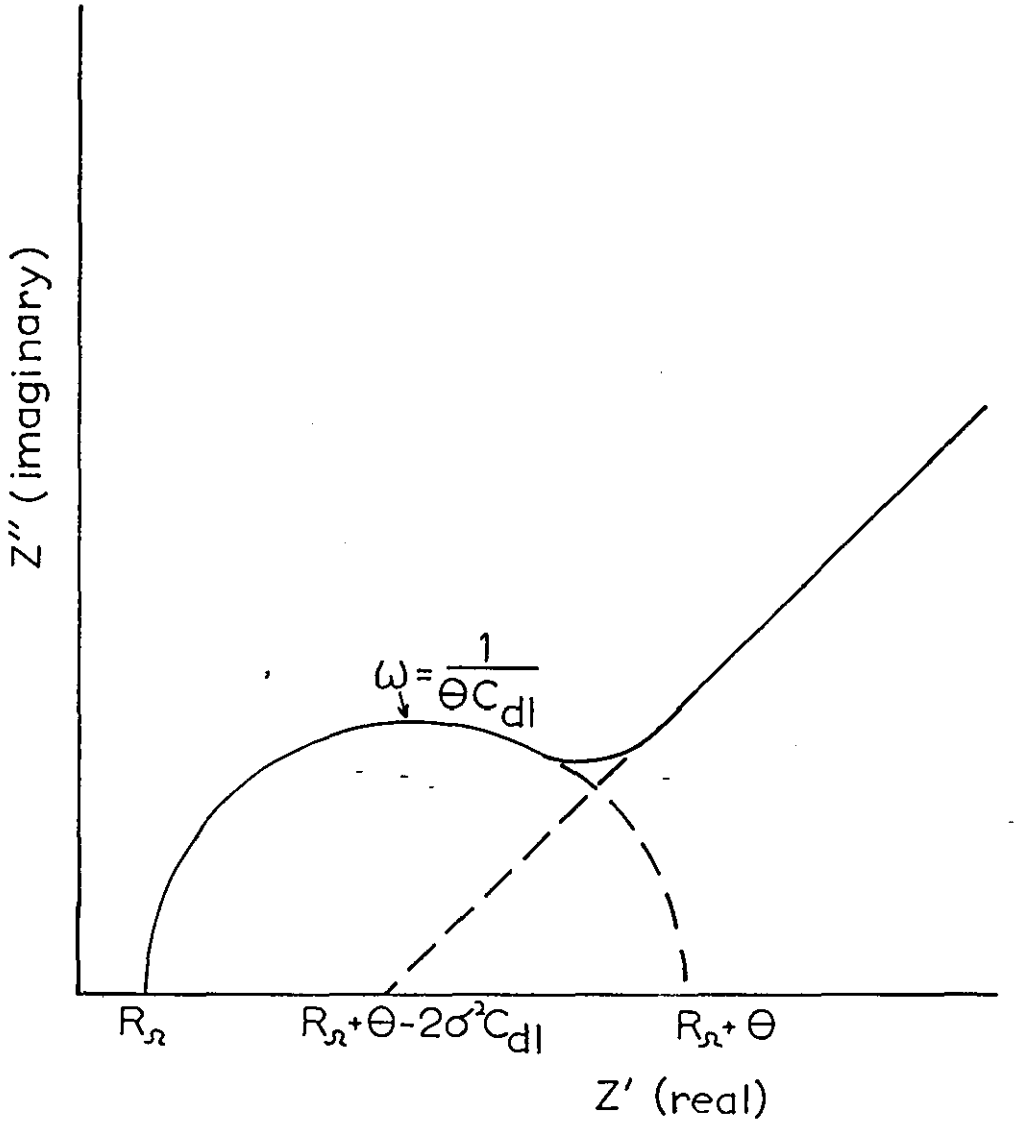

FIG. 3.6.3 COMPLEX PLANE (SLUYTERS) PLOT FOR A RANDLES CIRCUIT.

3.6.5 Extension of the impedance theory

(a) Alternative electrode analogues

The graphical method of obtaining kinetic parameters from impedance data, outlined above, is not always applicable. The Randles circuit in reality does not adequately model electrode behaviour for most systems. Usually an alternative equivalent circuit, with additional elements is devised. For such a circuit it is unlikely that there is a simple graphical method available for recovery of impedance parameters, in which case a numerical method is employed. Even for a simple Randles circuit a numerical computer based method for the analysis of impedance data is likely to yield more accurate results. The development of such a method is described in more detail in Appendix 1.

Additional resistances and capacitances in the electrode analogue have been used to represent the behaviour of adsorbed species on the electrode [149, 155, 156]. Complex reactions which involve adsorbed and soluble intermediates, and reactions with electrolyte dissolution, deposition and active-passive transition have also been studied by using the impedance technique. A review of such work has been written by Armstrong and Metcalfe [157].

(b) Porous and rough electrodes

Robert de Levie considered the electrochemical response of porous electrodes [158-160] on the basis of a model describing the pores as essentially cylindrical in shape and semi-infinite in length. He was able to give a unified and generally applicable treatment for the combined effects of double layer capacity and Faradaic processes.

Hampson et al [161] suggested that for electrodes possessing surface roughness a factor, γ, should be introduced. This factor could range in value from 1 for a perfectly smooth electrode, down to 0.5 for an electrode roughened to the extent that it is considered porous. This treatment arises from the work of de Levie [160] who concluded the following:

1. the phase angle of the impedance of a porous electrode is half that of the equivalent flat electrode, and

2. the absolute magnitude of the impedance of a porous electrode is proportional to the square root of that of the equivalent flat electrode.

From this, the complex impedance of a rough electrode may be expressed as follows:

$$Z_R = |Z_S|^{\gamma} \arg(\gamma\phi_s) \qquad (3.6.21)$$

where the subscripts R and S refer to rough and smooth electrodes respectively. Values of γ ranging between 0.5 and 1 represent various degrees of surface roughness.

3.6.6 Impedance Measurement

Impedance measurements have traditionally been carried out using an a.c. bridge network. This contains variable resistors and capacitors which can be balanced at given frequencies to determine the behaviour of the electrode.

More sophisticated techniques for carrying out impedance determinations have recently been developed. These involve the use of frequency response analysers (FRA's) which are normally used in conjunction with an electrochemical interface used to control the potential. The FRA consists of a progammable generator which provides the perturbating signal, measures the response of the system and analyses the result, which it can display in a number of possible ways. The FRA can be programmed to select a frequency and measure the response, or more usually to measure the responses over a range of frequencies from up to 1 MHz to as low as 1 mHz. The response can be averaged over a number of cycles.

It is possible to interface the FRA to a remote computer which can control the experiment and store the data in its memory.

CHAPTER 4

EXPERIMENTAL METHODS

4.1 The handling of Li-$SOCl_2$ cell components

Experiments with lithium-thionyl cells and other similar systems necessitate the exclusion of moisture from the working environment. Additional safety hazards are involved with these cells compared with most conventional battery systems, these include the danger of lithium ignition and the toxic asphyxiating effect of $SOCl_2$ vapour. On an industrial scale cell assembly takes place in a 'dry room', where the relative humidity is maintained at a low level.

For this study all experiments were carried out in a dry argon atmosphere. This was provided by an argon filled dry box (Fig. 4.1) which contained less than 40 ppm of water, a value well below the maximum permissible level for working with lithium. As a further precaution the lithium anode material was stored in airtight polythene containers, within the box. Initially a commercial moisture meter was used to monitor the water content in the box, however it was withdrawn after the detrimental effects of $SOCl_2$ on the internal workings of the meter were discovered. It was found that the moisture in the box was best monitored by observing a piece of lithium which was left continually exposed to the argon atmosphere.

Low relative humidity was maintained by passage of the argon atmosphere through molecular sieve resin (13-X, Union Carbide). The resin was contained in steel cylinders adjacent to the box, the atmosphere was circulated using a compressor. The resin was changed periodically or at the slightest sign of any lithium deterioration. A slight positive gas pressure was maintained inside the box, any fall in pressure was detected by sensors, which then activated a solenoid to admit fresh argon into the system. Passage of apparatus between the box and the outside environment was achieved via evacuable transfer ports.

FIG 4.1 ARGON FILLED DRY BOX.

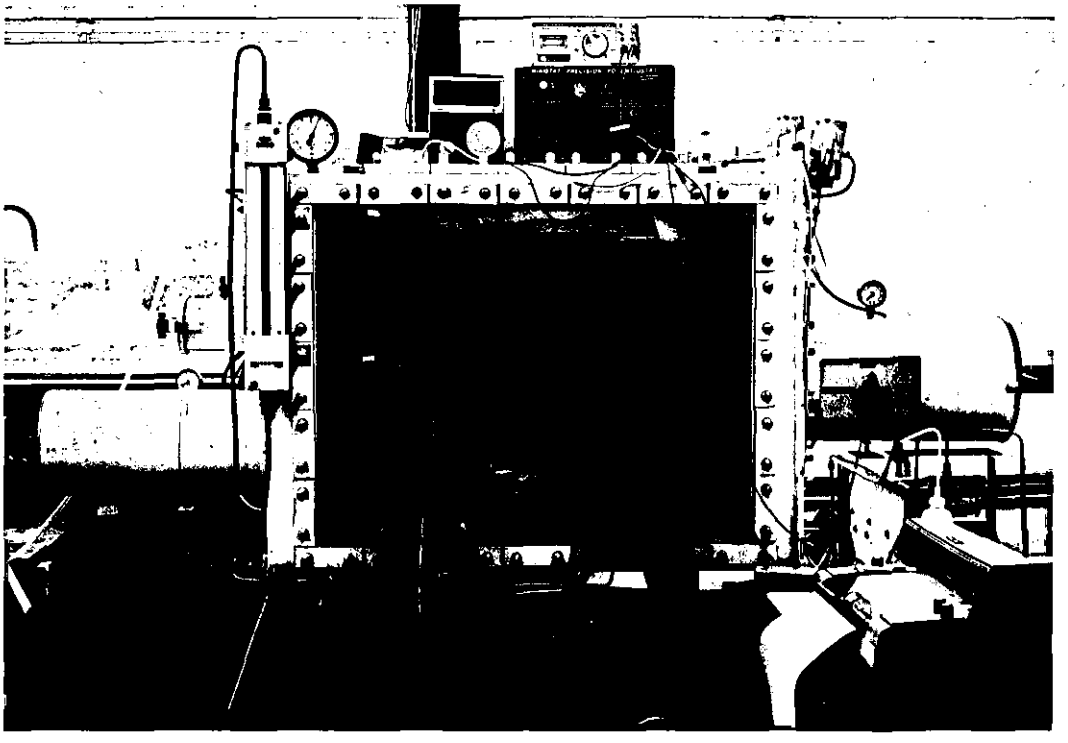

4.2 Apparatus and Materials

4.2.1 Electrolyte Solutions

These fall into two categories, neutral and (Lewis) acid electrolyte. The neutral electrolyte was lithium aluminium chloride in thionyl chloride. This was made by adding a stoichiometric quantity of $AlCl_3$ (Fluka, >99%) and a slight excess of LiCl (Fluka >98%) to $SOCl_2$ (Fisons Ltd., >98%), and stirring to dissolve. Any undissolved solid remaining was assumed to be LiCl, this was rinsed three times with $SOCl_2$, the washings being added to the rest of the electrolyte in a volumetric flask. The flask was then made up to the mark with $SOCl_2$. Such a procedure endeavoured to ensure complete neutralization of $AlCl_3$. The acid electrolyte employed consisted of either pure $AlCl_3$ in $SOCl_2$ or of $LiAlCL_4$ containing an excess of $AlCl_3$.

4.2.2 Porous Carbon Electrodes

These were used as cathodes for electrochemical cells and were composed of amorphous carbon and PTFE (10% $^{w}/_{w}$, ICI Plastics). Unless otherwise stated, the type of carbon powder used as a cathode material was Shawinigan Acetylene Black (SAB). Two methods were used for fabricating these electrodes.

(a) Spraying

The carbon and PTFE, with a quantity of surfactant (Triton X-100, BDH Chemicals), were combined in Analar grade 1,1,1-trichloroethane (BDH Chemicals), and stirred for about five hours until fully homogenised. This mixture was then sprayed onto nickel studs (Fig. 4.2a) using a portable spray gun. After being coated with carbon in this way the studs were dried in an oven at 100°C for four hours. A microtome (Fig. 4.3) was then used to remove layers of carbon from the electrode until the required loading was attained. This was achieved by careful weighing of the nickel studs before and after spraying. The microtome (Anglia Scientific) could be set to obtain slices from a sample of between 1 and 30 μm, this was achieved by rotating the drum which moved the stud the required distance towards the blade. The knife edge was carefully aligned to the surface of the electrode, using a plain stud.

The nickel studs were all pretreated by a surface etch with a solution of 10% HCl containing iron (III) chloride, followed by a thorough rinse in triply distilled water and drying in an oven.

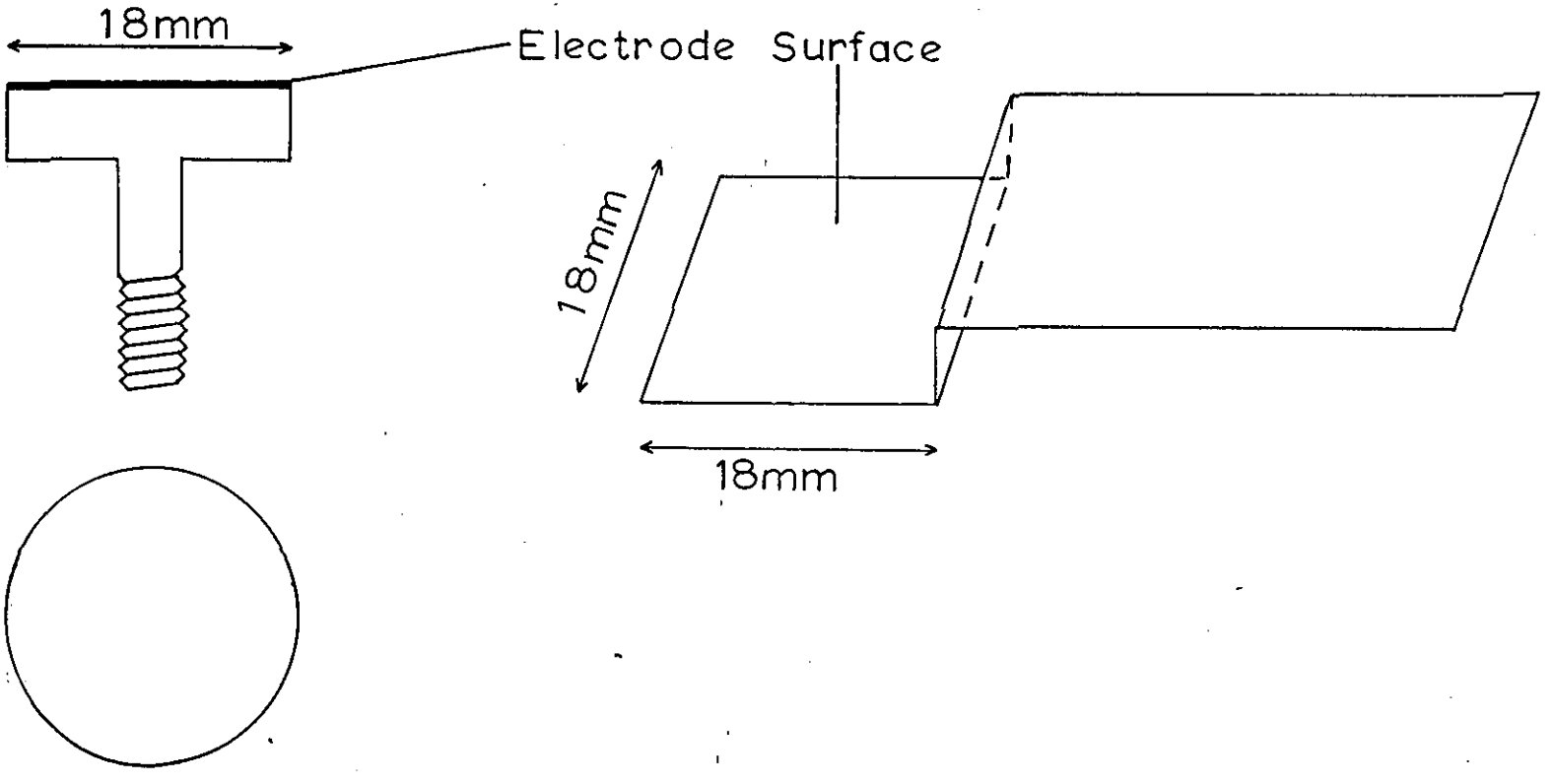

a) Nickel Stud

b) Nickel Gause

FIG 4.2 ELECTRODES.

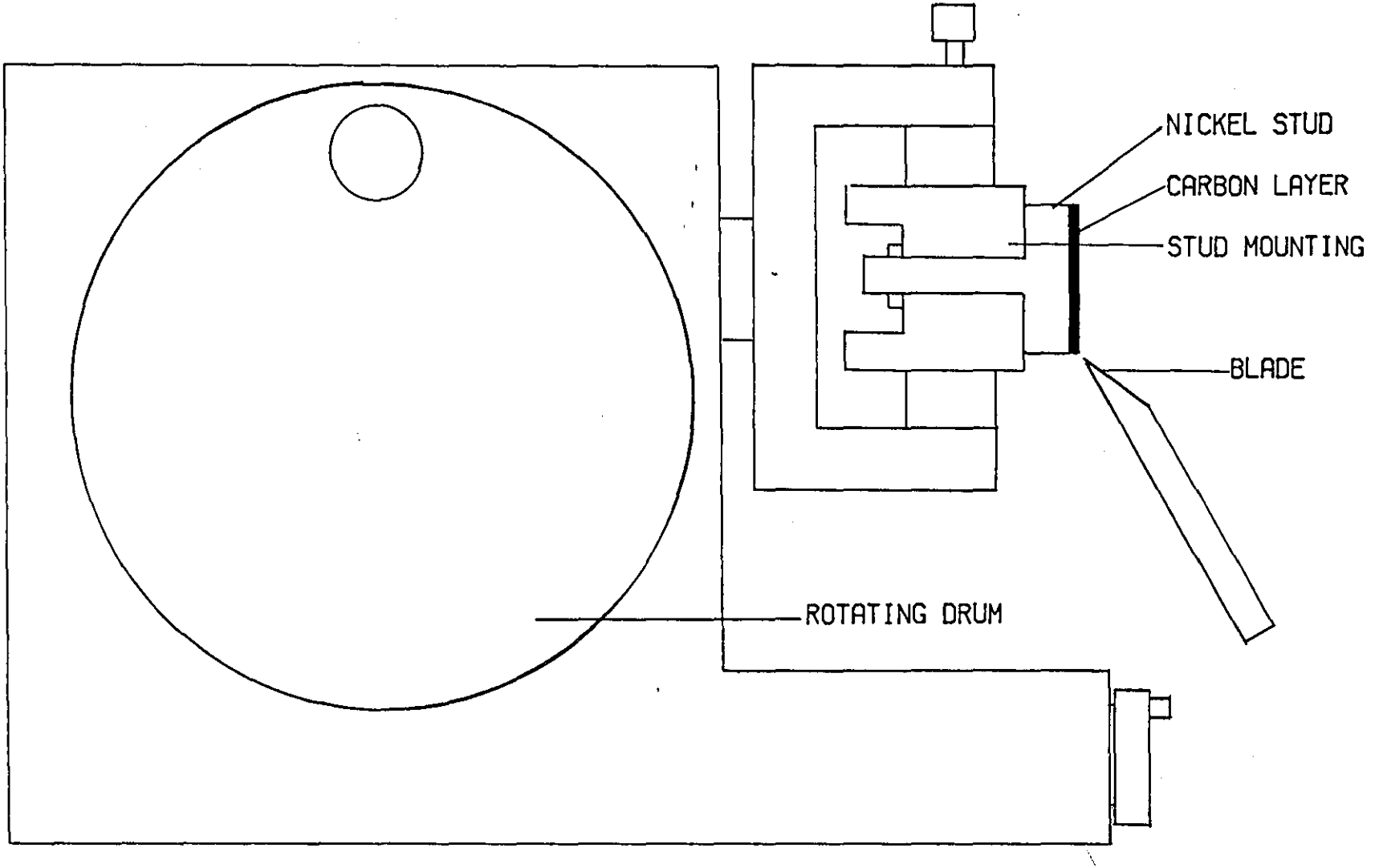

FIG 4.3 MICROTOME

(b) Pressing

In this process the carbon/PTFE mix was slurred in propan-1-ol and dried in an oven at 100°C. The solid mixture was then reduced to fine powder using a commercial blender. A carefully weighed portion of powder was pressed at a pressure of about 3 $kNcm^{-2}$ to form discs of Carbon/PTFE with a reasonable degree of integrity, which after further drying in an oven and storage in the dry box for at least 48 hours were used as cathodes.

4.2.3 Lithium Electrodes

The lithium anodes were prepared by trimming lithium foil (Lithco Ltd., 99.9%) to the dimensions shown in Figure 4.2b and pressing onto a nickel gauze current collector (99% Expamet. Co. minimesh). The nickel mesh was pretreated with the $FeCl_3$/HCl etching solution in a similar manner to the nickel studs.

Lithium reference electrodes were used for some experiments, these consisted of two forms. Some were similar in design to the anodes, but much smaller in area (0.4 cm^2), others consisted of a lithium wire shrouded in a piece of plastic tubing (2 mm in diameter).

4.2.4 Electrolytic Cells

For most experiments carried out in this work a PTFE cell was used, this was designed to accommodate the electrodes (Fig. 4.4). The basic cell consists of two halves, the top half is modified according to requirements. For cell discharge experiments the cell provided accommodation for the nickel stud, although if necessary could be modified so that the cathode was further back into the PTFE top.

For some experiments involving a large volume of electrolyte, an open glass cell such as shown in Figure 4.5 was employed.

4.3 Electrochemical Techniques

4.3.1 Cell discharge and cathode passivation experiments

A potentiostat (Thompson Electrochem. Ltd.) was used as a current source for all of these experiments, a Y-T type chart recorder (Curken) recorded the cell performances. Digital multimeters monitored the current output and cell voltages. The discharges were carried out galvanostatically at various current densities. Experiments specifically monitoring the cathode passivation process employed a lithium reference electrode, against which the cathode

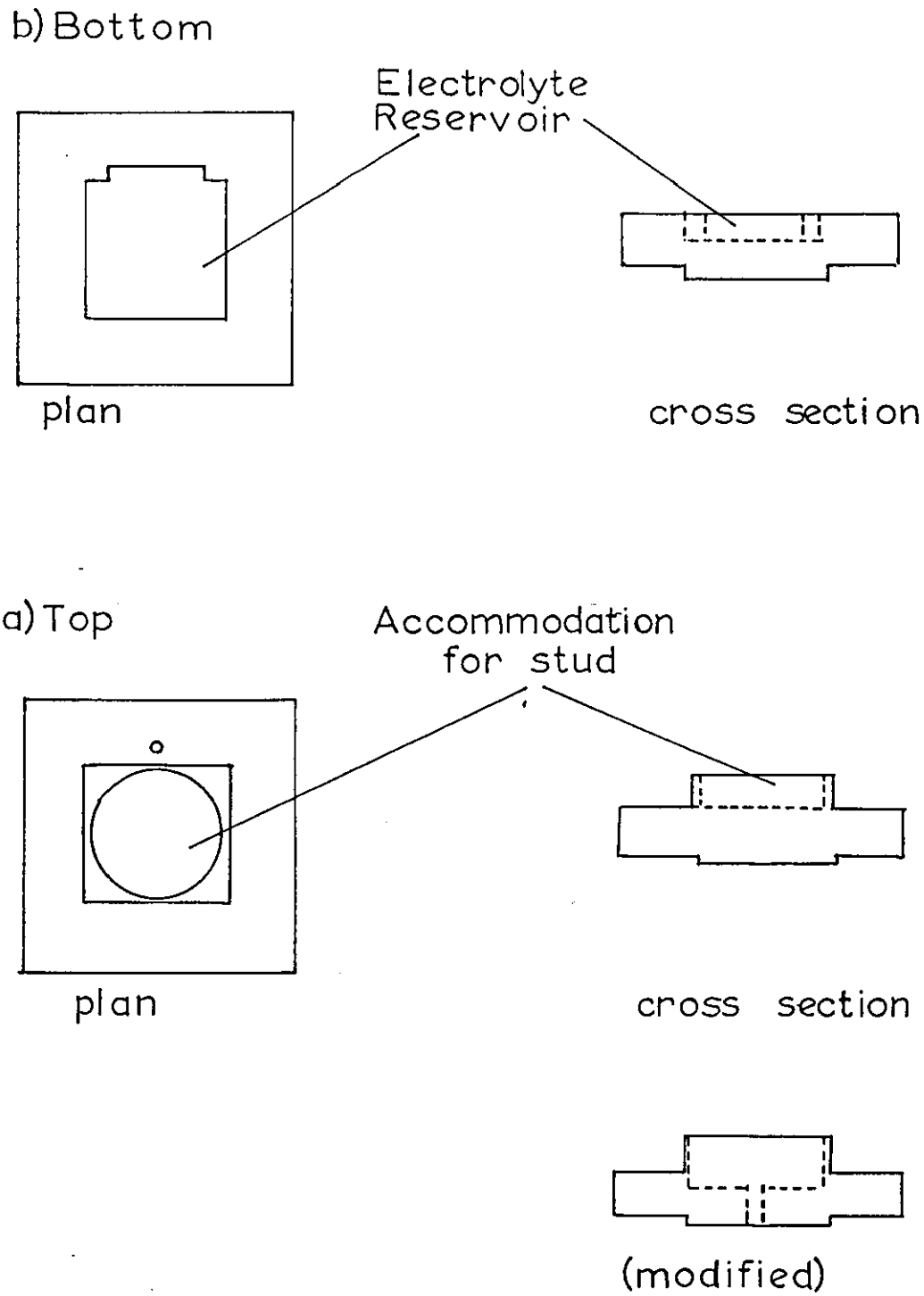

FIG 4.4 PTFE CELL HOLDER

Key to Fig. 4.5

A = Nickel fly lead attached to a nickel backing disc with a hole for electrolyte entry.

B = Pyrex cylinder.

C = Nitryl rubber 'O' rings.

D = Electrolyte solution.

E = Lithium anode.

F = Ceramic separator paper.

G = Glassy carbon disc.

H = Nickel fly lead attached to a nickel backing disc.

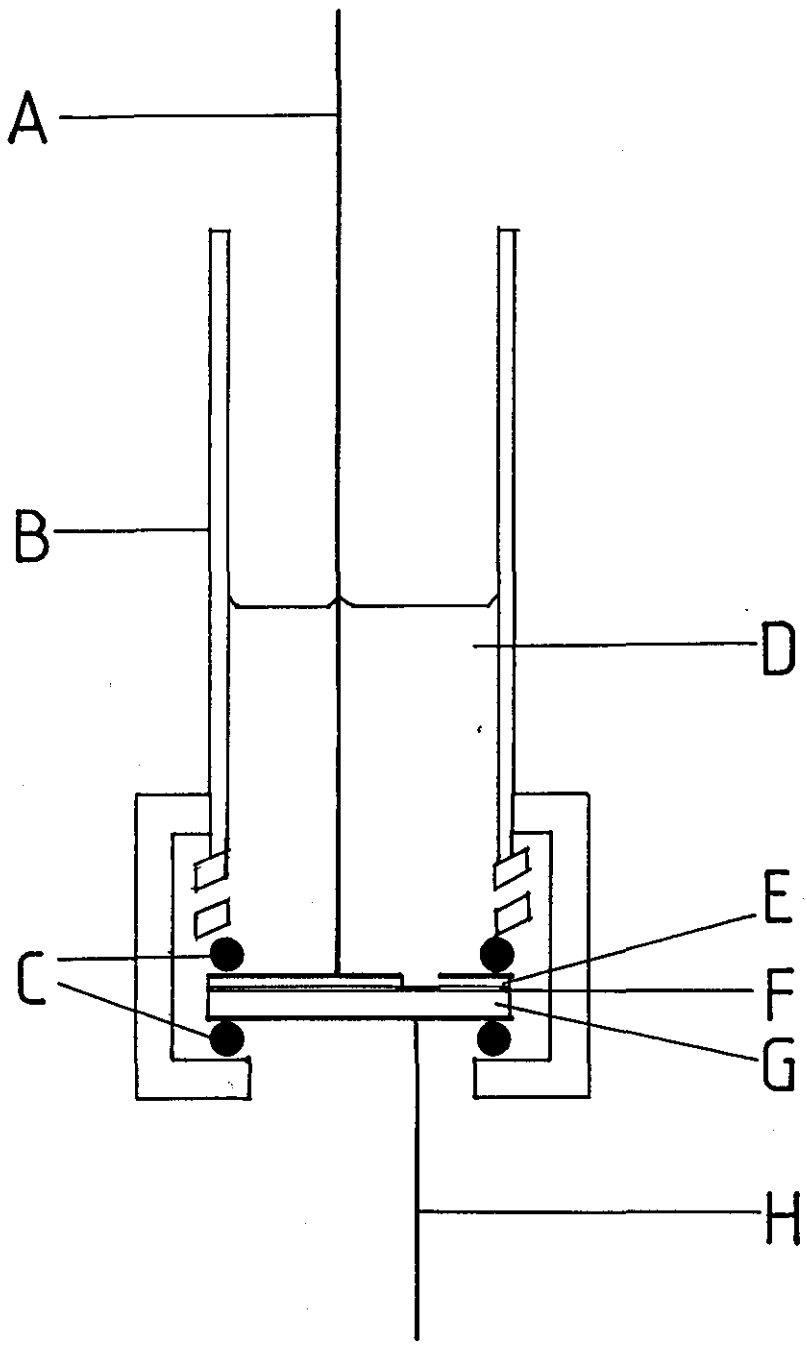

FIG 4.5 GLASS CELL.

potentials were measured. The circuits used are shown diagramatically in figure 4.6. Electrical contacts to the cell were made via the nickel stud and gauze current collectors.

4.3.2 Faradaic Impedance Measurements

The modules used to determine the impedance data are shown in the schematic diagram of Figure 4.7. The impedance measurements were carried out using a Solatron 1170 Frequency Response Analyser (FRA). A Solatron 1186 Electrochemical Interface maintained the cell at a predetermined potential. The response was analysed using the correlator in the FRA, the results were displayed in cartesian format as Z' and Z'', the real and imaginary parts of the impedance. The frequency was scanned logarithmically from high to low frequency, starting from 60 kHz. The response was usually averaged over 10 cycles. There are however a variety of ways in which the FRA may be programmed [163].

The FRA was interfaced to a N.E.C.PC-8001B micro-computer using an IEEE-488 interface bus. Thus the FRA was remotely controlled using the computer which stored data on $5\frac{1}{4}$" floppy disc and could display the same on the screen in the form of a Sluyters plot as the experiment proceeded. More detail pertaining to the interfacing procedure is given in Appendix 2. Subsequent data analysis was carried out with the help of a Honeywell Multics mainframe computer.

4.4 Analytical Techniques

It was necessary during this study to carry out analyses for lithium and aluminium ions from discharged cathodes, and for various metals in lithium samples. The aluminium ions were determined using a colorimetric method, the remaining analyses were carried out using flame spectroscopy. A brief description of each method follows.

4.4.1 Atomic Absorption Spectroscopy

This was found to be a satisfactory method for lithium determination. It is a very sensitive method, the detection limit for lithium ions is reportedly as low as 0.0015 $\mu g\ ml^{-1}$ [164]. Figure 4.8 shows the basic instrumentation necessary for atomic absorption spectroscopy. A solution containing the ions of interest is sucked through a capillary tube into an air/acetylene flame in which the constituents are atomised. The ground state atoms are then excited by an external light source, the radiation absorbed is measured and related to the concentration of ions present. The light

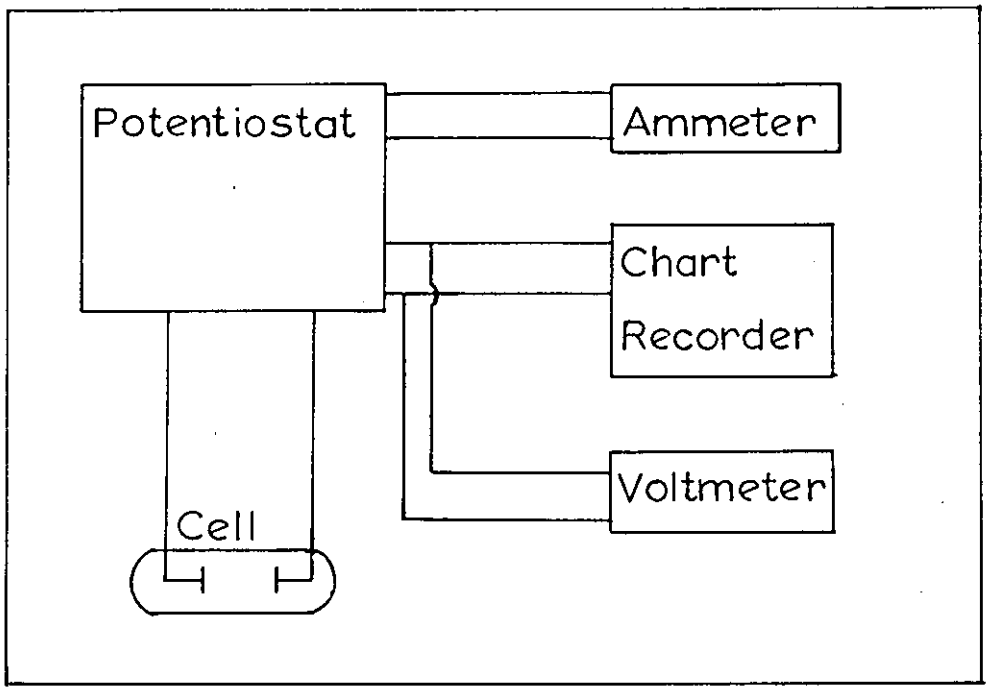

a) DISCHARGE CIRCUIT.

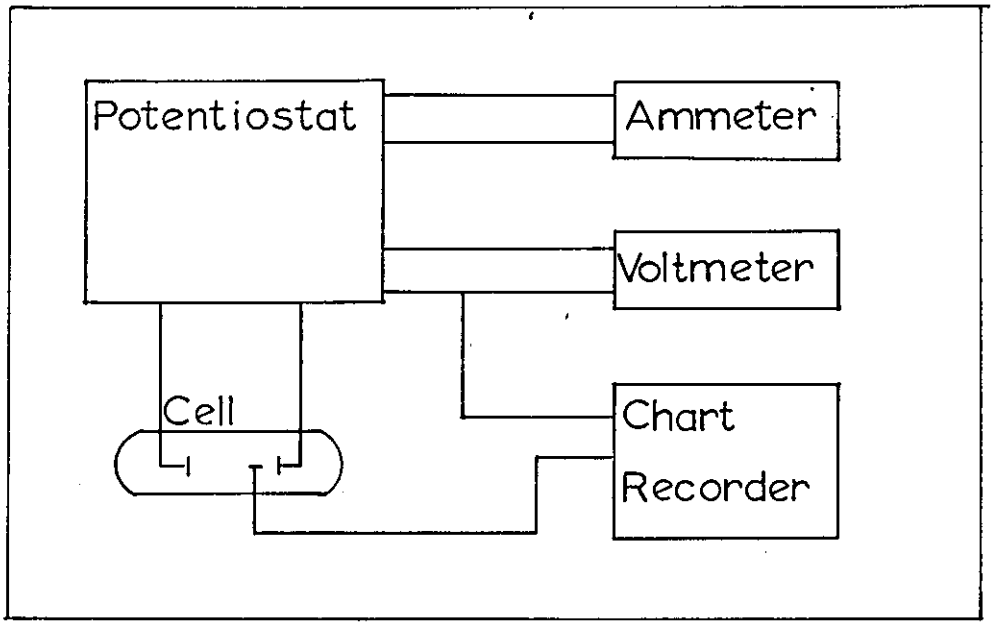

b) PASSIVATION CIRCUIT.

FIG 4.6 ELECTRICAL CIRCUITS.

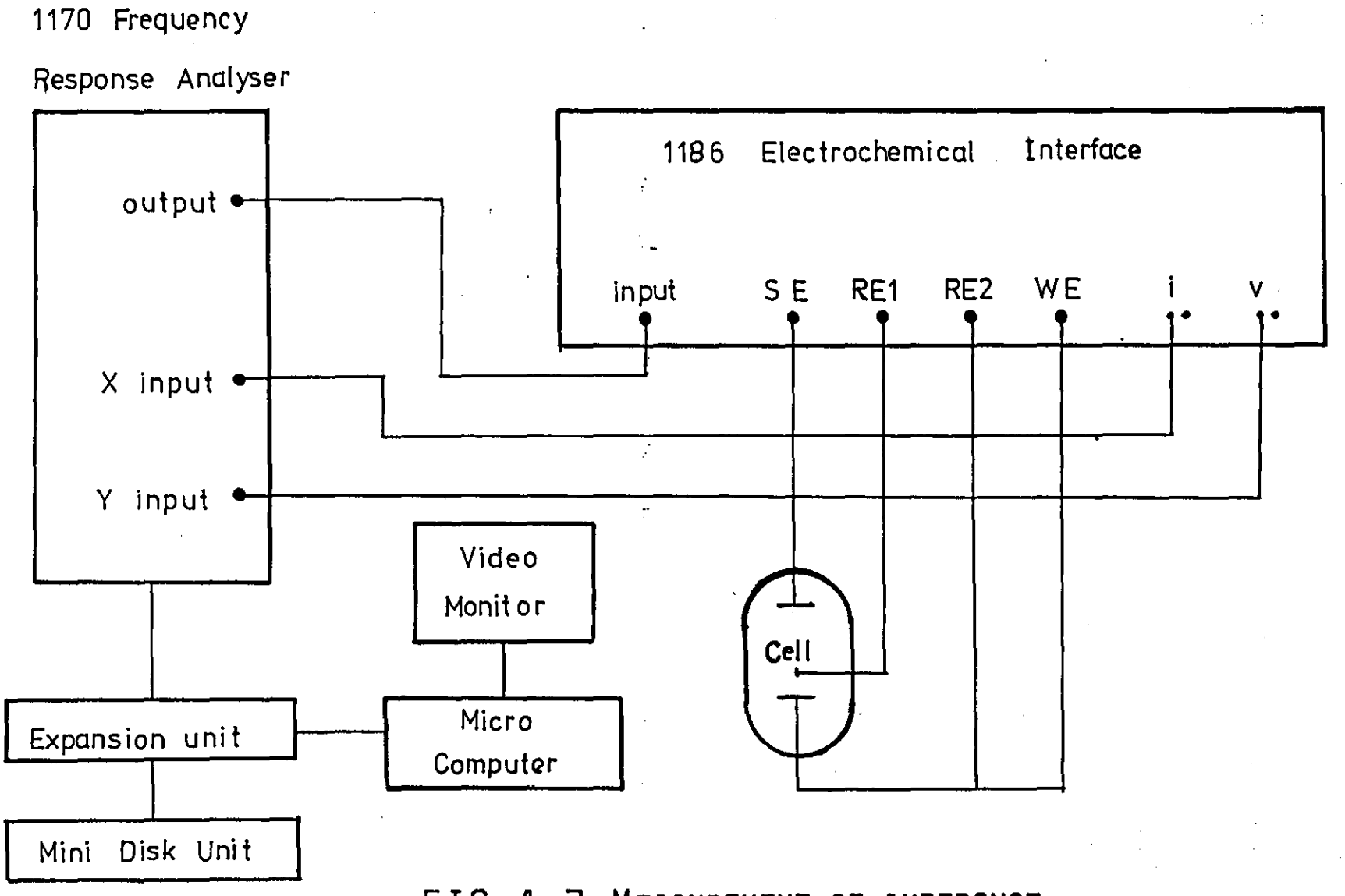

FIG 4.7 MEASUREMENT OF IMPEDANCE

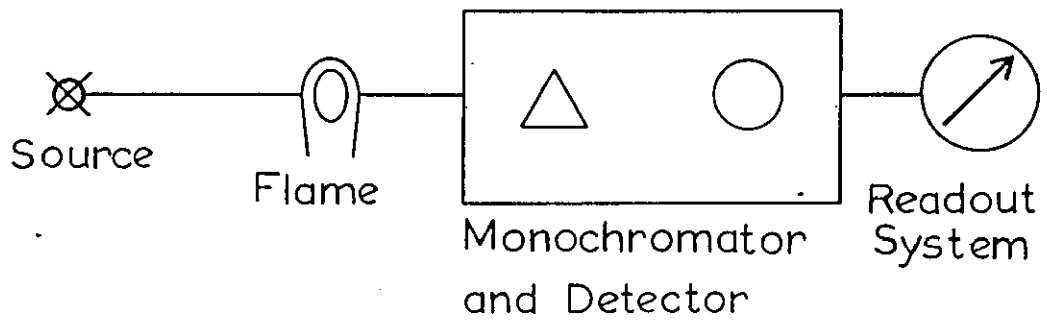

FIG 4.8 BASIC INSTRUMENTATION FOR ATOMIC ABSORPTION SPECTROSCOPY

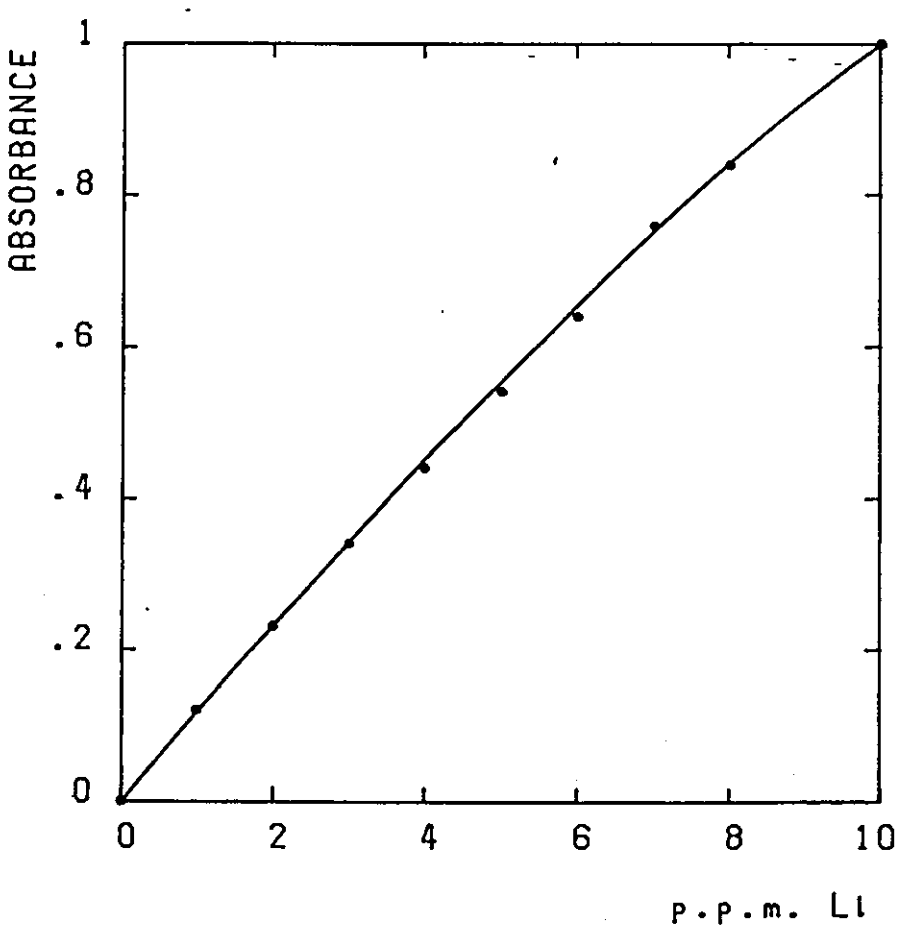

FIG 4.9 CALIBRATION CURVE FOR LITHIUM

source used was a lithium element hollow cathode lamp, the wavelength 670.8 nm was isolated by the monochromator to give maximum sensitivity. The components of the instrumentation were incorporated in a Shandon Southern A3300 Spectrophotometer. A calibration curve was constructed, Figure 4.9, the zero and 10 ppm settings were checked before each determination.

Atomic emission spectroscopy is similar to atomic absorption, except that the radiation emitted as the excited state atoms return to the ground state is measured. Also the flame itself can be used to excite the atoms. A glass filter isolates the line relevent to the element of interest.

4.4.2 Colorimetric Analysis

This method was used for the determination of aluminium ions in discharged cathodes. The colorimetric method is based on converting the constituent to be determined into a substance whose solution is coloured. The percentage of light at suitable wavelength, absorbed by the solution is measured. Preparation of the solutions can be a tedious process, particularly where it is required to carry out a large number of determinations. For this work the preparation was relatively straight forward, the absorbing solution was prepared by dissolving two proprietary test tablets (The Tintometer Ltd.), in 10 cm^3 of the sample. One tablet was a pH buffer, the other contained the complexing reagent eriochrome cyanine R. Figure 4.10 shows the absorption curve for the solution containing 0.3 ppm Al^{3+} ions. A Pye-Unicam PU8600 uv/visible spectrophotometer was used to determine the absorbance of the solution at 532 nm, the wavelength of maximum absorbance. A calibration curve was constructed (Fig. 4.11) for determinations of up to 0.5 ppm of Al^{3+}, the region for which the calibration is linear. In the absence of aluminium the complexing solution is yellow, becoming orange, pink and then deep purple as increasing quantities of Al^{3+} are added. The absorbance of each solution was measured after 10 minutes. This time interval allows full colour development, if left for much longer the colour begins to fade.

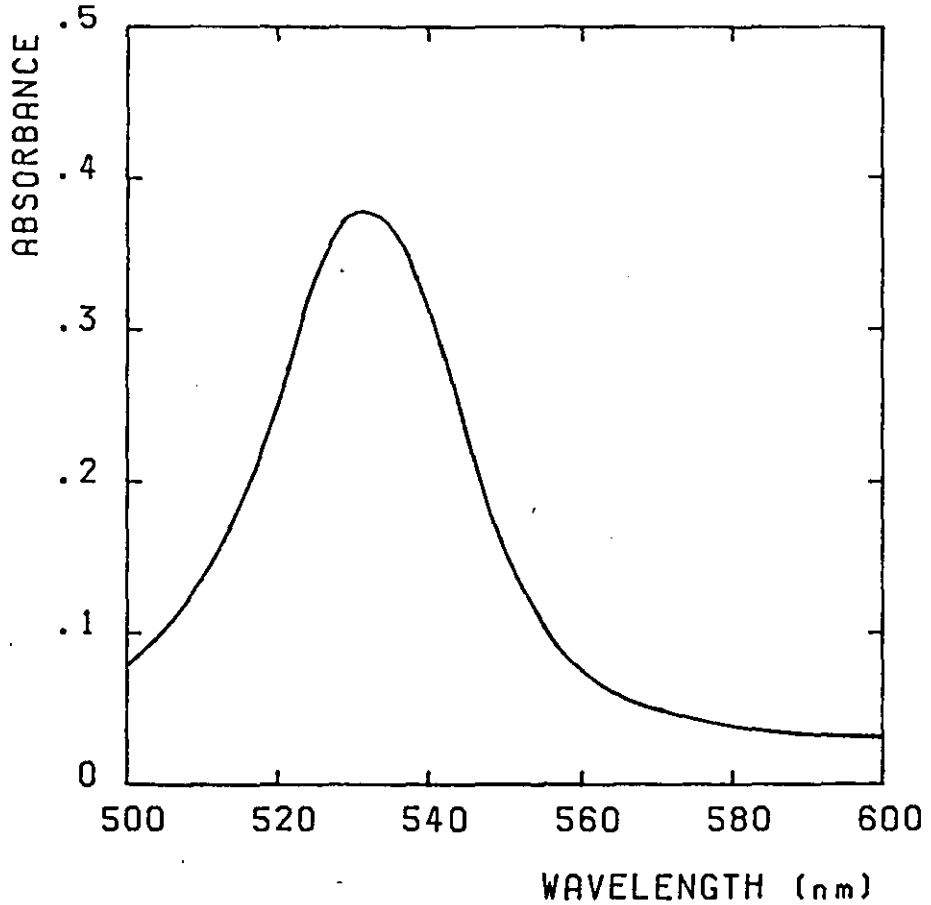

FIG 4.10 ABSORBTION CURVE FOR ALUMINIUM

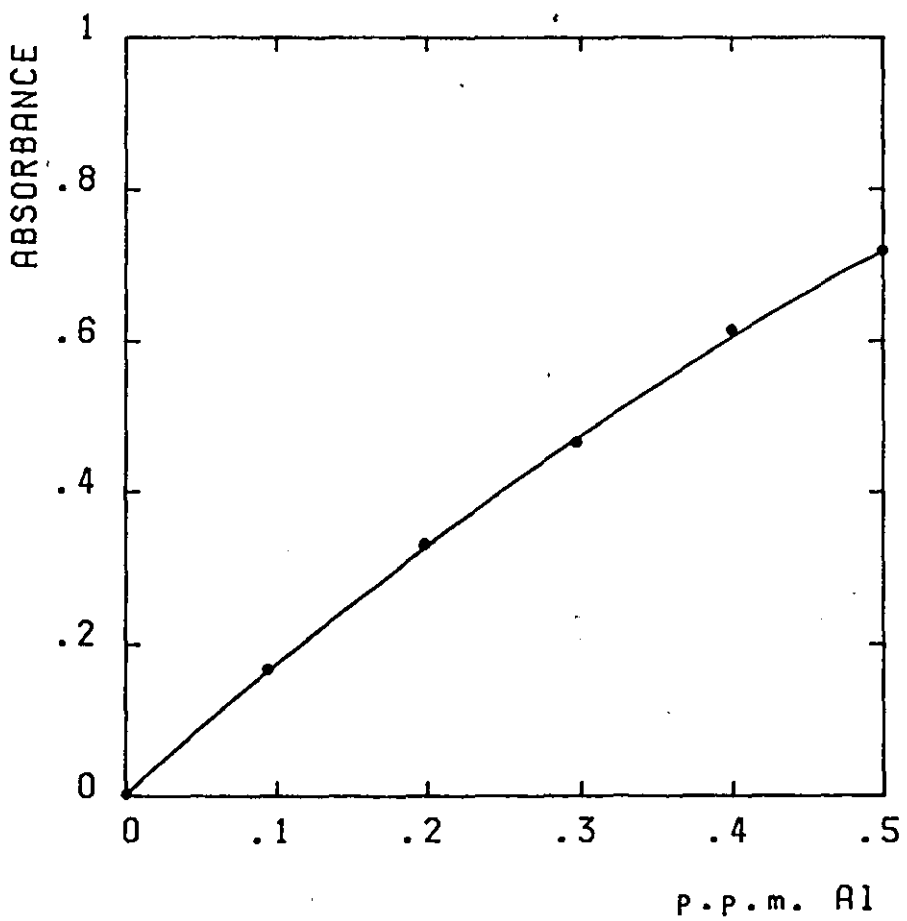

FIG 4.11 CALIBRATION CURVE

CHAPTER 5

THE IMPEDANCE OF THE Li^+/Li ELECTRODE IN $SOCl_2$:

I IN NEUTRAL ELECTROLYTE

5.1 Introduction

The Li-$SOCl_2$ discharge reaction mechanism is fairly complex, it is thought that various intermediates must be involved [13, 17]. The presence of such intermediates along with cell reaction products may complicate the behaviour of the lithium electrode for which the anodic reaction:

$$Li \rightarrow Li^+ + e^- \qquad (5.1)$$

results in the production of lithium chloride. Although the majority of this product is deposited in the cathode matrix, the anode is to some extent protected by a film of LiCl. The presence of this surface film [32, 34], which forms as the electrode and electrolyte make contact, results in the high stability of lithium in $SOCl_2$-$LiAlCl_4$ solutions.

The Li^+/Li exchange in Li-SO_2 cells has been studied previously by making deductions from the total system [165] and by incorporation of a Li reference electrode in a sealed cell [166]. In the present work neither is desirable.

The simplest method for studying the Li^+/Li exchange reaction in $SOCl_2$ is by using a cell consisting of two Li electrodes and a lithium reference in the electrolyte solution. Such arrangements have been used previously in connection with Li/$SOCl_2$ (C) electrochemistry [20, 43], for both impedance and cyclic voltammetry. It is the intention of this work to study the kinetic parameters of the Li^+/Li exchange in electrolyte solutions of conventional, commercial cell concentration, in order to assess the magnitude of the kinetic constants.

5.2 Experimental

The PTFE electrolytic cell arranged for a working electrode (area 0.0415 cm^2) to be isolated from a counter electrode (area 3.5 cm^2) by a ceramic separator. The reference electrode was a strip of lithium placed between the electrodes in such a way as to not shield the working electrode. The electrodes themselves were made from lithium and fabricated as in Section 4.2.3. A nickel plate with a hole in the centre defined the working electrode area. The electrolyte solution used was 1.8 M $LiAlCl_4$ in $SOCl_2$.

The cell was assembled and the electrolyte solution was added in an Argon filled dry box (Section 4.1). The cell was then placed immediately into a special polythene container which could be transferred to the test equipment in the ambient atmosphere. Connections between the cell and test circuits were made via metal leads through the polythene isolation box. Thus it was possible to carry out all the electrochemistry without the intrusion of oxygen or moisture to the lithium system.

Impedance measurements were made using a Solatron 1170 Frequency Response Analyser. The computer control of the instrument incorporated software routines developed in these laboratories [167, Appendix 2] which ensured that accurately standardised data were obtained when the cell was interfaced through the 1186 electrochemical interface. Generally the electrochemistry was carried out within 60-100 minutes of initial electrode/electrolyte contact. The results of experiments in this range were found to replicate within experimental error. After the impedance measurements had been obtained on disc, the cell impedance was processed using a least squares technique with a Taylor series approach so that a series of models could be matched to the experimental data. Decomposition of the data into the appropriate circuit elements was accomplished using a Honeywell Multics main-frame computer.

5.3 Results and Discussion

Figure 5.1 shows the impedance spectrum of the cell with no external d.c. polarization. It consists of an elongated semicircle going off into a Warburg region which shows a definite return to the real axis at low frequencies. On repeating the experiment after the electrode had been immersed in the electrolyte solution for 50 h the impedance locus was significantly altered, this change continuing for some time as indicated by the data of Figure 5.2. Similar changes in

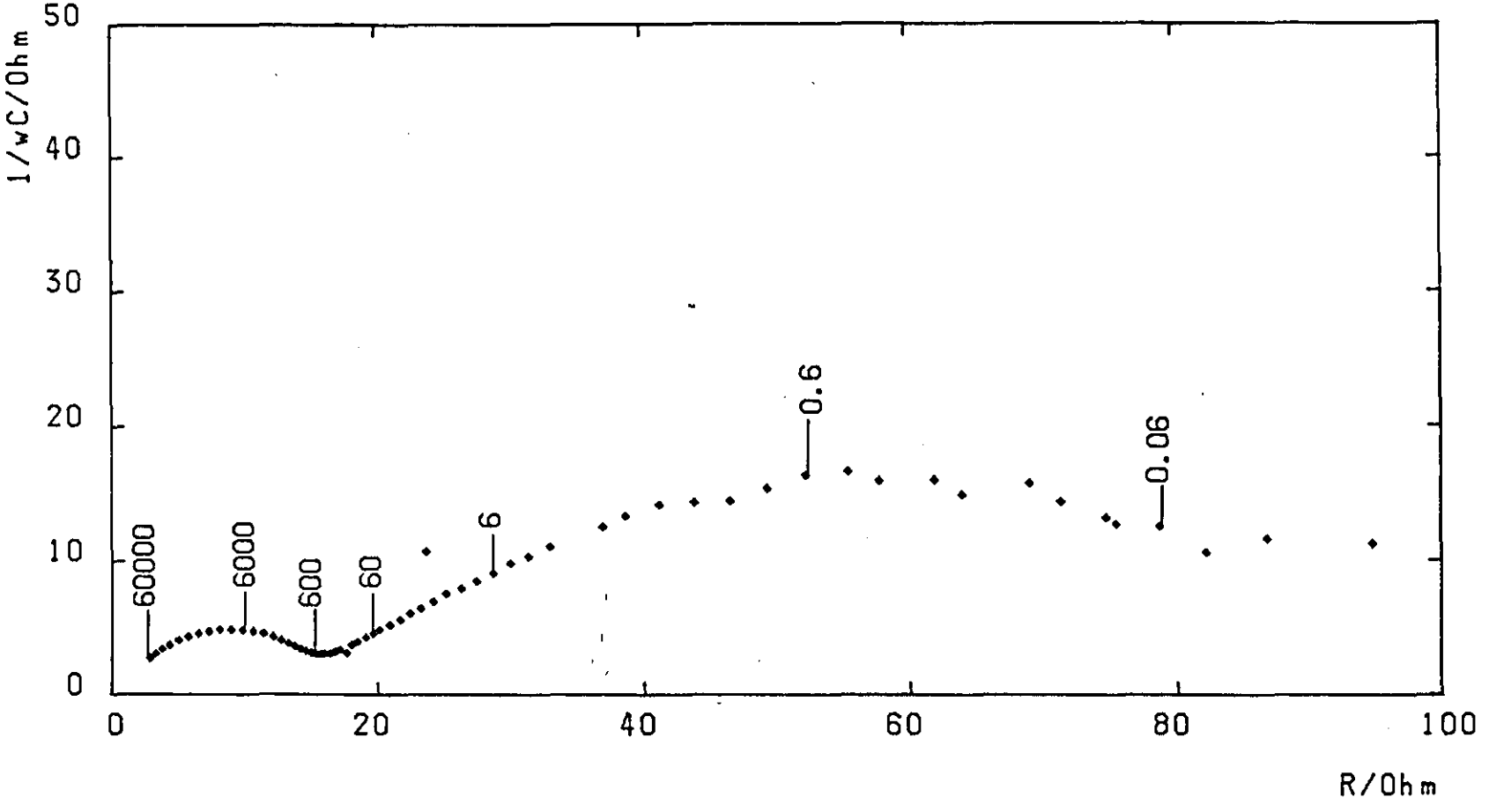

FIG 5.1 IMPEDANCE DATA FOR A LITHIUM ELECTRODE IN 1.8M $LiAlCl_4 + SOCl_2$. NUMBERS ARE FREQUENCIES (IN Hz). IMMEDIATELY AFTER CELL ASSEMBLEY.

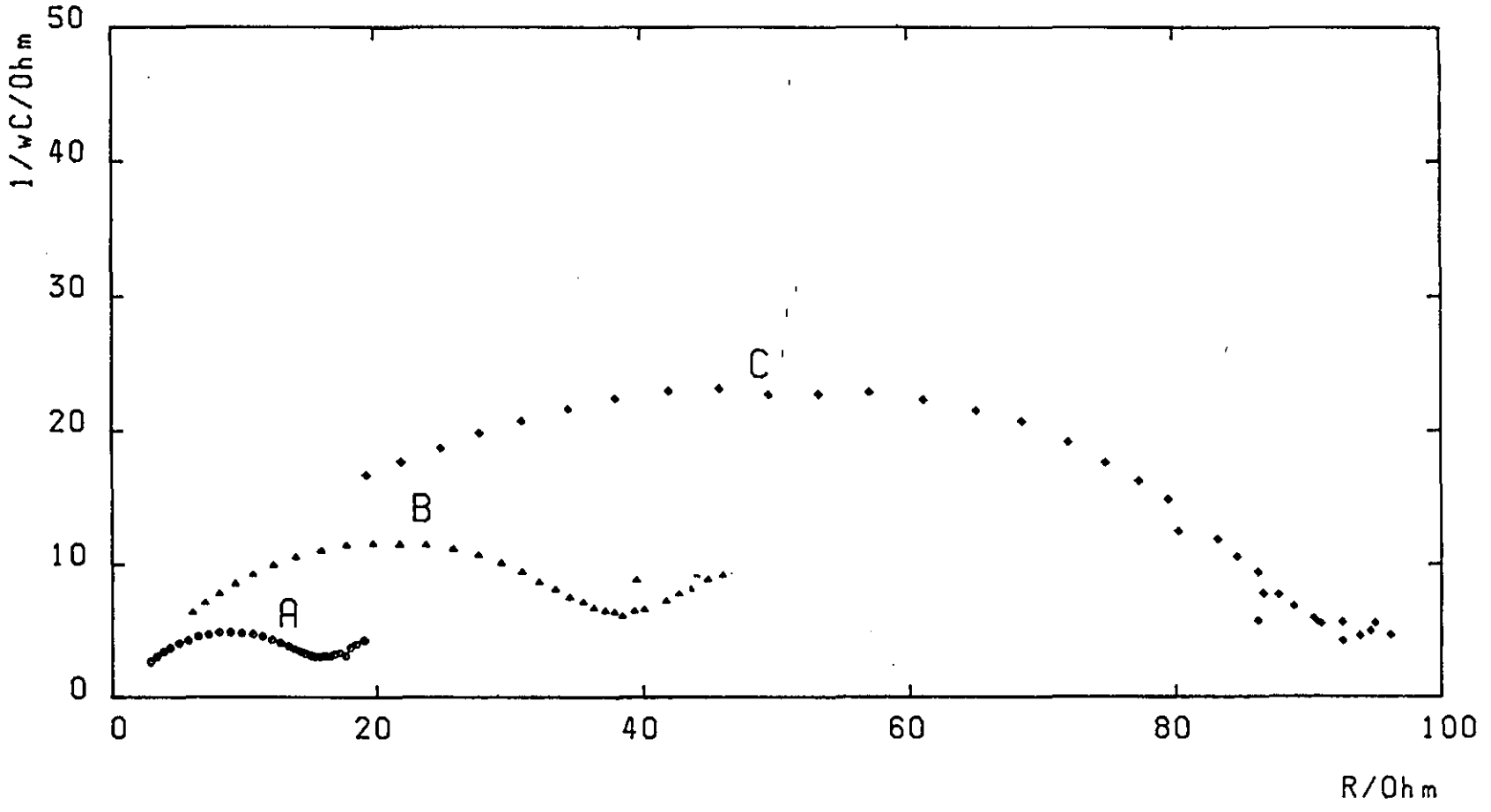

FIG 5.2 IMPEDANCE LOCI AFTER VARIOUS ELECTROLYTE CONTACT TIMES. (A) FRESHLY MADE ELECTRODE; (B) AFTER 50 HOURS CONTACT BETWEEN ELECTRODE AND ELECTROLYTE; (C) AFTER 7 DAYS ELECTRODE/ELECTROLYTE CONTACT.

the cell impedance have been observed previously for electrodes stored in $SOCl_2$[43, 168] and SO_2Cl_2 [41] and demonstrate the generally ascribed development of a LiCl film on the Li electrode. The present impedance data support this for it is clear that the surface is covered by a film which immediately forms, and continuously thickens. Under these conditions it is not possible to obtain impedance values characteristic of the clean lithium surface. It was decided that the most satisfactory procedure would be to estimate the impedance as rapidly as possible. This would enable a series of measurements to be carried out on a cell for which the effect of the variation of the impedance with time could be neglected since it would be small. The frequency range was therefore restricted to a limit sufficient to enable us to obtain the desired kinetic data.

In the initial stages the impedance was observed to approximately double every 24 h. The experiments were made in ∿40 min. so that the developing film on the anode is not much affected in this time span. Furthermore, the experimental procedural time from the initial electrode/electrolyte contact (∿1 h) itself would not significantly modify the impedance data in comparison with that arising from the effects of the applied potential and the general uncertainty (±10%) always associated with a polycrystalline solid metal electrode.

This procedure is the best identified in order to obtain impedance data characteristic of the system. The use of fully aged electrodes yields heavily filmed systems of relatively high impedance and consequential increased uncertainty of accurate mathematical analysis.

The elongated semicircles obtained for the impedance spectra are characteristic of a porous or rough electrode. At low frequencies the Warburg line rises initially at an angle of 25° to the real axis. This is close to the 22.5° angle expected for a porous electrode [158, 160]. We consider this to be due to the porous film on the lithium electrode which will both obscure and roughen the electrode surface. As can be seen from Figure 5.1 the Warburg line returns to the real axis at lower frequencies. This phenomenon has been encountered by Karunathilaka et al [169] in previous work involving cells in which the distance between the electrodes was small. It was considered that this behaviour was due to the effective distance between the electrodes being of the same order as $(\omega/D_i)^{\frac{1}{2}}$ at low frequencies. (D_i is the diffusion coefficient of species i, ω is the angular frequency of the perturbing signal). For this situation the Warburg, mass transport impedances are modified as follows [149]:

$$Z'_w = \sigma_i \omega^{-\frac{1}{2}} \left[\frac{\sinh (Ui) + \sin (Ui)}{\cosh (Ui) + \cos (Ui)}\right] \qquad (5.2)$$

$$Z''_w = \sigma_i \omega^{-\frac{1}{2}} \left[\frac{\sinh (Ui) - \sin (Ui)}{\cosh (Ui) + \cos (Ui)}\right] \qquad (5.3)$$

$$Ui = (2a)^{\frac{1}{2}} \left[\frac{\omega}{D_i}\right]^{\frac{1}{2}} \qquad (5.4)$$

These equations govern the return of the spectrum to the real axis. Where "a", the electrode separation is large, both equations (5.2) and (5.3) become equal to $\sigma_i \omega^{-\frac{1}{2}}$. In a well-defined situation with an electrode separation, estimated to be 0.017 cm these workers found that a return to the real axis occurred in the frequency range investigated, which is the order of the present distances involved. Using similar modelling from these results the electrode separation was calculated to be 47 μm. This was found to be a reasonable value since it is similar to the thickness of the ceramic separator paper employed in the cell arrangement. Figure 5.3 shows a computer match for the data of Figure 5.1.

It is recognised that the present experiments are complicated by the presence of a ceramic separator. It is difficult to quantify the effect of this for it introduces uncertainty regarding the effective area of the electrode due to shielding and also a media effect. The latter has been dealt with by Oldham and Tapol [170] who showed that the effect simply adds a constant multiplier to the electrode response function. The former complication is impossible to predict in the absence of any theory for it. The effect of the separator presence was therefore tested for by repeating measurements in the absence of a separator. These experiments were difficult to set up, however, similar impedance spectra were obtained for cells which did not involve ceramic separator paper between between the electrodes (Fig. 5.4). It was concluded that the use of a separator did not influence the electrode response in our high frequency domain extending down to 10 Hz.

The presence of LiCl on the front of the electrode is a further complicating factor which would be expected to reduce the Warburg slope from the ideal value of 45°. The film is non-blocking, our electrometric results confirming characteristics reported by others [34]. Under these conditions the electrode is free of films. This confirms the explanation that the shape of the impedance locus in

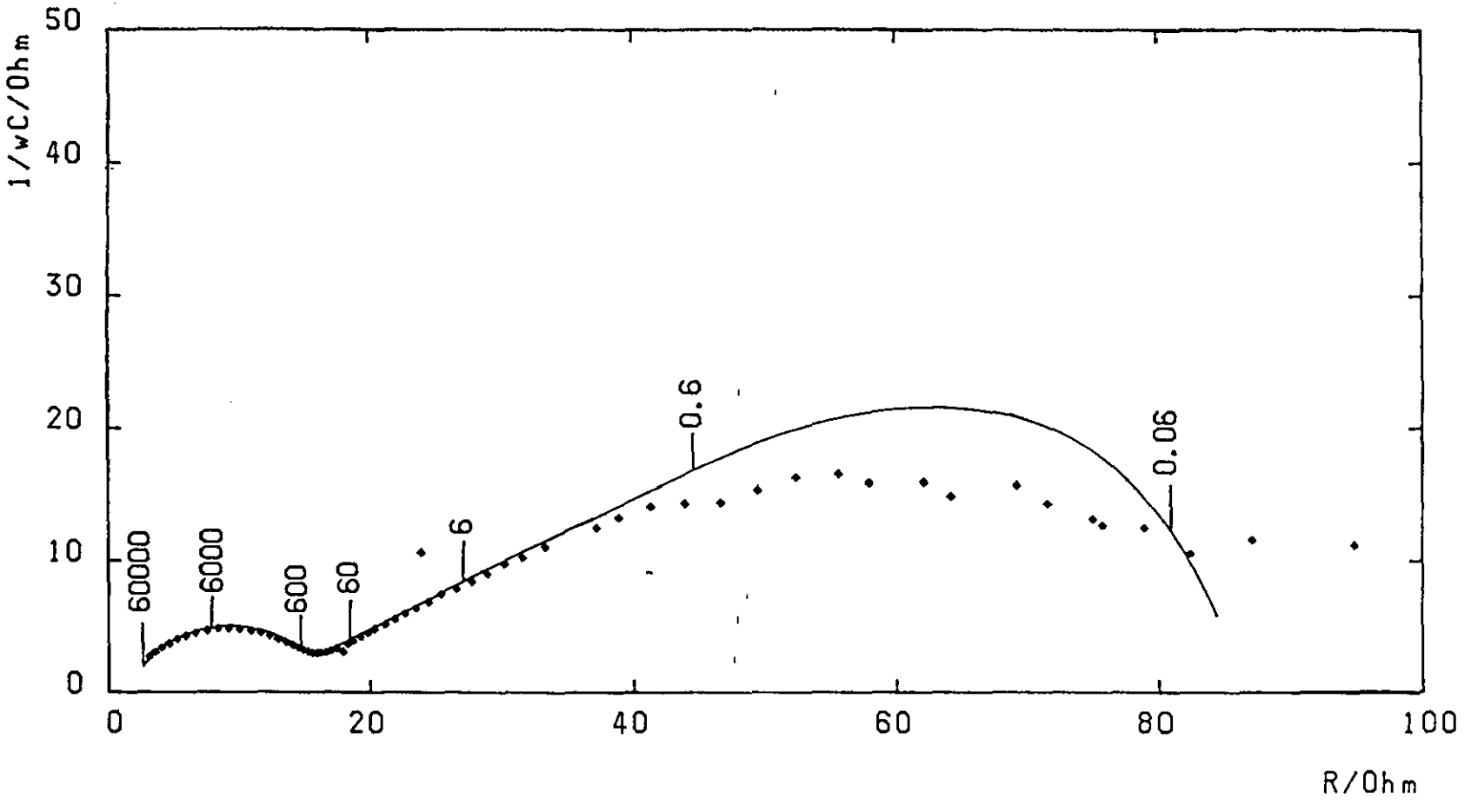

FIG 5.3 IMPEDANCE DATA WITH COMPUTER MATCH.

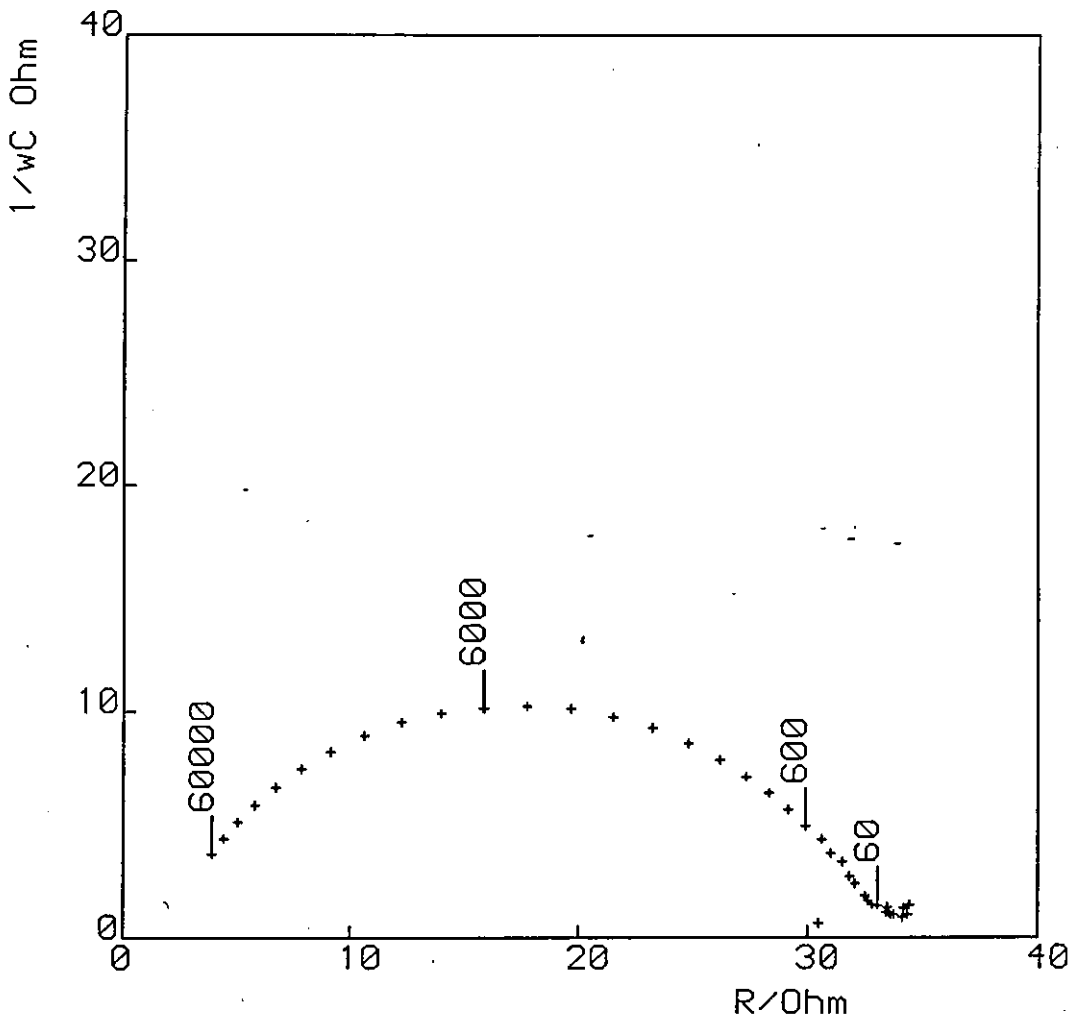

FIG 5.4 IMPEDANCE DATA FOR A LITHIUM ELECTRODE IN A CELL WITHOUT THE PRESENCE OF A SEPARATOR. OTHERWISE CONDITIONS ARE AS BEFORE.

neutral electrolyte is due to a porous film on the electrode.

The effects of polarizing the working electrode are shown in Figure 5.5 which are impedance spectra for cells at various over-potentials with respect to unpolarized Li. These are characteristic of the spectra obtained from cells throughout the whole potential range investigated. The shapes of the loci are generally unchanged indicating that the potential does not engender a change in electrode process. The impedance was clearly seen to vary with potential.

Application of a positive potential between the working and counter electrodes causes dissolution of the lithium working electrode according to equation (5.1). Negative potentials cause the reverse reaction to take place, lithium ions from the solution being deposited on to the working electrode, and also tend to reductively remove the protective layer.

The model which best represented the experimental data was that of a simple charge transfer and solution diffusion [151, 171] with a modification for electrode roughness (porosity). This model was used to match the experimental data and was found to be adequate for evaluation of impedance parameters, i.e. θ, the charge transfer resistance, R_s the solution resistance, σ the Warburg coefficient and C_{dl} the double layer capacity. The results of all these evaluations are displayed in Table 5.1. Figure 5.6 shows the matched curve for impedance data as a potential of +25 mV is applied. This is typical of all the matches. It may be possible to improve the match slightly by inclusion of an additional capacitance term allowing for the influence of the film on the electrode surface.

The relationship between E and $\ln R_D$* for a simple charge-transfer (anodic) reaction is:

$$(\partial E/\ln R_D) = -(RT/nF)(1-\alpha)^{-1} \qquad (5.5)$$

Thus a plot of applied potential versus log θ should yield a slope of $59/(1-\alpha)$mV in the manner of a Tafel plot, at 298 k.

It was noted that the double layer capacitance, C_{dl}, varied with applied potential. This was taken as an indication of the way in which the surface area of the electrode varied. With increasing positive

---

*Footnote

R_D and θ become identical for an unfilmed electrode.

Table 5.1 Impedance Data

Applied Potential/mV	Rs/Ω	θ/100Ω	$C_{dl} \times 10^6/Fcm^{-2}$	$\sigma/100\Omega s^{-1}$
0.0	1.11	13.22	0.98	32.29
1.0	1.00	12.65	1.00	33.46
2.0	0.99	12.20	1.01	32.81
5.0	0.84	11.53	1.02	32.85
7.5	0.96	10.84	1.06	34.06
10.0	0.89	9.84	1.09	31.72
15.0	0.82	9.24	1.14	31.38
25.0	0.80	7.29	1.23	22.78
35.0	0.81	5.16	1.41	13.60
50.0	0.88	3.09	1.76	7.67
65.0	1.42	1.84	2.40	3.72
80.0	1.61	1.22	3.00	2.17
0.0	0.44	1.96	4.48	23.41
-1.0	0.33	2.12	4.42	26.89
-2.0	0.55	2.22	4.28	22.37
-3.0	0.31	2.30	4.14	24.79
-4.0	0.33	2.41	3.82	27.18
-5.0	0.21	2.46	3.95	27.61
-7.5	0.29	2.53	3.89	25.06
-10.0	0.01	2.54	4.02	27.72
-12.5	0.11	2.61	3.70	28.22
-15.0	0.10	2.69	3.60	28.99
-20.0	0.10	2.53	3.43	27.19
-25.0	0.02	2.49	3.47	23.02
-35.0	0.06	1.82	3.72	15.52
-50.0	0.13	1.21	4.28	7.21

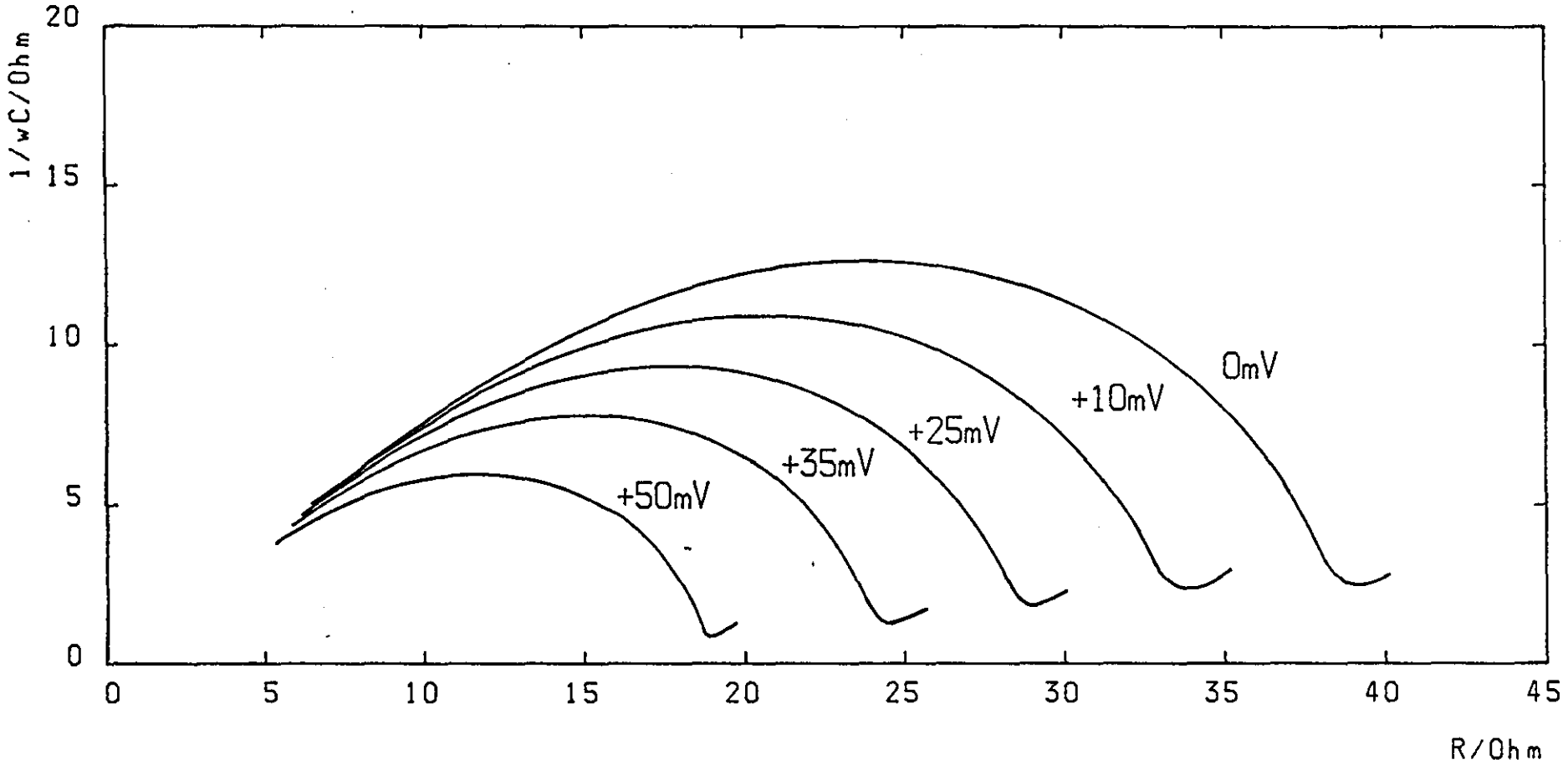

FIG 5.5 IMPEDANCE SPECTRA FOR A LITHIUM ELECTRODE WITH IMPOSED DC POLARIZATIONS. HIGH FREQUENCIES ONLY EXAMINED. THE COMPUTER FITS ONLY ARE DISPLAYED.

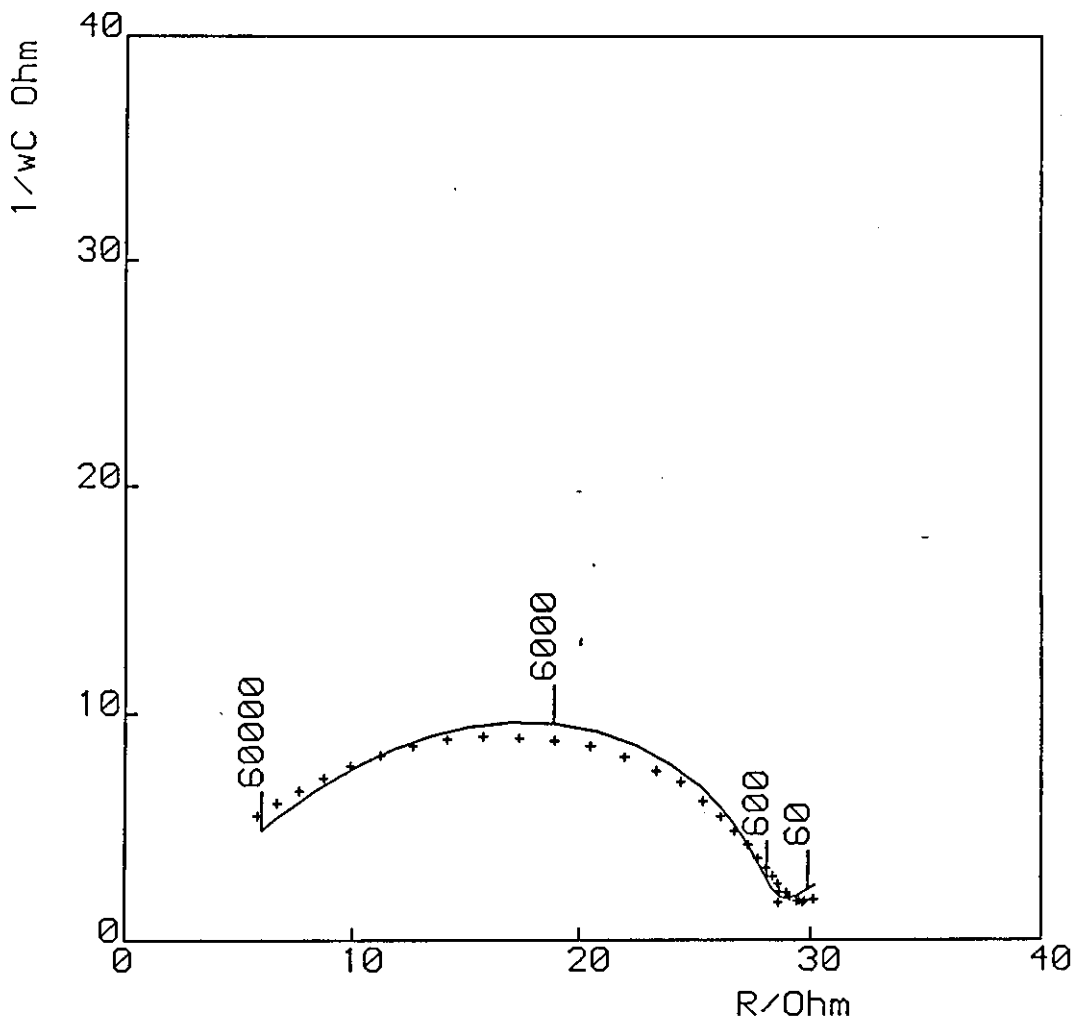

FIG 5.6 IMPEDANCE SPECTRUM FOR A LITHIUM ELECTRODE. WITH +25mV APPLIED DC POLARIZATION. DIAGRAM SHOWS A TYPICAL COMPUTER MATCH FOR THE DATA.

potential C_{dl} increased (Table 5.1). This was thought to be indicative of the surface film being disrupted, exposing more of the electrode. Secondly, lithium dissolution could cause 'pits' to form on the electrode surface, with a consequential increase in the surface area.

It is desirable to correct the value of θ for the area of lithium reacting and it was considered that a plot of log θ C_{dl} versus applied potential would lead to a more accurate estimation of kinetic parameters. This represents a relationship corrected for the development of an intruding film, assuming that the electrode double layer capacitance reflects the electroactive electrode surface. This relationship is shown in Figure 5.7.

For anodic overpotentials the area corrected log θ versus potential relationship (Fig. 5.7) yielded a slope of 143 mV/decade, indicating a charge-transfer coefficient of 0.59.

The exchange current at zero potential was estimated to be 0.0198 mA (0.48 mA cm^{-2}). Since it is not possible under practical conditions to obtain a value of i_o uncomplicated by the intrusion of LiCl, this value represents the best estimate under cell conditions. A value of k°, the standard rate constant was not determined since it is very difficult to obtain a meaningful figure which can be compared with other systems.

Such an analysis of the data for polarization in the negative region proved impossible due to the non-linearity of the log θ versus potential relationship. It appears that there exists a barrier to the dissolution reaction since a rise in θ was expected as increasing negative potentials were applied, due to a decrease in the concentration of Li^+ ions, the oxidised species at the electrode. However, the effect of the negative potential in reducing the barrier layer of LiCl must also be taken into account. At the lower over-potentials the direction of change in θ is as expected, at high over-potentials when LiCl is removed by reduction from the surface this is reversed.

The area-corrected relationship between σ and applied potential is shown in Figure 5.8. The expected straight line with a slope of 2.303 RT/nF of 60 mV for a single species is drawn on the curve. This indicates that Li^+ ions are in equilibrium with the electrode in the voltage domain between about 20 mV and 60 mV. Here the reaction is sufficiently fast to be considered reversible enough to justify the kinetic argument used [172].

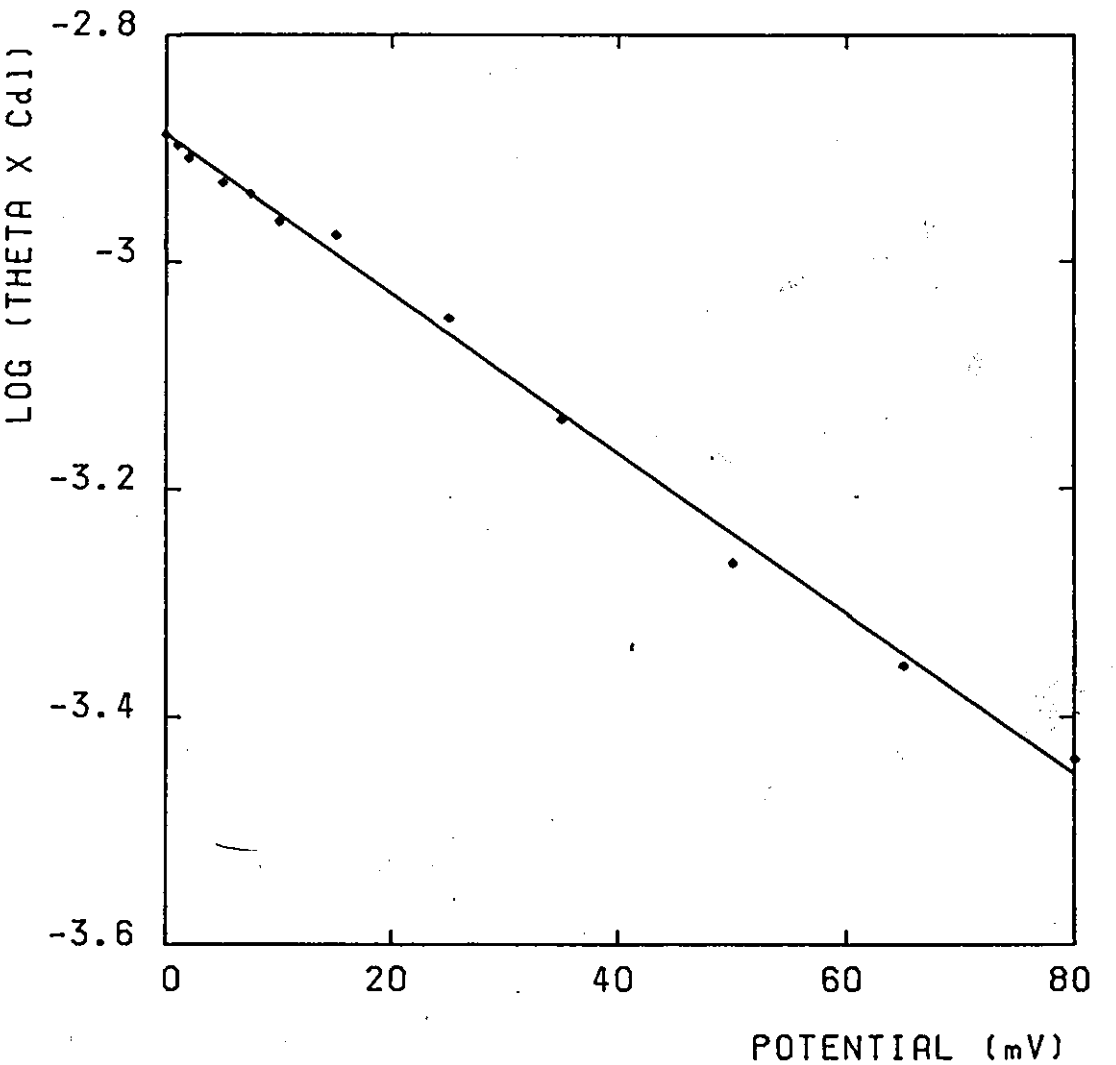

FIG 5.7 GRAPH SHOWING LOG(θCdl) VS. APPLIED POTENTIAL FOR INCREASING POSITIVE POTENTIALS.

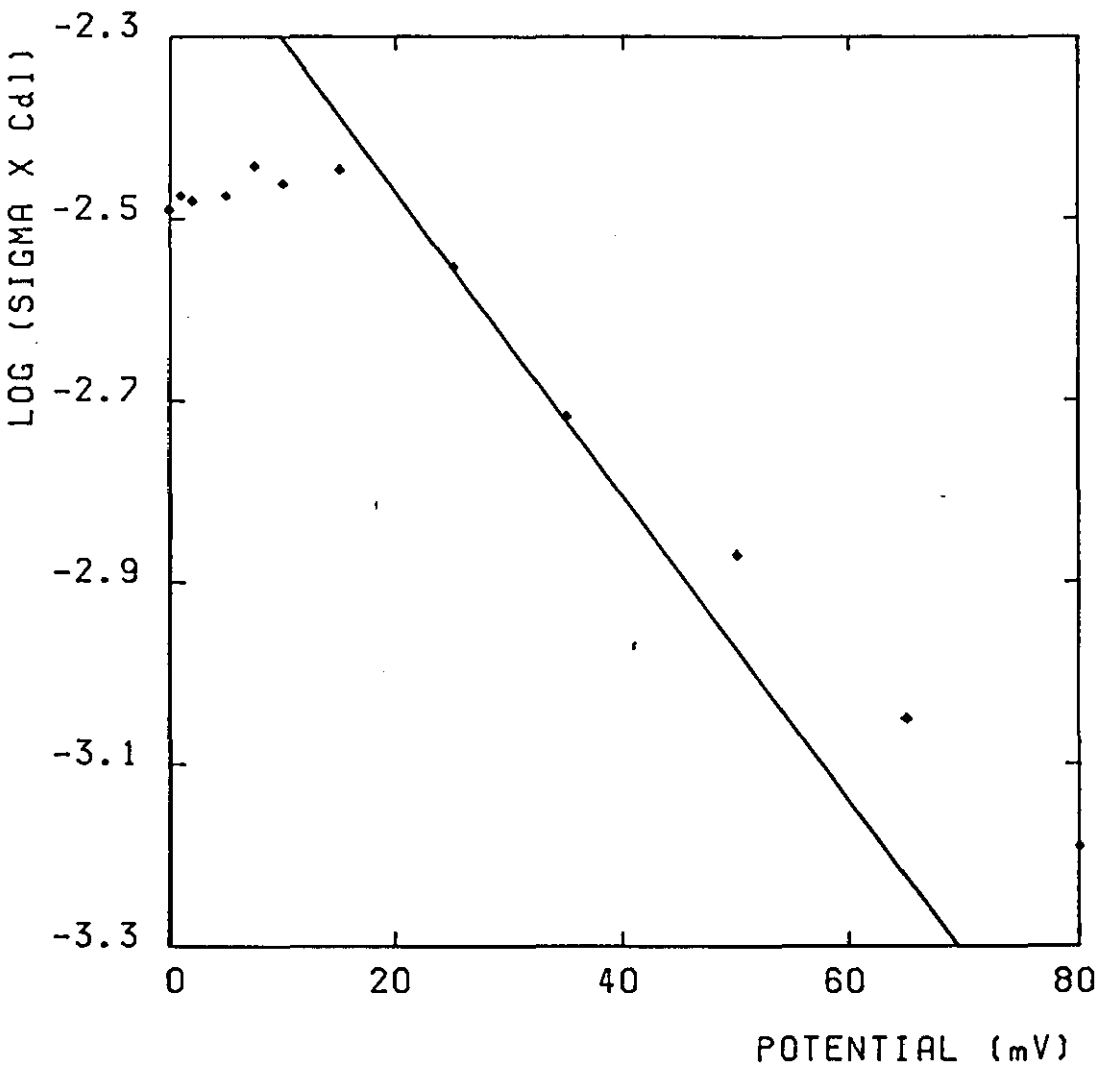

FIG 5.8 GRAPH SHOWING LOG(σCdl) VS. APPLIED POTENTIAL FOR INCREASING POSITIVE POTENTIALS.

At potentials more than ~70 mV it appears that the reaction has been driven too fast for the mass transport processes to maintain the system in a quasi-reversible condition. At the lower overpotentials it is clear that some intrusion of the nucleating LiCl film may be affecting the electrode area, so that at more negative potentials an effectively higher electrode "diffusing area" is observed. This occurs despite area adjustment using the double layer capacitance. It should be emphasised in this connection that the important points in the extraction of θ from the raw data come overwhelmingly from the high frequency region which reflects the true area of the electrode. On the other hand the low frequency points which reflect the diffusing area of the electrode are dominant in the extraction of the Warburg slope.

It must also be borne in mind that in these experiments with a limited Warburg region, the log σ plots involve a much greater uncertainty than the log θ plot.

The value of α obtained in this work is to be compared with those of Hughes et al [165] for Li in $SO_2(CH_3CN)$. These workers obtained a value of 0.37 for α by investigating the change in θ with concentration. It is difficult to compare these values in view of the lack of information regarding the amounts of stabilisation which the Li^+ has in the two solutions. However, α might be expected to be greater for the $SOCl_2$ system than the SO_2-CH_3CN system in view of the superior ionising character of the former. Exchange current densities are similar for each system, Hughes et al [165] obtaining a value of 0.7 mA cm^{-2}.

This value of i_o is only about 1% of that for zinc in KOH and LiOH [173]. This is in keeping with the relatively high overpotentials (up to 1 volt) noticed when Li-$SOCl_2$ cells are discharged at high rates, and accounts, in part, for the high temperatures obtained. It may well transpire that a significant contribution to this polarization (and low value for the apparent i_o) is due to the film.

The results clearly indicate that this film breaks down on passing anodic current across the lithium, and in practice this would explain initially rising voltage time discharge transients from Li-$SOCl_2$ cells. Voltage delay at room temperature, due to the LiCl film is only minor, although it is more noticable at high temperature [32].

5.4 Conclusions

(1) The Li^+/Li exchange in $SOCl_2$ is a charge transfer process followed by diffusion.

(2) The lithium electrode is progressively blocked by a film of LiCl.

(3) The charge transfer coefficient and exchange current are 0.59 and 0.48 mA cm^{-2} in 1.8 M $LiAlCl_4$ respectively.

CHAPTER 6

THE IMPEDANCE OF THE Li^+/Li ELECTRODE IN $SOCl_2$:

II IN ACID ELECTROLYTE

6.1 Introduction

This study represents a continuation of the work from the previous chapter. The results from Chapter 5 amongst other things confirm the existence of a thick, porous film on the lithium electrode surface which gives rise to impedance behaviour normally characteristic of severely roughened or porous electrodes. Although this film gives lithium a high stability in $SOCl_2$ solutions and other solvents [32-34], it is also the cause of voltage delay in the Li-$SOCl_2$ system. Attempts have been made to reduce the extent of filming on the anode, these include addition of sulphur dioxide to the electrolyte [51] and alternative electrolyte salts [56].

Free Lewis acid in the electrolyte as $AlCl_3$ would be expected to reduce the extent of the LiCl anode film. However use of such an electrolyte is restricted to reserve cells, where the electrolyte is only admitted to the electrode stack as power is required. This is to prevent anode corrosion which would otherwise occur when such an electrolyte is used, thus the use of free Lewis acid electrolyte is not a viable solution to the voltage delay problem. However it was considered of interest to study the anodic process for a lithium electrode in such an electrolyte, in order to contrast with the behaviour in neutral electrolyte.

6.2 Experimental

The experimental procedure is as described in the previous chapter, the electrochemical cell containing only lithium electrodes. The electrolyte solutions used contained an excess of $AlCl_3$, most of the work employed 3.0 M $AlCl_3$. Other electrolytes used were 1.0M $LiAlCl_4$ + 0.8M $AlCl_3$ and 0.5M $LiAlCl_4$ + 2.5M $AlCl_3$.

6.3 Results and Discussion

Figure 6.1 shows a typical impedance spectrum for a lithium electrode in a cell containing a 3.0M $AlCl_3$-$SOCl_2$ electrolyte solution. In contrast to results in 1.8M $LiAlCl_4$ + $SOCl_2$, the impedance spectrum consists of a near-perfect semicircle, which is characteristic of loci from smooth electrode surfaces. The likelihood therefore is that the porous LiCl film which previously roughened the electrode is not present to such an extent. This is reflected in the values obtained for the apparent double layer capacitance, after matching the experimental data with a Randles circuit model. In this instance values of about $10^{-4}F/cm^2$ were obtained, whereas previously for neutral electrolyte $10^{-6}F/cm^2$ was more usual. This confirms a much greater effective surface area for the electrode in acid electrolyte, which is to be expected for a less filmed surface.

It is likely that the apparent second semicircle is due to a Warburg diffusion line which rises initially at an angle close to 45° and then returns to the real axis at low frequency. A similar effect was observed previously with neutral electrolyte and attributed to the small inter electrode distance. The solid line on figure 6.1 shows a computer match for the data using a simple charge-transfer and solution diffusion model with adaption for this low frequency behaviour. The electrode separation was calculated from this data and yielded a similar value to that previously obtained (Chapter 5).

At this stage it is interesting to look at an impedance spectrum for a Li^+/Li electrode in $SOCl_2$ containing no added electrolyte, Figure 6.2 shows such a plot. The origin of the semicircle in this diagram is shunted a considerable distance from the origin of the complex-plane. From this a value for R_s the solution resistance of about 200Ω is yielded. This is much greater than for systems containing added electrolyte and is a result of the very low conductivity of thionyl chloride. The diameter of the semicircle is similarly large, with a likely low exchange current at the surface. The semicircle is greatly flattened, indicating the presence of a LiCl film on the electrode, but the Warburg line rises at an angle of 45°. This angle is as expected for a diffusion controlled process at a smooth electrode. Thus the cell behaviour can not be modelled using a simple Randles circuit. It may be that the film on the electrode surface is different under these conditions. There is no apparent return to the real axis of the Warburg tail in Figure 6.2, this suggests that $(\omega/D_i)^{\frac{1}{2}}$ will remain large in comparison with the low frequencies, since the diffusion coefficient in pure $SOCl_2$ is expected to be very low.

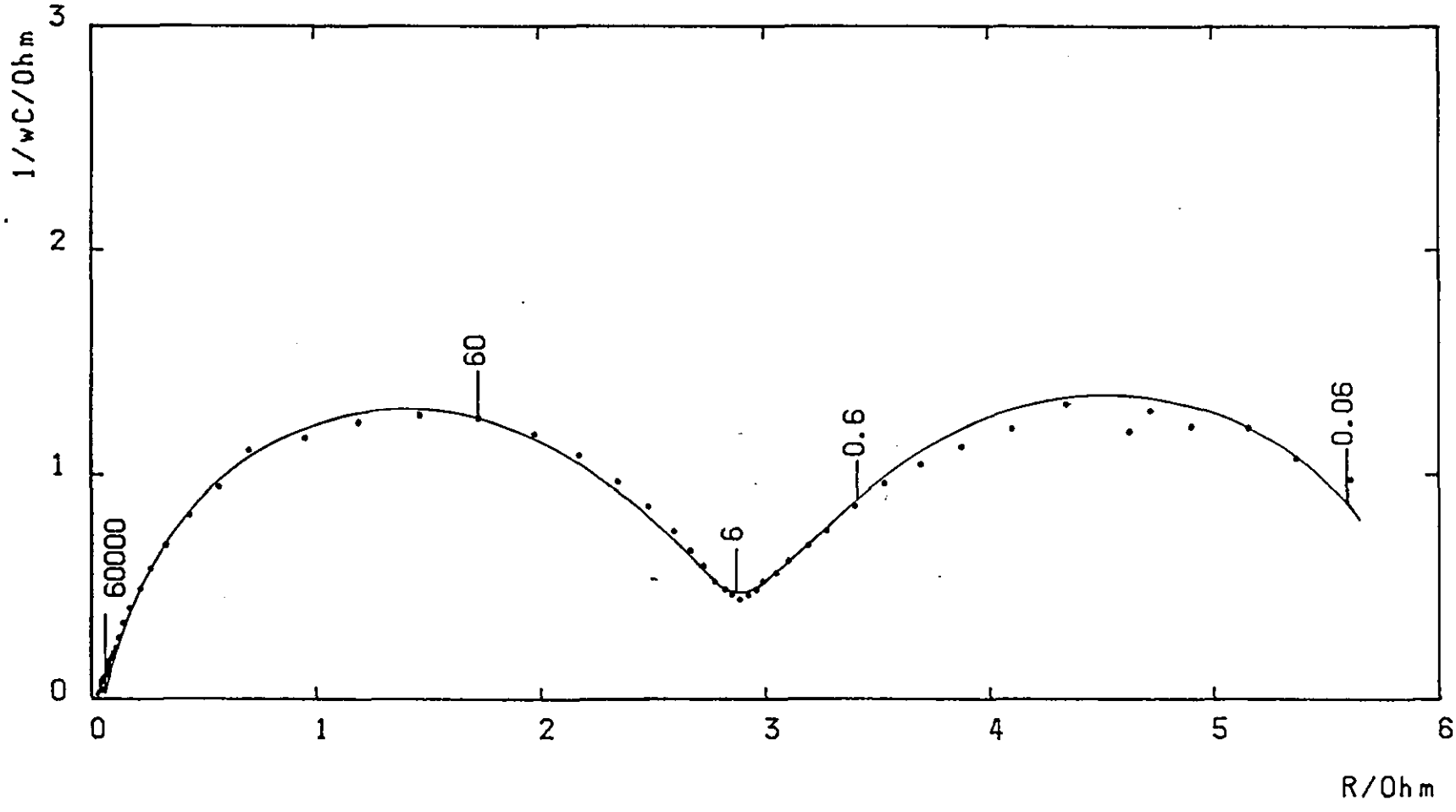

FIG 6.1 IMPEDANCE DATA FOR A LITHIUM ELECTRODE IN 3.0M $AlCl_3$+$SOCl_2$. THE SOLID LINE REPRESENTS A COMPUTER MATCH FOR THE DATA.

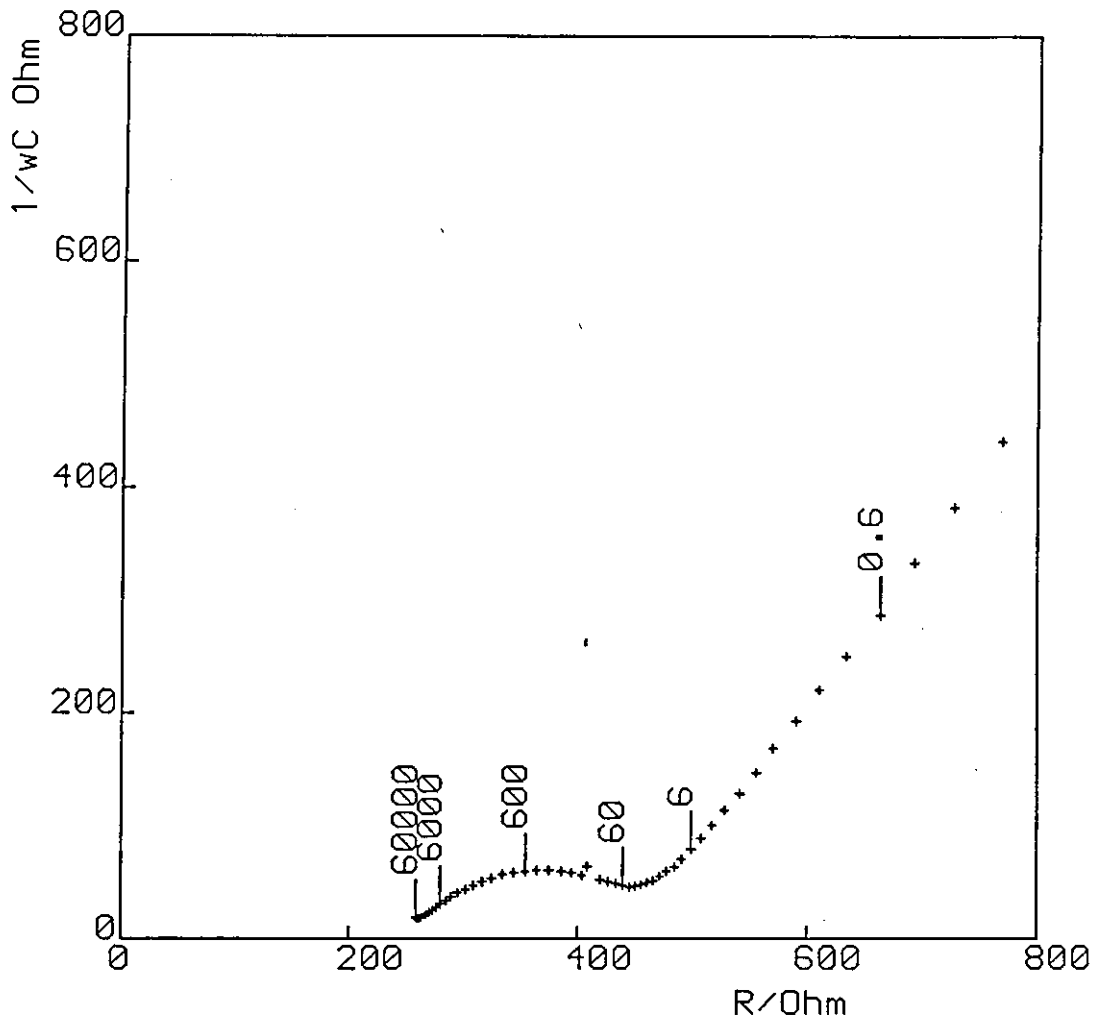

FIG 6.2 IMPEDANCE SPECTRUM FOR A LITHIUM ELECTRODE IN $SOCl_2$ WITH NO ADDED ELECTROLYTE.

Some of the spectra resulting from polarization of the working electrode are shown in Figure 6.3. As positive potentials are applied to the working electrode there is a decrease in the magnitude of the impedance. Table 6.1 shows the results obtained from matching the experimental data to the impedance parameters of the equivalent circuit. The semicircles could all be modelled to a simple Randles circuit, although for some experiments the analogue needed to be slightly modified to allow for the effect of adsorbed species on the electrode, which slightly altered the behaviour of the Warburg tail.

The values obtained for θ, the charge-transfer resistance, are much lower than for the corresponding ones obtained in neutral electrolyte, even after making allowance for experimental error. From the value of θ at zero potential, the exchange current (i_o) was calculated to be 45 mA/cm^2, which is almost one hundred times greater than the value in neutral electrolyte. This value of i_o is therefore likely to be characteristic of a clean lithium surface and is more in keeping with known battery performance.

Under these conditions the variation of double layer capacitance with potential is small, indicating that the effective surface area of the electrode remains fairly constant throughout the experiment.

Figure 6.4 shows the variation of log θC_{dl} with potential for these experiments. For applied potentials of greater than 30 mV, θ was observed to decrease with applied potential, which is expected as the rate of lithium dissolution at the working electrode increases. At low overpotentials however it would appear that there is not sufficient driving force for the reaction to raise the concentration of lithium ions at the electrode surface by a significant amount. It must be borne in mind that the results from this work are likely to be impaired by corrosion of the lithium electrodes according to the following reaction:

$$4Li + 4AlCl_3 + 2SOCl_2 \rightarrow 4LiAlCl_4 + SO_2 + S \qquad (6.2)$$

Corrosion effects were minimised as much as possible by restricting the frequency range in order that measurements could be made rapidly and in quick succession. The slope of the graph of Figure 6.4 is 107 mV/decade, from which a value of α, the charge transfer coefficient of 0.45 was calculated. This was lower than the corresponding value of 0.59 obtained in neutral electrolyte. This value of α is closer to other values obtained for this reaction (0.5 or less) [44].

Table 6.1 Impedance data

Applied Potential/mV	$10^2 Rs/\Omega$	θ/Ω	$10^3 C_{dl}/Fcm^{-2}$	$\sigma/\Omega s^{-1}$
0.0	14.77	13.88	2.60	15.05
10.0	13.04	14.94	2.55	17.09
20.0	5.31	15.39	2.47	17.24
30.0	26.20	14.18	2.36	19.69
40.0	7.21	12.66	2.27	19.01
50.0	5.71	10.24	2.38	19.79
60.0	6.99	8.18	2.46	19.75
70.0	10.88	6.14	2.52	21.19
80.0	12.03	4.86	2.38	23.07
100.0	11.54	2.02	4.17	17.37

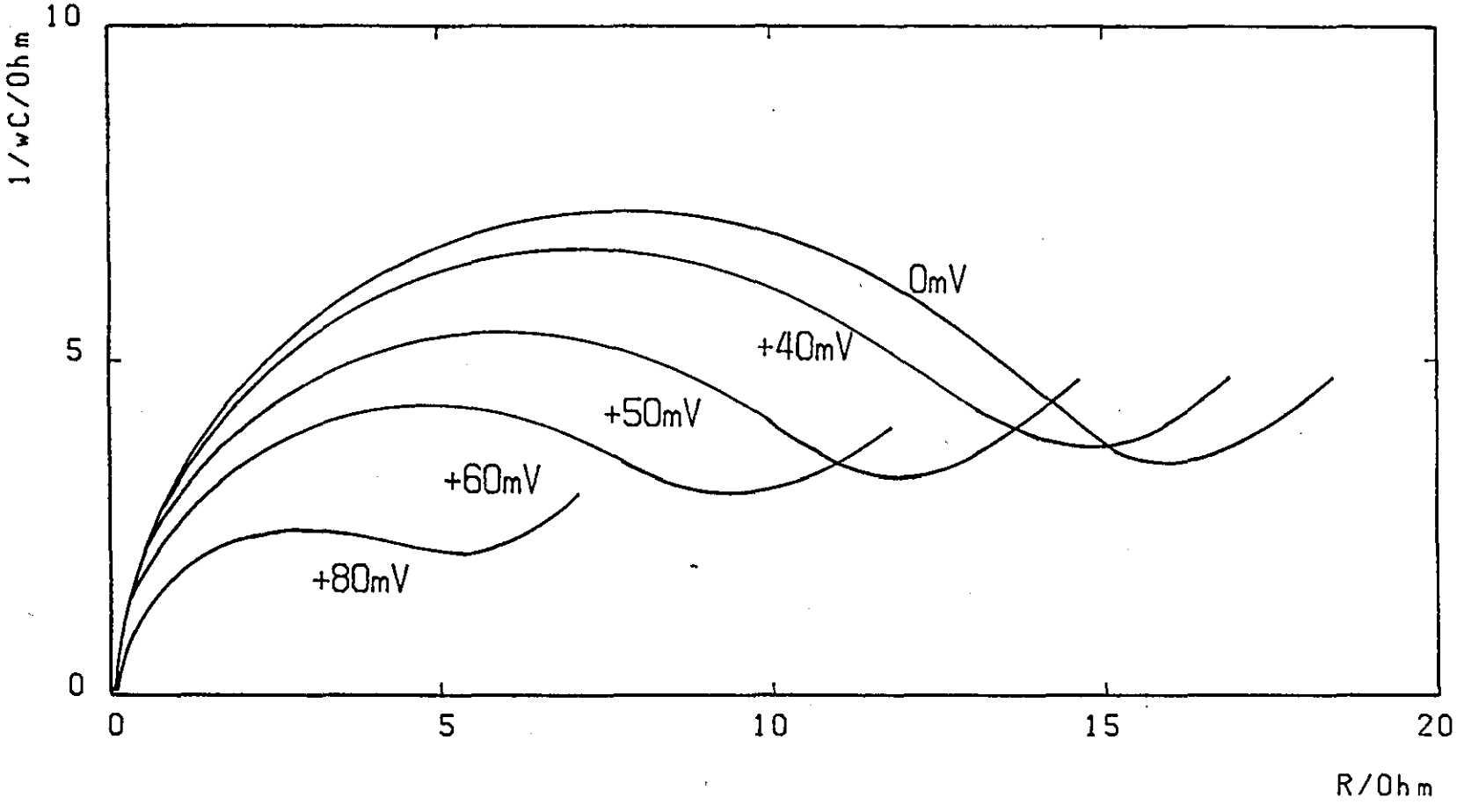

FIG 6.3 IMPEDANCE SPECTRA FOR A LITHIUM ELECTRODE WITH DC POLARIZATIONS. THE COMPUTER FITS FOR THE DATA ARE DISPLAYED.

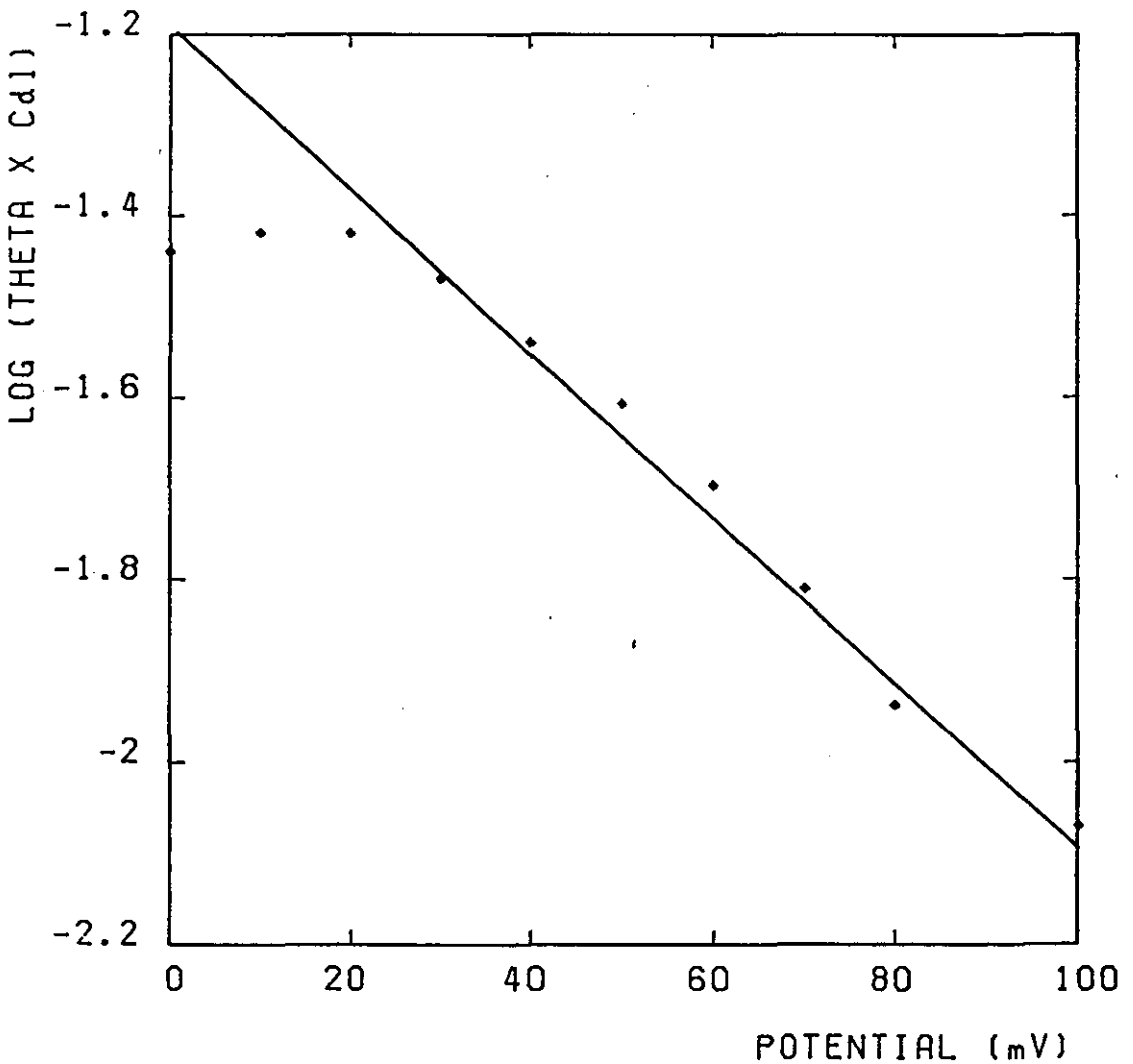

FIG 6.4 GRAPH SHOWING LOG(θCdl) VS. APPLIED POTENTIAL FOR INCREASING POSITIVE POTENTIALS.

It was decided to extend this work further by examining the Li^+/Li exchange in solutions of $LiAlCl_4$ containing an excess of free $AlCl_3$. The results could only give qualitative information about the electrode process. A typical impedance spectrum for a Li^+/Li electrode in a 1.0M $LiAlCl_4$ + 0.8M $AlCl_3$ solution is shown in Figure 6.5. Close inspection of this reveals that the semicircle is somewhat flattened indicating a partly roughened electrode surface. Although this flattening is less than for neutral 1.8M $LiAlCl_4$ electrolyte, there still clearly exists a film on the electrode surface in spite of free Lewis acid in the electrolyte. Attempts to determine impedance parameters by polarizing the working electrode as before, proved meaningless. This was because the roughness of the electrode increased continually with time throughout the experiment in such a way as to distort the kinetic data. Calculated values of the charge transfer resistance increased with time, due to the rapidly developing film. Even applied potentials of up to 100 mV were insufficient to reverse this behaviour. This was further emphasised by a decrease of the measured double layer capacitance with time. Even using 0.5M $LiAlCl_4$+ 2.5M $AlCl_3$ as the electrolyte a similar effect was noted.

It would appear that the existance of LiCl initially in the electrolyte, even as little as 0.5M in a large excess of $AlCl_3$ is sufficient to form a film which has a roughening effect on the electrode surface and whose rate of formation is greater than its removal by free $AlCl_3$.

Film formation is likely to take place according to the following discharge type reaction:

$$4Li + 2SOCl_2 \rightarrow 4LiCl + SO_2 + S \qquad (6.3)$$

Any breakdown of this film in acid electrolyte is likely to occur as follows:

$$AlCl_3 + LiCl \rightarrow LiAlCl_4 \qquad (6.4)$$

However it would appear that the corrosion rate of equation (6.1) is greater than the rate at which the LiCl film reacts with $AlCl_3$. Therefore pure $AlCl_3$ initially present in the electrolyte may suppress the formation of a noticeable film on the electrode surface, but can not prevent the growth of a film once it is established.

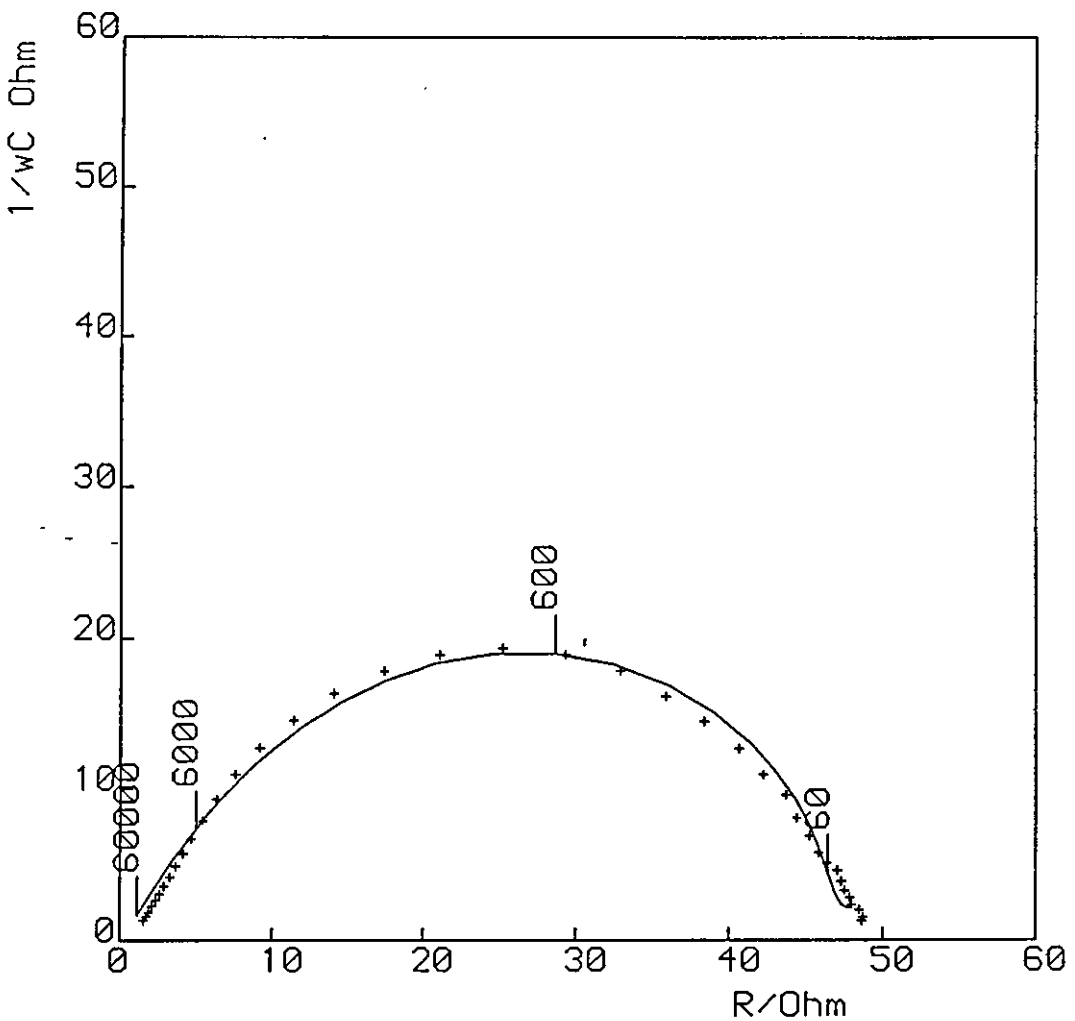

FIG 6.5 IMPEDANCE SPECTRUM OF A LITHIUM ELECTRODE IN $SOCl_2$ CONTAINING 1.0M $LiAlCl_4$ + 0.8M $AlCl_3$.

6.4 Conclusions

(1) The shapes of the impedance loci and the magnitude of determined double layer capacitance values have shown that the LiCl film in 3.0M $AlCl_3$ - $SOCl_2$ usually present on the Li electrode was insignificant.

(2) Lithium chloride initially present in the electrolyte, even with an excess of free $AlCl_3$ results in an anode film.

(3) In 3.0M $AlCl_3$ the charge transfer coefficient and exchange current density are 0.45 and 46 mA/cm^2 respectively.

CHAPTER 7

THE IMPEDANCE OF THE C-$SOCl_2$ ELECTRODE IN $SOCl_2$

7.1 Introduction

In the previous two chapters the impedance technique has been used to study the Li-$SOCl_2$ cell anode process. This chapter represents a complementary cathode study, in which the reduction and oxidation of $SOCl_2$ at a glassy carbon electrode is investigated. According to the generally accepted cell discharge reaction thionyl chloride is reduced at a cathode substrate according to the following reaction:

$$2SOCl_2 + 4e^- \rightarrow 4Cl^- + SO_2 + S \qquad (7.1)$$

The precise mechanism is thought to be rather more complex than the above equation suggests, several intermediate species are involved in the process. Many workers believe that the SO radical is an intermediate species, this has been known to form in the reaction between thionyl chloride and metals, for some time [174, 175].

The cathodic reduction mechanism is undoubtedly complicated by the presence of reaction products, particularly LiCl, which become deposited on the electrode surface. Passivating films on vitreous carbon electrodes have been shown to affect the reaction as examined by cyclic voltammetry [15, 20, 176]. The cell used for this study consisted only of carbon electrodes, in order to isolate the cathode reaction. Electrolytes used were of conventional cell composition, and the results are discussed with respect to other impedance studies on this and similar systems.

7.2 Experimental

For this work a glassy carbon disc shaped working electrode was used (area = 1.77 cm^2, Le Carbone). A porous carbon counter electrode was employed. This electrode which weighed about 50 mg was made by dry pressing a Carbon/PTFE mixture (Section 4.2.2). A reference electrode was not employed during this study since as demonstrated by Randles [151], the impedance of a large area counter electrode can be considered as negligible compared to that of the working electrode.

Although the apparent area of the counter electrode is only 2.54 cm^2, the BET surface area of Shawinigan Acetylene Black (SAB) the carbon used is 60 m^2/g. Thus even allowing for the fact that only a fraction of this BET area is electrochemically active [65, 177] the counter electrode area is still likely to be more than 100 times greater than the working electrode area. A PTFE cell was used to house the electrodes (Fig. 4.2), which were connected to test leads via a nickel gauze and a nickel stud current collector. The electrolyte solutions were 1.8M $LiAlCl_4$ and 3.0M $AlCl_3$, prepared as in Section 4.2.1. The procedures for cell assembly and impedance measurements are as outlined in Chapter 5.

7.3 Results and Discussion

Figure 7.1 shows a typical impedance spectrum for a glassy carbon electrode in a 1.8M $LiAlCl_4$-$SOCl_2$ solution, with no applied potential. It apparently consists of the beginning of a depressed semicircle and is likely to yield high values for θ, the charge transfer resistance (>1000Ω). Such slow kinetics are confirmed by cyclic voltammetry [15, 18, 20, 178] which has shown the irreversible behaviour of $SOCl_2$ reduction.

Figures 7.1 to 7.3 illustrate the way in which the impedance varies with applied negative potential. Polarization in this direction results in $SOCl_2$ reduction, which also occurs during normal cell operation. The characteristics observed on polarization in this direction, warrant a comparison with the results of Madou and Szpak [20] who carried out a similar study, but all measurements were carried out against a lithium reference electrode.

The expected regular decrease in the magnitude of the impedance with applied potential is not initially observed. The results show little change in impedance characteristics for overpotentials of between 0 and -500 mV, this is largely in agreement with the results of Madou and Szpak [20]. It is therefore likely that near the equilibrium potential some additional reduction process (or processes) takes place, which together with the reaction of equation (7.1) result in a smaller than expected value of θ. One such process has been attributed to the reduction of Cl_2, produced by $SOCl_2$ oxidation [20]. The decrease in magnitude of the impedance between -500 mV and -750 mV is then great, the semicircle becomes clearly visible at this latter overpotential. At -1000 mV the semicircle is smaller, as expected for the increased current flowing.

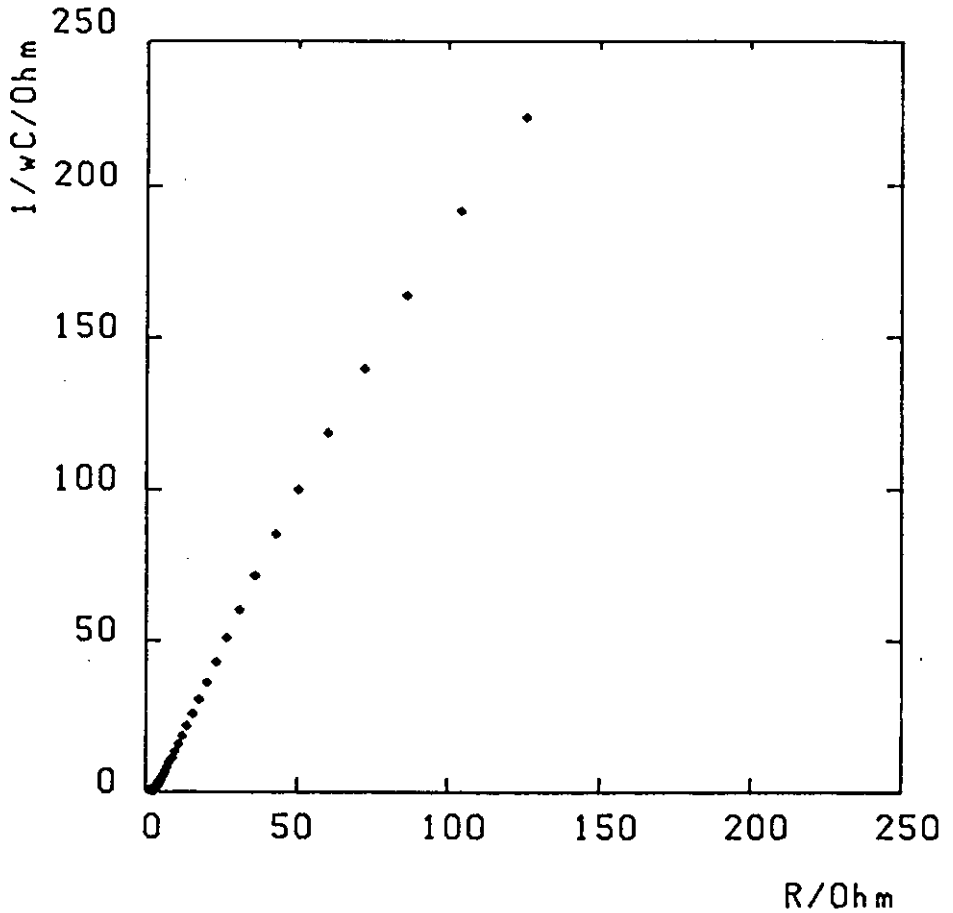

FIG 7.1 IMPEDANCE LOCUS OF A GLASSY CARBON ELECTRODE IN $SOCl_2$, NO APPLIED POTENTIAL.

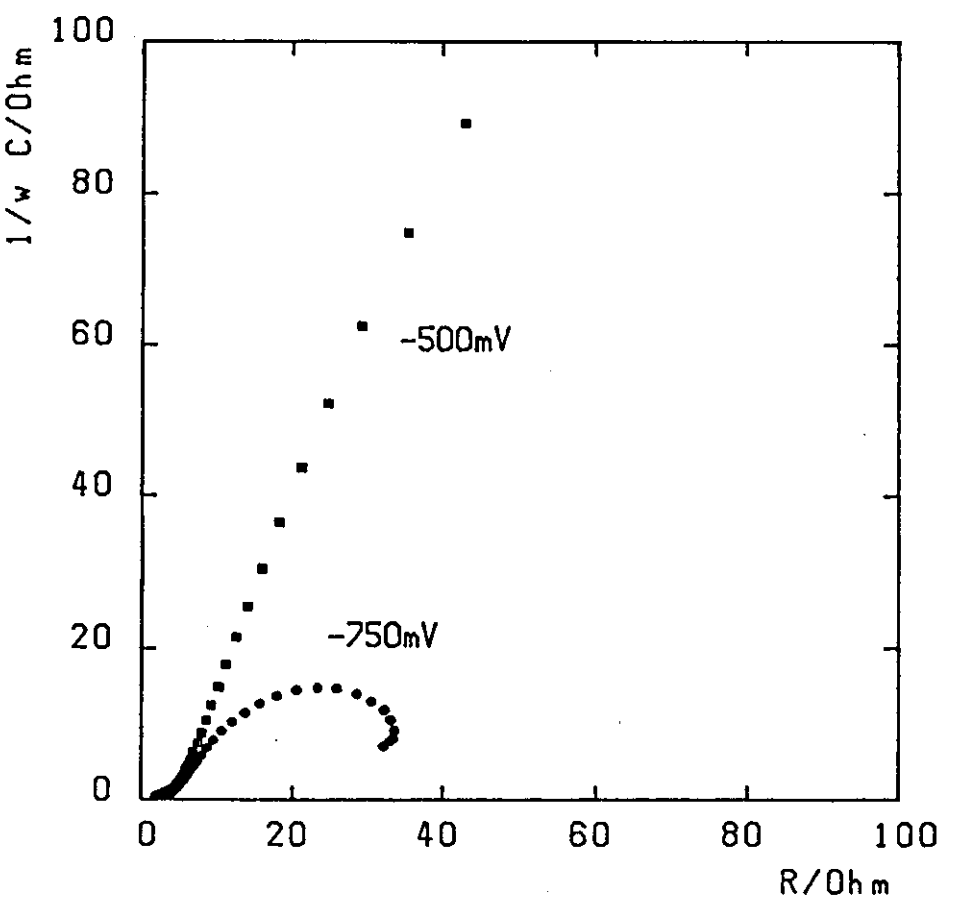

FIG 7.2 AS ABOVE, BUT APPLIED POTENTIALS OF -500mV AND -750mV.

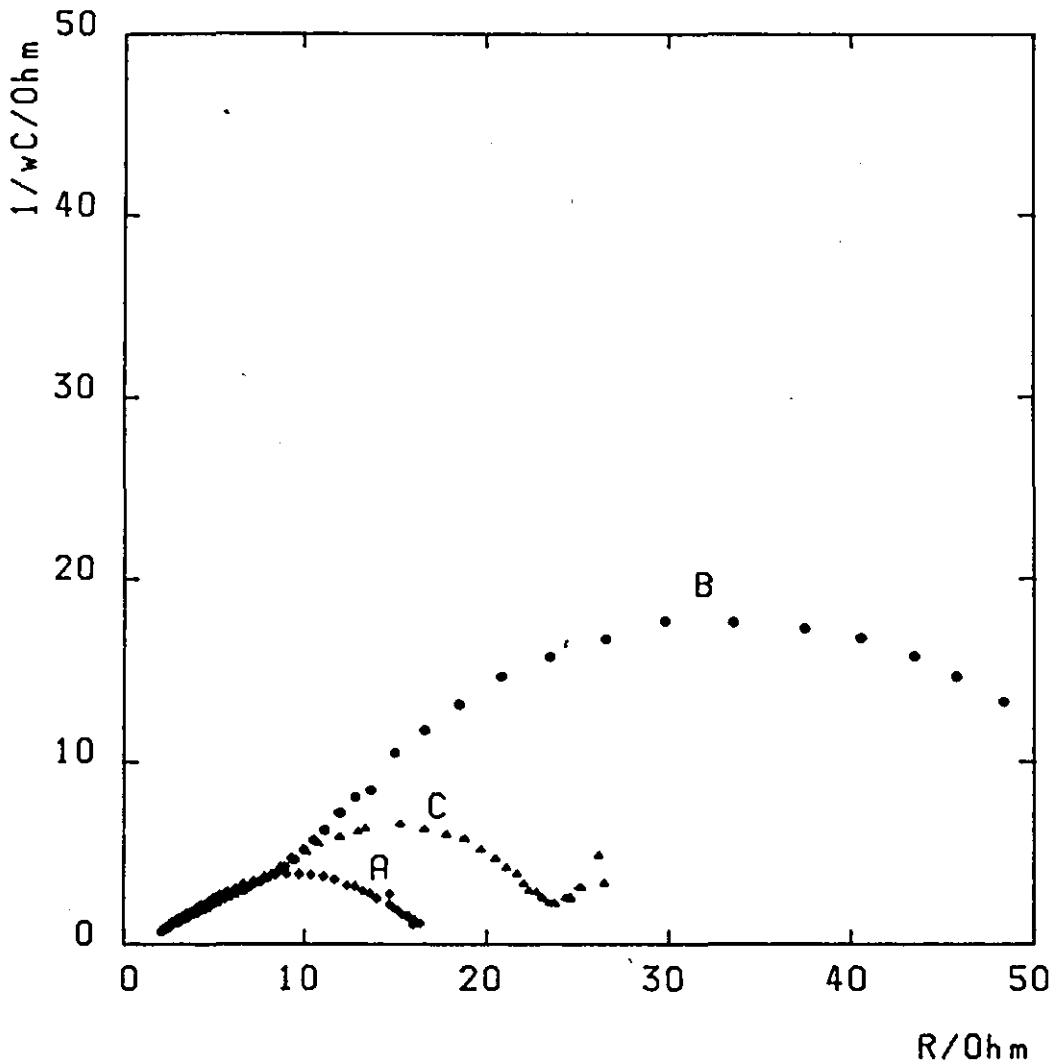

FIG 7.3 IMPEDANCE LOCI FOR A GLASSY CARBON ELECTRODE SUBJECTED TO APPLIED POTENTIALS OF: -1000mV (A), -1200mV (B), -1400mV (C).

Madou and Szpak found that for potentials less than 2.9V versus a lithium reference (i.e. increasing cathodic overpotentials beyond -800 mV), the impedance of a glassy carbon electrode increased. This they attributed to a film of insoluble reaction products on the electrode surface giving rise to a diffusion layer resistance the magnitude of which is proportional to the film thickness. The results of this work also show that a point is reached where the impedance semicircles actually increase with applied negative potential. An increase in the impedance was noted between -1000 mV and -1200 mV (Fig. 7.3). However unlike for the work of Madou and Szpak, when the cathodic potential was increased further the semicircle once again decreased in diameter. Because of the complex impedance behaviour it was decided not to extend the study too far by trying to obtain any kinetic data from the results.

This study was extended further in order to investigate the $SOCl_2$ oxidation process. This was achieved by applying positive potentials to the glassy carbon electrode (Figs. 7.4 and 7.5). For low overpotentials, unlike for the cathodic reduction process, the impedance decreased in a more regular fashion with potential. For example there was a noticeable change in the impedance characteristics between 0 and +500 mV. It is also apparent that in general the semicircles of figures 7.4 and 7.5 are about five times greater than the corresponding ones obtained for negative polarizations. This suggests that less current flows during the oxidation of $SOCl_2$ than during its reduction. Between +1000 mV and +2000 mV the impedance locus changes shape from a slightly flattened semicircle to a semicircle which is distorted at low and intermediate frequencies to a line rising at a slight angle to the real axis. The impedance at potentials between +1000 mV and +2000 mV (not displayed) shows intermediate behaviour with little change in the overall magnitude of the impedance. This suggests that species taking part in the oxidation of $SOCl_2$ are to a certain extent becoming adsorbed on the electrode.

According to Behl [179] the electrochemical oxidation of $SOCl_2$ in $LiAlCl_4$-$SOCl_2$ solutions is represented as follows:

$$2SOCl_2 + 2AlCl_4^- \rightarrow 2SOCl^+AlCl_4^- + Cl_2 + 2e^- \qquad (7.2)$$

This is in agreement with early work by Spandau [7]. Abraham and Mank [180] suggested that the oxidation of $SOCl_2$ was a two stage process, they also proposed a number of additional reactions which

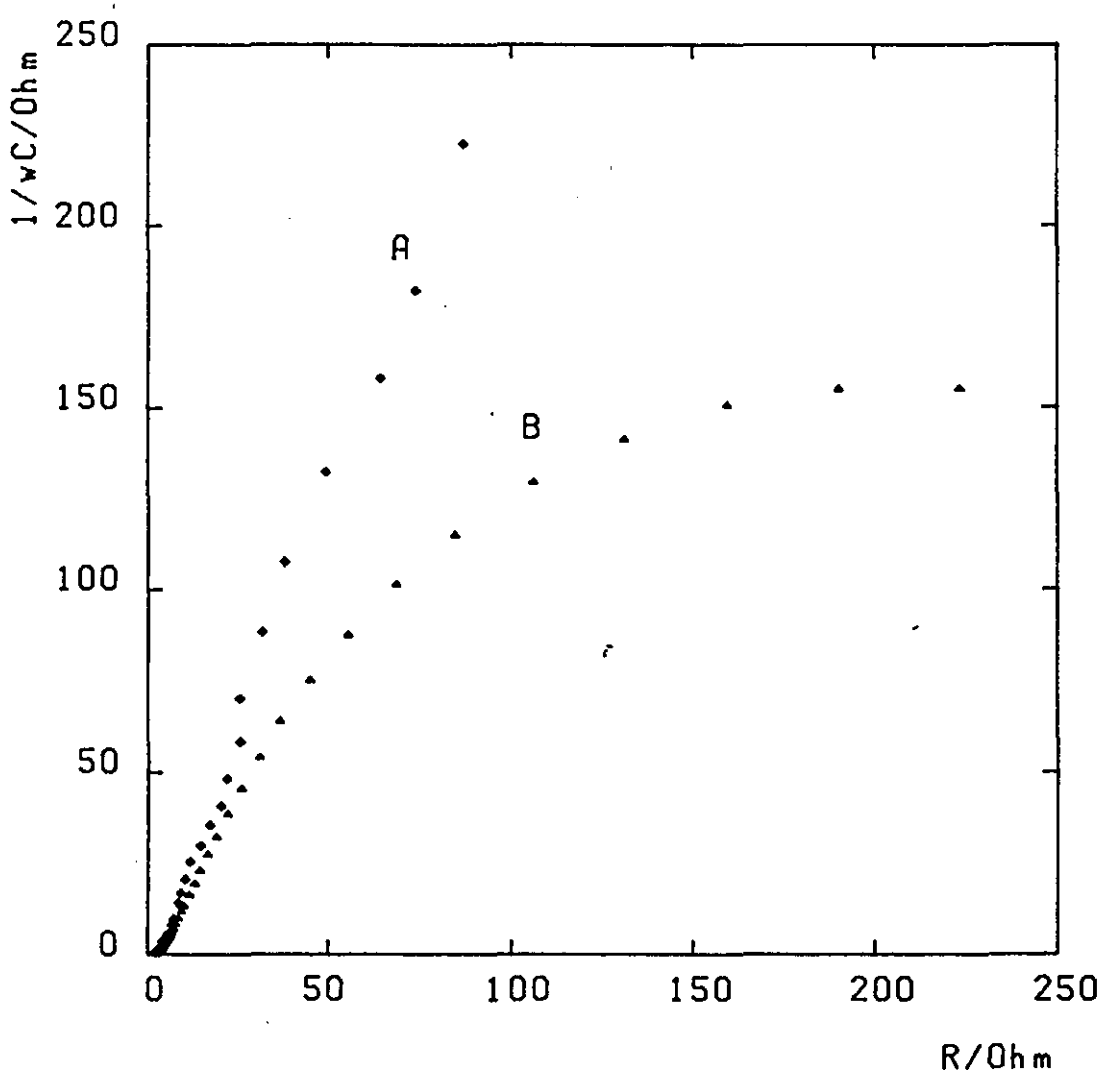

FIG 7.4 IMPEDANCE LOCI FOR A GLASSY CARBON ELECTRODE WITH NO APPLIED POTENTIAL (A), AND AT +500mV (B).

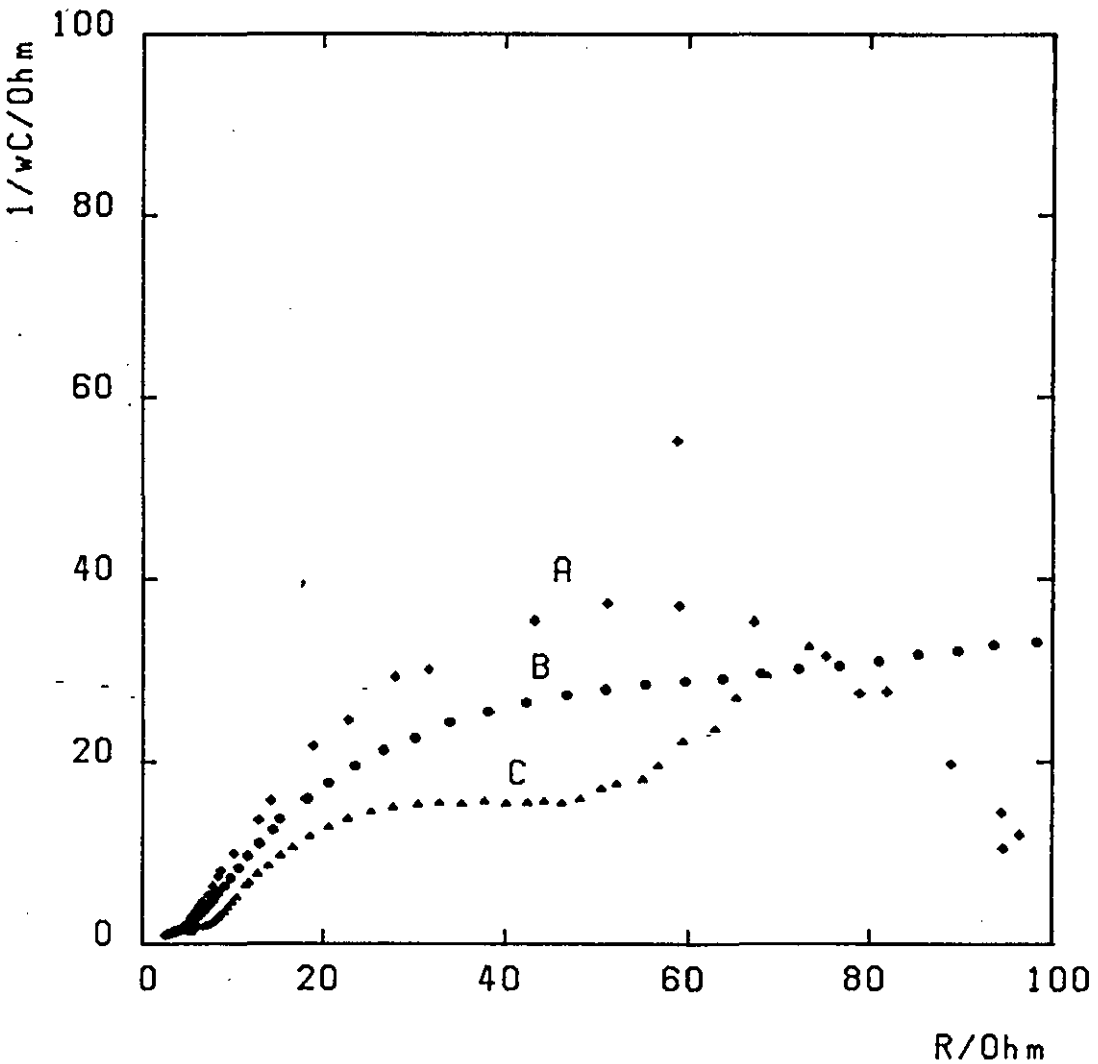

FIG 7.5 IMPEDANCE LOCI FOR A GLASSY CARBON ELECTRODE SUBJECTED TO APPLIED POTENTIALS OF: +1000mV (A), +2000mV (B), +3000mV (C).

were also thought to occur. Product analysis revealed the presence of SO_2Cl_2, $SOCl^+AlCl_4^-$, $AlCl_3$, SCl_2 and Cl_2, no LiCl was found. Therefore it is unlikely that LiCl precipitation is a factor influencing the anodic behaviour of glassy carbon in $SOCl_2$-$LiAlCl_4$, although it almost certainly takes part in the cathodic process.

It was decided to repeat the experiments using free Lewis acid electrolyte (3.0 M $AlCl_3$). Figures 7.6-7.7 show the results. One noticeable feature of the data is that the semicircles originate some distance from the origin of the complex plane. This yields values of about 20 Ω for the solution resistance which is about ten times greater than values for neutral electrolyte. This difference is due to the greater conductivity which 1.8 M $LiAlCl_4$-$SOCl_2$ electrolyte solutions have over solutions of $AlCl_3$ in $SOCl_2$.

The impedance data in acid electrolyte revealed little evidence for filming on the electrode during cathodic polarization, however this apart the spectra were of similar form to those obtained in neutral electrolyte.

7.4 Conclusions

(1) $SOCl_2$ oxidation and reduction at glassy carbon electrodes are complex processes, impedance data for which yield no straight forward kinetic interpretation. $SOCl_2$ reduction is apparently complicated by more than one reaction at low overpotentials, and influenced by LiCl filming at higher overpotentials.

(2) Impedance data suggests that the electrochemical oxidation of $SOCl_2$ at a glassy carbon electrode may involve some sort of filming on the surface, although not to the extent of the reduction process, and it is unlikely that the film is due to LiCl.

(3) The impedance results from solutions containing 3.0M $AlCl_3$ show similar shaped spectra to those obtained in neutral electrolyte, except that in pure acid electrolyte the solution resistance is considerably greater.

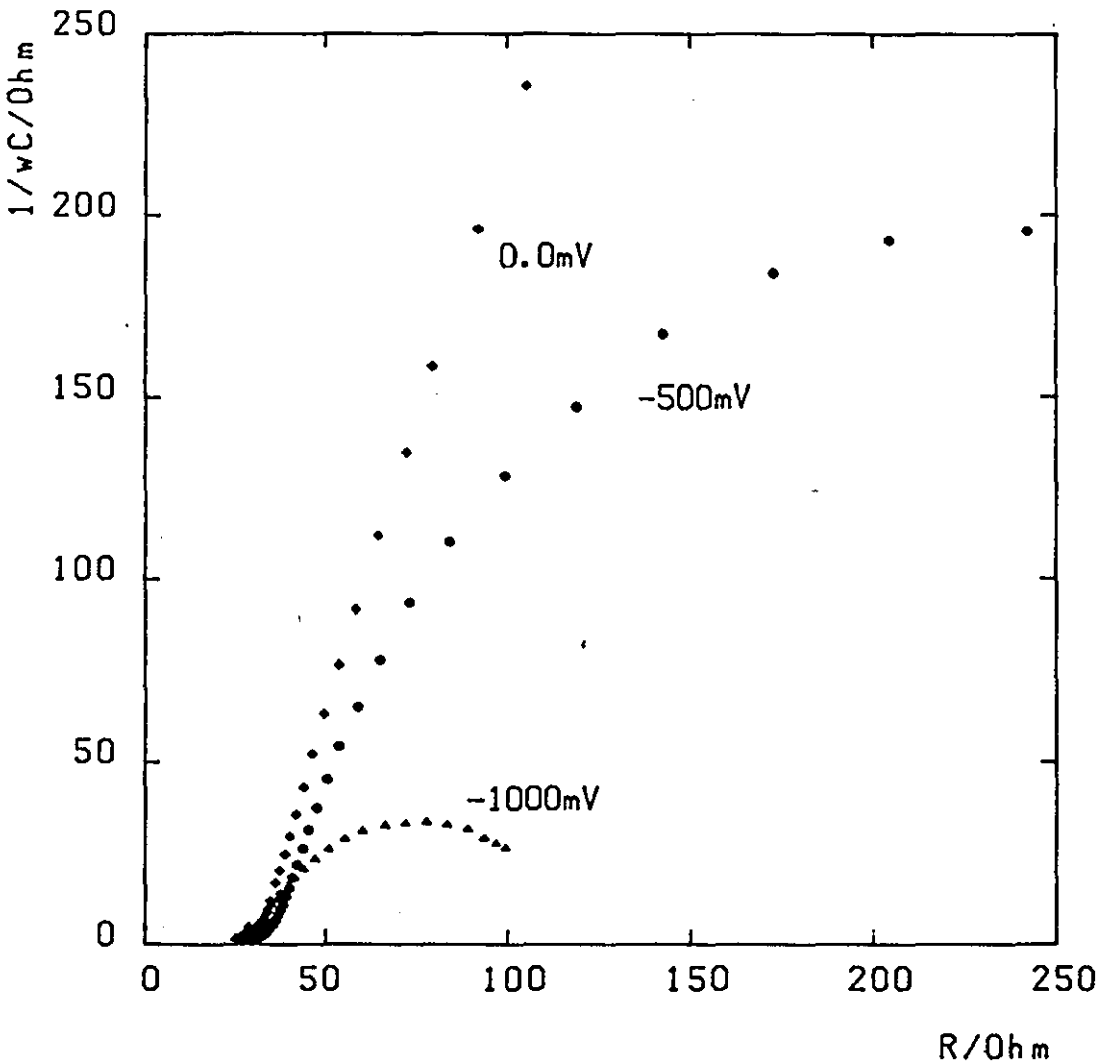

FIG 7.6 IMPEDANCE LOCI FOR A GLASSY CARBON ELECTRODE IN ACID ELECTROLYTE, SUBJECTED TO VARIOUS APPLIED NEGATIVE POTENTIALS.

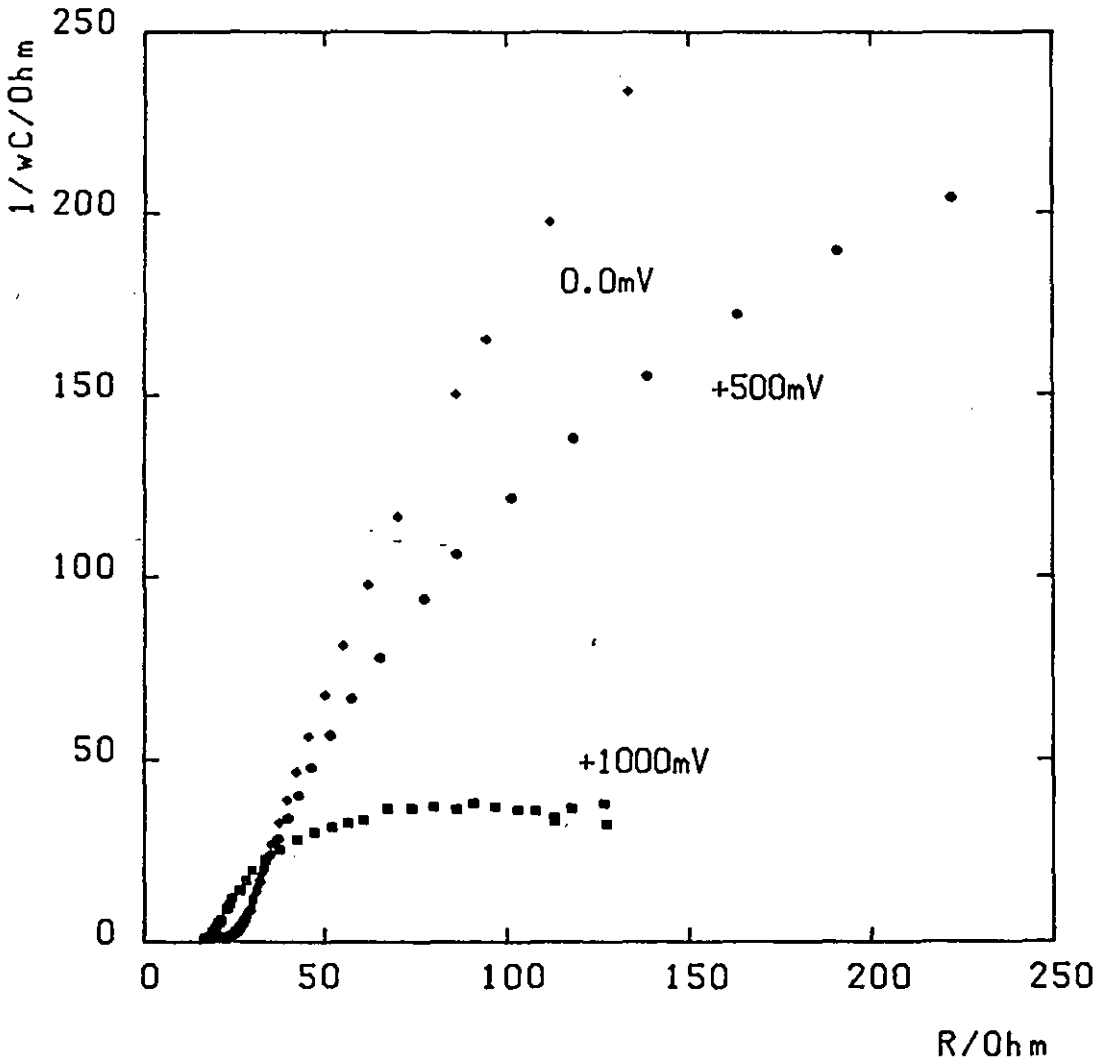

FIG 7.7 IMPEDANCE LOCI FOR A GLASSY CARBON ELECTRODE IN ACID ELECTROLYTE, SUBJECTED TO VARIOUS APPLIED POSITIVE POTENTIALS.

CHAPTER 8

THE PASSIVATION OF POROUS CARBON CATHODES

8.1 Introduction

Much work has been undertaken in recent years to improve the performance of the carbon cathode in high rate Li-$SOCl_2$ cells. This electrode is usually the cause of overall cell failure, which occurs as the carbon surface becomes progressively blocked by an insoluble deposit of LiCl. Other reaction products such as elemental sulphur may also contribute to this passivation process. Addition of electrocatalysts to the cathode have been shown to increase cell capacity, the best known being platinum [78], copper halides [81] and various metal phthalocyanines [85].

For this work it was considered of interest to engage upon a more fundamental study of the carbon cathode. Specifically, interest centred on the time taken to passivate various thicknesses of uncatalysed carbon cathodes. For these experiments it was possible to prepare a range of cathodes including very thin ones ($\sim$1 mg/cm^2). In addition smooth, glassy carbon was included for comparison purposes.

Similar work has actually been undertaken by Hagan et al [94] in which the transition times of porous carbon electrodes for different concentrations of $LiAlCl_4$ dissolved in the $SOCl_2$ were studied. This technique has been used for the study of smooth [181] and porous [182] zinc anodes in potassium hydroxide solutions. The results of the latter study showed that an insoluble deposit was formed within the porous matrix, in a similar manner to the LiCl on porous carbon.

Passivation usually results in an abrupt change in potential due to the surface concentration of the electroactive species reducing to zero at the electrode interface. For the carbon cathode in the Li-$SOCl_2$ cell this is due to the presence of LiCl which is a poor conductor, on the electrode surface, eventually preventing further reduction of thionyl choride, i.e. the electrode is blocked.

In the absence of convection, Sand [183] developed an equation governing transition time, τ, for a limiting concentration of species at an electrode surface, at a given current:

$$(1/\tau^{\frac{1}{2}}) = 2i/nF(\pi D)^{\frac{1}{2}}A \mid C-C_{crit} \mid \qquad (8.1)$$

where,

τ = time for the concentration of products at the electrode surface to change to a value necessary to cause passivation,

i = current density,

n = valency charge,

C = concentration of products in the bulk electrolyte, and C_{crit} is that concentration at the electrode necessary to bring about passivation,

D = diffusion coefficient of electroactive species,

F = Faraday constant,

A = electrode area.

The results for such a diffusion controlled reaction imply that a plot of $\tau^{-\frac{1}{2}}$ vs i should be a straight line with a gradient:

$$\partial\tau^{-\frac{1}{2}}/\partial i = 2/nF(\pi D)^{\frac{1}{2}}A\Delta C \qquad (8.2)$$

This relationship although originally derived for smooth electrodes in aqueous solution, has been found to hold for porous carbon in thionyl chloride at higher current densities [94]. (It is interesting to note that at these high rates the reaction is thought to be largely rate controlled by diffusion).

The aim of this study was to explore the relationship between passivation time (active reaction time) and other variables of interest to technologists and generally optimise the behaviour of the system.

8.2 Experimental

For this work, the cathodes were prepared using the spraying method outlined in Section 4.2.2a. Layers of carbon were removed from the sprayed cathode, until a pre-determined thickness was reached. Anode and electrolyte preparation are described in Section 4.2, a 1.8M $LiAlCl_4$-$SOCl_2$ electrolyte solution was employed throughout this work.

The electrodes were housed within a PTFE electrolytic cell, within which arrangement was made for a small lithium foil reference electrode, next to the cathode. All potentials were measured against this electrode, thus eliminating any possibility of the anode influencing cathode failure. Separators used within the cell were constructed of ceramic material.

8.3 Results and Discussion

Figure 8.1 shows a voltage-time transient for a 300 μm thick cathode, 50 mA/cm^2 being applied to it. This is typical of all the transients obtained. The curve is characterised by an initial rapid fall in potential from the open circuit voltage as the electrode is polarized, followed by a voltage ramp. As the electrode becomes completely blocked by a passivating layer of LiCl, there is a rapid decrease in potential, until the trans-passive region after which a steady potential is reached.

There is no well established method of measuring the transition time. This work involved a similar system to that used by Hagan et al [94] and consequently τ was evaluated in a similar way. The two approximately linear portions of the transient were extrapolated and the point on the rapidly rising portion which bisects the two lines was taken as the transition time. This method was generally found to be very satisfactory, since τ could be judged to a precision of $\sim$1% of the reaction time.

Voltage transients for carbon cathodes at various current densities were obtained and analysed. The current density applied to the cathode was found to be inversely proportional to the square root of the transition time.

Plots of $\tau^{-\frac{1}{2}}$ vs i for a range of cathode thicknesses are displayed in Figure 8.2. As can be seen a reasonable linear relationship exists for the current densities investigated. It is also apparent that each line in Figure 8.2 passes through the origin. This behaviour is characteristic of a diffusion controlled process, in this limited range of current densities. It has been demonstrated that for current densities below 20 mA/cm^2, this relationship does not hold [94].

Since the final passivating layer on the cathode is LiCl, the reaction is controlled by diffusion of the product away from the electrode. This process continues until the concentration of LiCl at the electrode becomes critical, when the solution capacity for LiCl is exceeded at the electrode and solid LiCl is deposited. This has been confirmed by allowing a passivated glassy carbon electrode to remain on open circuit for ten minutes, after which time, on re-polarization some of the capacity for $SOCl_2$ reduction was recovered. Figure 8.3 shows the results of successive discharges, interspaced with rest periods, for a Li-$SOCl_2$ cell containing a glassy carbon cathode. This experiment was then repeated using a large glass cell containing an excess of electrolyte (see Fig. 4.5). There was no significant increase in cell reaction time using such a cell, however

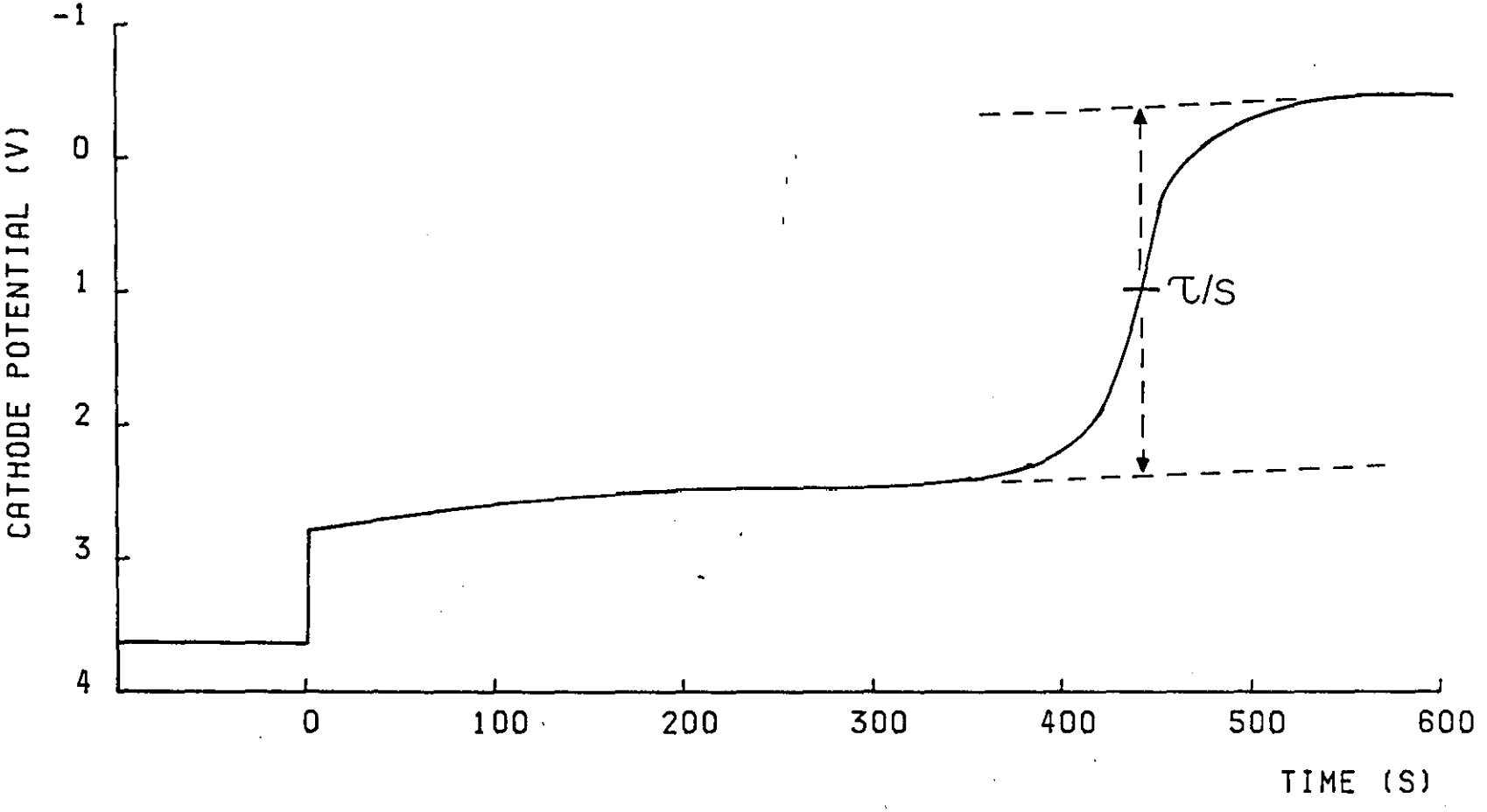

FIG 8.1 A TYPICAL VOLTAGE TRANSIENT FOR A CATHODE, 300 μm THICK, AT 50 mA cm^{-2}, SHOWING HOW THE TRANSITION TIME IS EVALUATED.

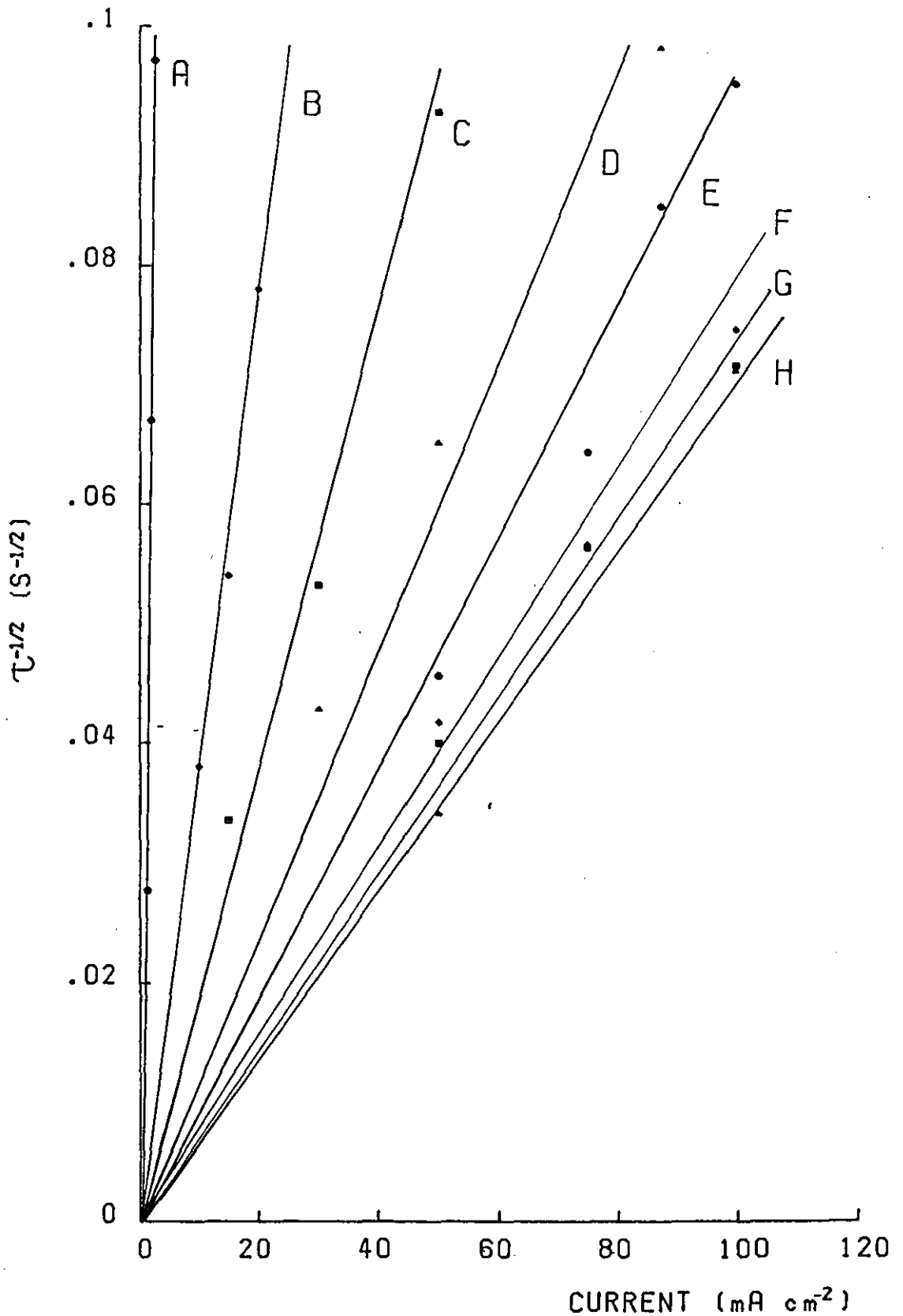

FIG 8.2 PLOTS OF $\tau^{-1/2}$ VERSUS i FOR VARIOUS THICKNESSES OF CARBON CATHODE (μm). (B) 50; (C) 100; (D) 200; (E) 300; (F) 400; (G) 500; (H) 600. (A) IS FOR A GLASSY CARBON CATHODE.

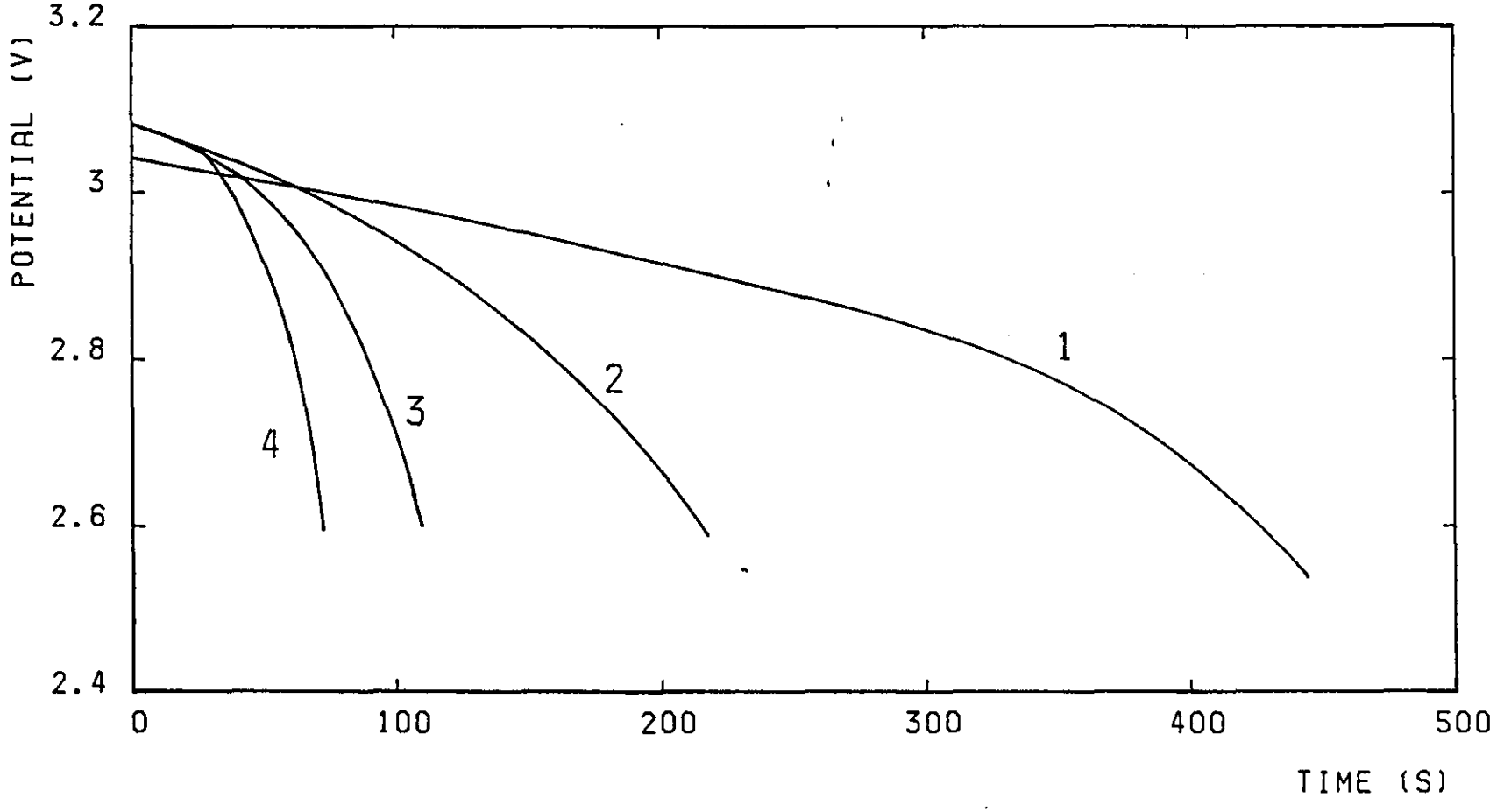

FIG 8.3 SUCCESSIVE DISCHARGES FOR A GLASSY CARBON CARBON CATHODE. CURVE 1 IS THE FIRST. CURVE 4 IS THE LAST. CELL WAS RESTED FOR 15 MINUTES BETWEEN EACH DISCHARGE. CURRENT DENSITY=1.14 mA cm^{-2}.

the extent of cathode recovery was much greater, almost all of the cell capacity was recovered. We consider that this arises since the solubility of LiCl in the electrolyte solution exceeds the stoichiometry required by $LiAlCl_4$ [94]. On standing the solid phase LiCl at the electrode back dissolves and the cathode depassivates. Dissolved SO_2 from the cathode reaction also complexes with LiCl produced and thereby increases the solution capacity to remove LiCl.

Using porous electrodes it was found that in an open glass cell, without the presence of separator paper between the electrodes, the thinnest (50 μm) cathodes recovered about one third of their original capacity on resting for 30 minutes, after passivation at 15 $mAcm^{-2}$. 100 μm Cathodes, after passivation at 30 $mAcm^{-2}$ recovered about 20% of their capacity after 30 minutes rest time.

Further examination of Figure 8.2 shows that a limit is reached; after thickening the cathode beyond ∿400 μm little increase in passivation time is observed. This is clearly demonstrated by the slope $\partial\tau^{-\frac{1}{2}}/\partial i$. This relationship is non-linear with thickness and the thinner deposits are behaving as intermediates in the progression from a truly planar electrode to one which is 'infinitely porous' in the sense of de Levie [158]. A plot of $(slope)^{-1}(\partial i/\partial\tau^{-\frac{1}{2}})$ (Fig. 8.4) versus the cathode thickness was found to be approximately linear for the range up to 400 μm, this behaviour is in accordance with the results of Frumkin [184]. Beyond this thickness it was found that there is virtually no increase in passivation time for current densities of 100 mA/cm^2. However, the passivation time is still increasing with cathode thickness when current densities of 50 mA/cm^2 are applied. This accounts for the slight continuing increase in $\partial i/\partial\tau^{-\frac{1}{2}}$ shown in the graph Figure 8.4 beyond 400 μm. This can be predicted from the theory of de Levie who showed that the penetration depth of a porous electrode decreases with increasing current density.

The linear portion of Figure 8.4 is in accordance with equation (8.2), the slope $\partial\tau^{-\frac{1}{2}}/i$ is inversely proportional to A, the effective electrode area, which increases with the thickness. From this relationship it was possible to calculate effective diffusion coefficients, D, for each thickness, based on the apparent surface area of the electrode. The ΔC term in equation (7.2) was taken as being 6.5×10^{-4} mol cm^{-3} of LiCl. This is the amount of additional LiCl which can be accommodated within a 1.8M $LiAlCl_4$ solution without precipitation based on previous results [94]. D was found to increase with deposit thickness, as expected, however, the value for glassy carbon, $1 \times 10^{-7} cm^2 s^{-1}$

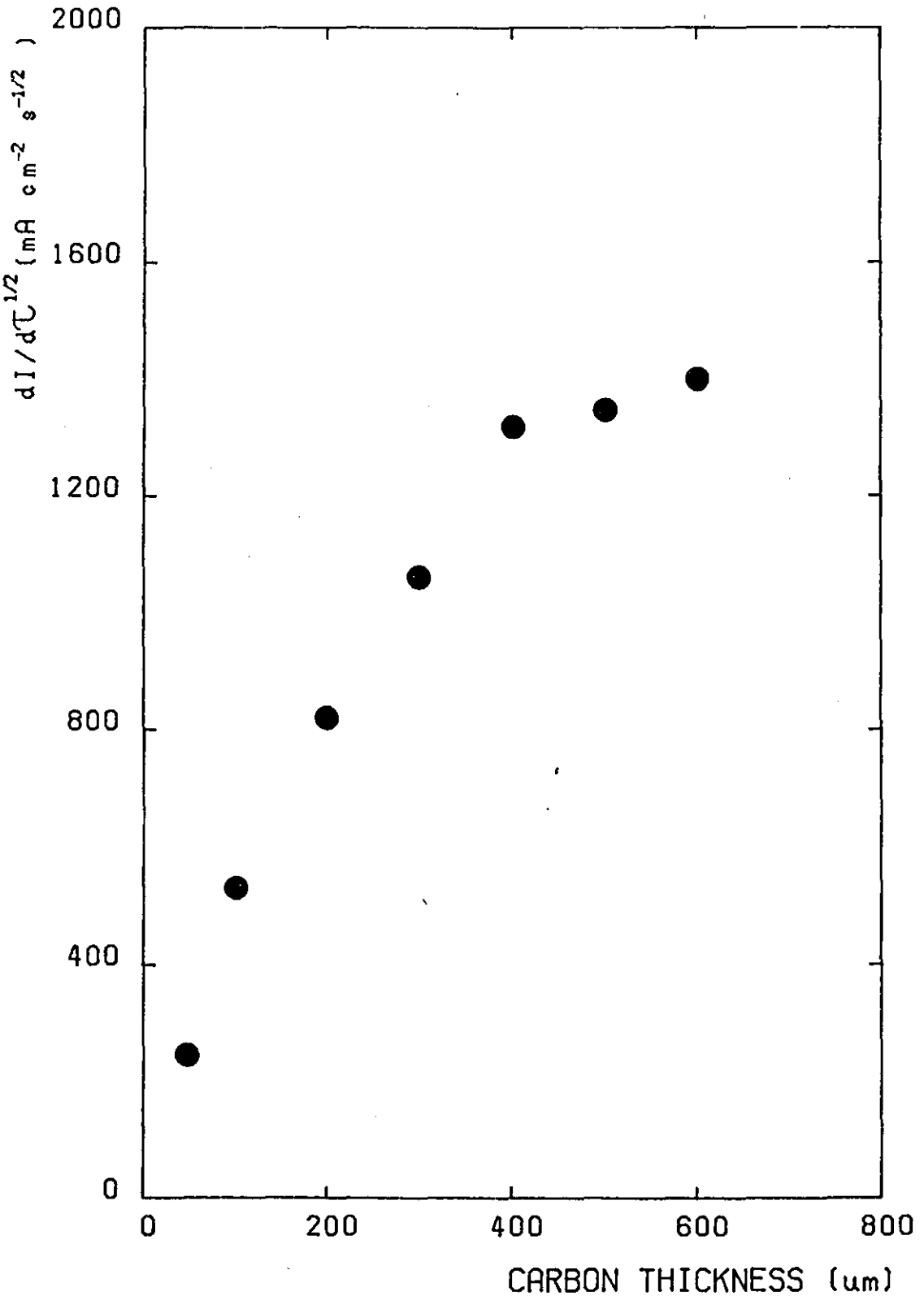

FIG 8.4 GRAPH SHOWING THE RELATIONSHIP BETWEEN (1/SLOPE) OF THE LINES IN FIG 8.2 AND THICKNESS.

indicates that the surface is not wholly active. Diffusion coefficients for Li^+ in $SOCl_2$ have not been reported in the literature, so an accurate assessment of the active electrode area [185] cannot be made with certainty. However, assuming a value of 1.3×10^{-5}cm s^{-1} which is characteristic of Li^+ in 1.0M LiCl aqueous solution, it seems that less than 1% of the surface is active for $SOCl_2$ reduction. We could also assume a true value of D to be $\sim 3 \times 10^{-6}$cm s^{-1} which is characteristic of Li^+ in a 0.7 M LiCl-propylene carbonate solution. Using such a value, this would imply that about 4% of the surface was active [186].

It must also be borne in mind that these diffusion coefficients were calculated from results based on the 'sandwich' type cells employed in this work. More realistic results would be expected using cathodes in open cells, without the complication of the ceramic separator. Knowing the surface area of Shawinigan carbon black to be 60 m^2 g^{-1} the area-corrected diffusion coefficients for porous carbon cathodes could be calculated (Table 8.1). These however, were found to be very small, therefore most of this surface is unavailable for LiCl deposition.

It was decided to investigate the effects of electrode separation on cell performance, it has previously been shown that where the cathode is allowed to expand during discharge capacity is increased by up to 33% [73, 74, 76]. Figure 8.5 shows the discharge characteristics for a cell where the anode and cathode are in close contact, and one for which the cathode is set back slightly in the lid of the cell, giving an electrode separation of about 0.5 mm. The results confirm the increase in cell lifetime possible by allowing the cathode to expand, however, the electrode separation also leads to greater ohmic polarization which results in a lower overall cell voltage. Figure 8.6 compares the $\tau^{-\frac{1}{2}}$ vs i behaviour of cells where electrode separation is allowed for and where it is not. This confirms the beneficial effect of electrode separation on cathode passivation times, at different current densities.

Polarization curves for cells containing glassy carbon and thin porous carbon cathodes (50 μm and 100 μm) are shown in Figure 8.7. Further increases in cathode thickness, yield slightly higher load voltages, although the improvements in polarization are less for greater thicknesses which confirms the findings of Klinedinst [78]. As expected the glassy carbon cathode undergoes severe polarization and cannot sustain a current of greater than about 4 mA/cm^2. Because of its low geometric surface area, glassy carbon is rapidly

Table 8.1 Values of apparent and area-corrected diffusion coefficients for a variety of cathodes

Cathode Employed	Apparent Diffusion Coefficient D′	Diffusion Coefficient (Area Corrected)
	(cm^2s^{-1})	(cm^2s^{-1})
Glassy carbon	1.06×10^{-7}	1.06×10^{-7}
50 μm porous carbon	3.06×10^{-5}	8.79×10^{-11}
100 μm porous carbon	9.12×10^{-5}	6.54×10^{-11}
200 μm porous carbon	2.17×10^{-4}	3.90×10^{-11}
300 μm porous carbon	3.64×10^{-4}	2.90×10^{-11}
400 μm porous carbon	5.55×10^{-4}	2.51×10^{-11}
500 μm porous carbon	5.88×10^{-4}	1.69×10^{-11}
600 μm porous carbon	6.46×10^{-4}	1.29×10^{-11}

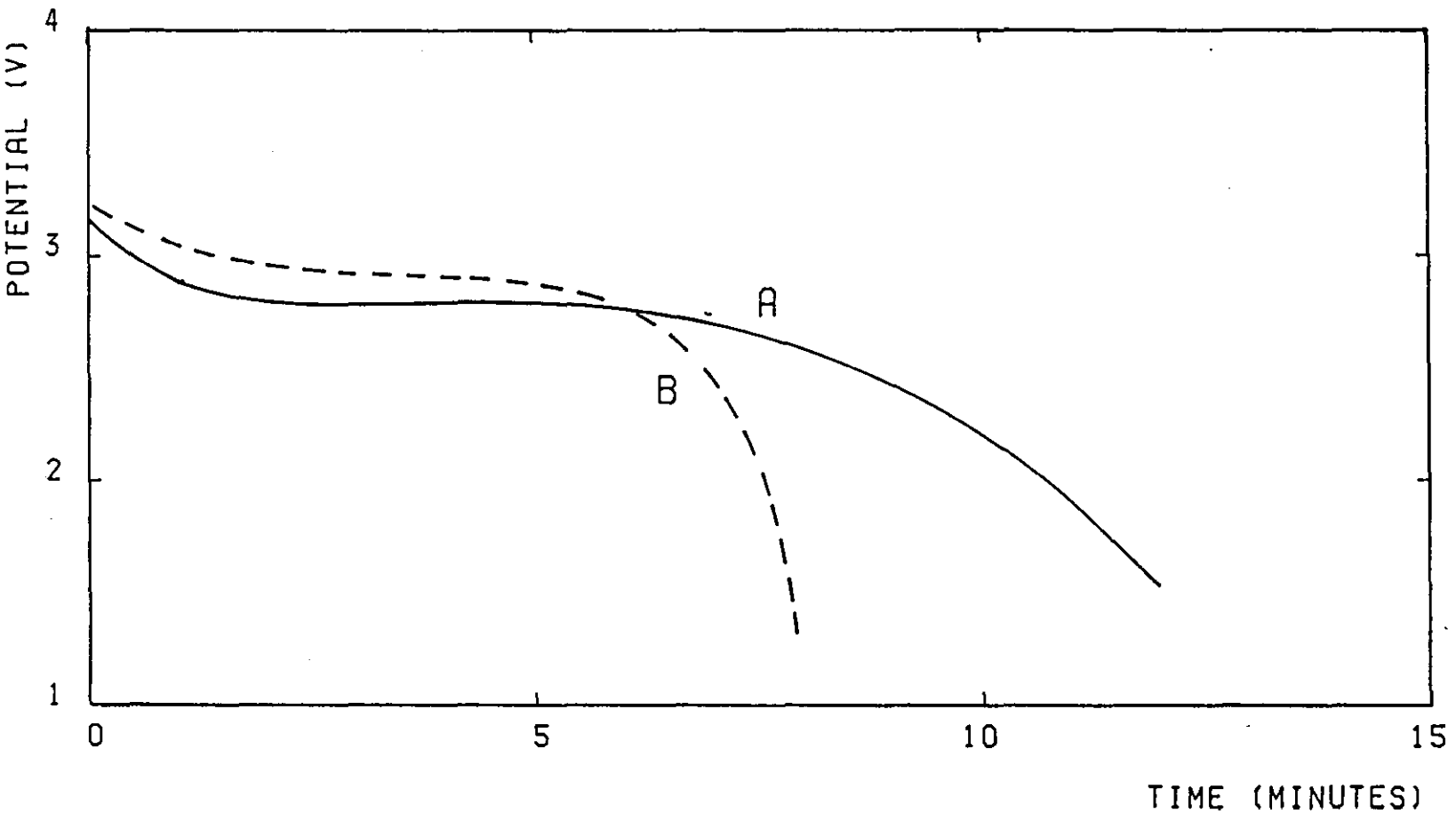

FIG 8.5 DISCHARGE PROFILES FOR A CELL WHICH ALLOWS FOR ELECTRODE EXPANSION (A) AND FOR ONE WHICH DOES NOT (B). CATHODE THICKNESS =200 μm. CURRENT DENSITY =30mA cm^{-2}.

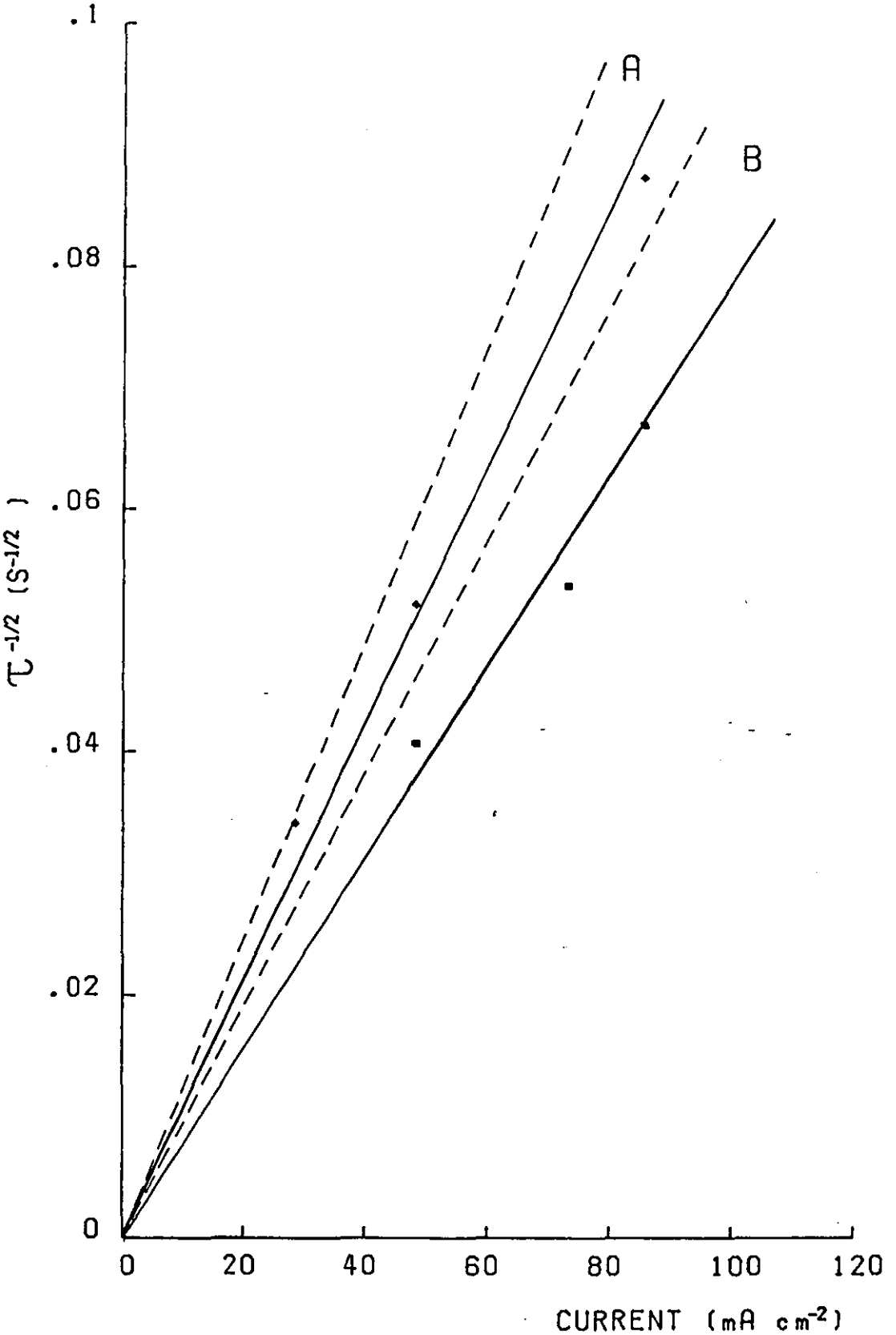

FIG 8.6 $\tau^{-1/2}$ VERSUS i CHARACTERISTICS FOR 200μm (A) AND 300μm (B) THICK CATHODES. THE DASHED LINES ARE FOR CELLS WHICH HAVE NO ALLOWANCE FOR ELECTRODE EXPANSION, THE SOLID LINES FOR CELLS WHICH DO. THE SQUARE SHAPED DATA POINTS (▪), DEFINE THE SOLID LINE B, THE DIAMOND SHAPED POINTS (◆) DEFINE A.

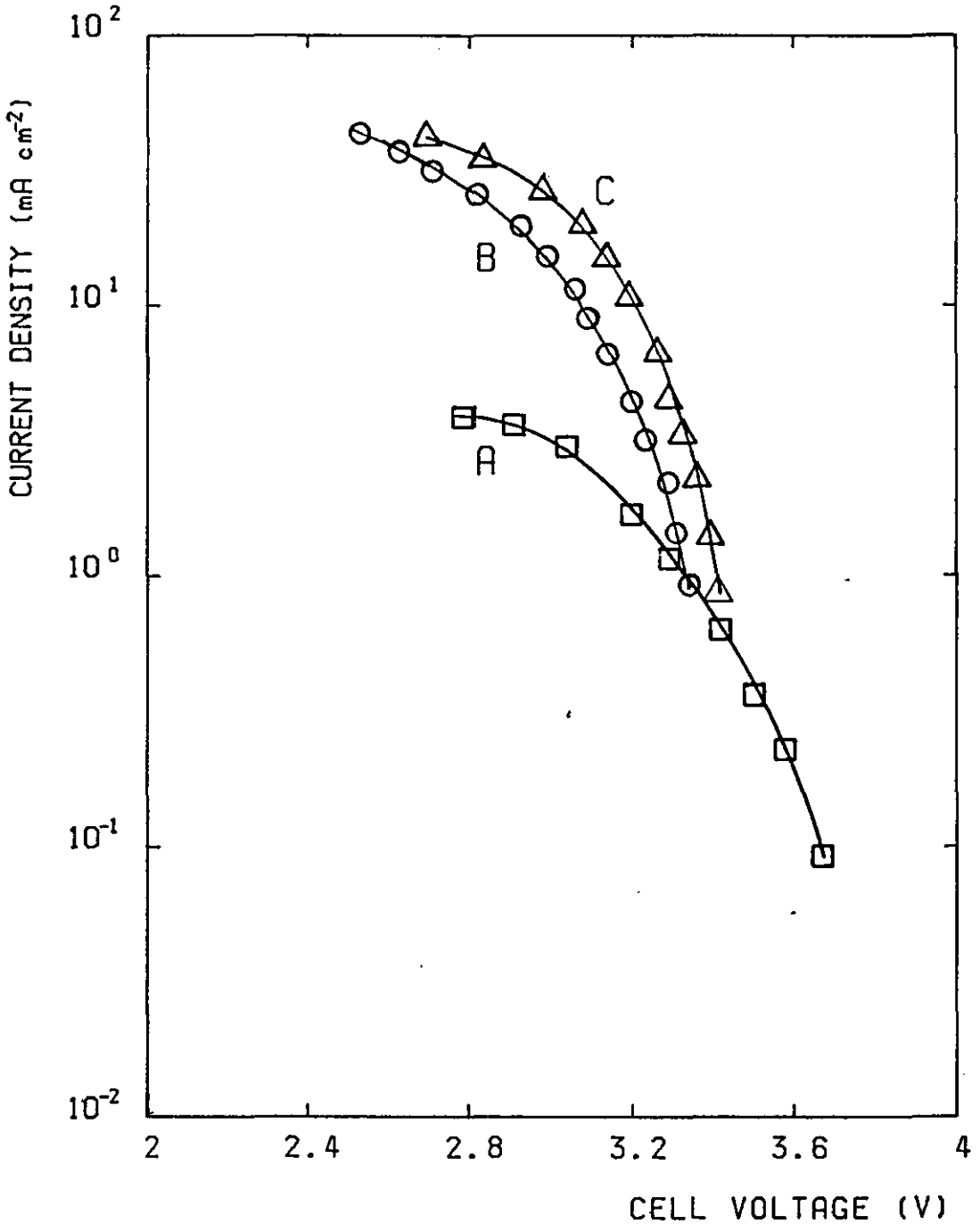

FIG 8.7 POLARIZATION CHARACTERISTICS FOR VARIOUS CARBON CATHODES: GLASSY CARBON (A), 50 μm POROUS CARBON (B), AND 100 μm POROUS CARBON (C).

passivated by LiCl as soon as any current is applied. The open circuit voltage however is higher for cells containing glassy carbon cathodes, as well as higher cell voltages being obtained at low currents (>0.3 mA/cm^2). This is probably due to the greater conductivity which a glassy carbon disc has over a solution filled porous carbon electrode.

8.4 Conclusions

(1) Earlier findings that the reduction of $SOCl_2$ at a carbon surface is controlled by the solubility of LiCl in the electrolyte immediately surrounding the electrode, have been confirmed.

The electrode remains active until the LiCl is unable to leave the electrode by diffusion (mass transport).

(2) On standing in the cell after passivation, a glassy carbon cathode recovers capacity for further reduction of $SOCl_2$, as the LiCl product is removed into the bulk solution. This occurs to a lesser extent with porous carbon cathodes.

(3) As little as 1% of a glassy carbon surface may be active for the reduction process; at a porous carbon cathode only a very small fraction of the calculated surface area is active.

(4) There exists a porous carbon black electrode thickness above which the reaction time is unaffected by thickness increases. This thickness is greater for lower current densities.

(5) Cathode reaction time is enhanced by allowing the carbon electrode room to expand during discharge, however the overall cell voltage is lower under these circumstances.

CHAPTER 9

FREE LEWIS ACID EFFECTS IN $SOCl_2$ ELECTROLYTE SOLUTIONS

9.1 Introduction

Li-$SOCl_2$ cells for high power, high rate applications often have a reserve construction in which the electrolyte is contained in a separate compartment from the electrode stack area and is admitted only as power is required. As well as giving the cell an almost indefinite shelf life by preventing the build up of a thick porous LiCl film on the anode, this arrangement favours the use of aluminium chloride in the electrolyte solution. Aluminium chloride behaves as a Lewis acid (electron pair acceptor) in thionyl chloride by increasing the relative concentration of $SOCl^+$. In this media chloride ions behave as Lewis bases, partaking in the following neutralization reaction:

$$Cl^- + AlCl_3 \rightarrow AlCl_4^- \qquad (9.1)$$

Free $AlCl_3$ in the electrolyte has been found to substantially increase the cell capacity and the average discharge voltage [77, 95-97]. It is thought to achieve this by complexing with LiCl produced during the cell reaction, thereby delaying passivation of the cathode. The reserve design prevents $AlCl_3$ dissolving the protective LiCl layer on the anode, which would otherwise allow premature reaction between lithium and $SOCl_2$. Any capacity loss due to lithium corrosion and leakage currents during discharge is likely to be minimised for short cell lifetimes. The concentrations of Lewis acid used are not often mentioned in the literature although Klinedinst [77, 95] found 3.0M $AlCl_3$ most suitable for cells with thick carbon cathodes, and 4.5M $AlCl_3$ more effective for thinner ones (37 μm). The aim of this chapter was to comprehensively examine a range of electrolyte compositions with respect to performance in lithium-thionyl chloride cells. In this way the optimum electrolyte composition could be identified.

Additionally it was considered of interest to investigate free Lewis effects at other carbon surfaces with different BET surface

areas. This was thought to be particularly relevant as many high surface area carbon blacks are being considered as possible cathode materials for high rate Li-$SOCl_2$ cells [67, 71].

Other Lewis acid electrolytes have been considered for Li-$SOCl_2$ cells [99], $GaCl_3$ in particular offers an improvement in cell capacity [100]. However the very high cost and relative scarcity of $GaCl_3$ compared with $AlCl_3$ mean that it is unlikely to ever be a suitable alternative.

9.2 Experimental

Details of cell design, electrolyte and anode preparation are as outlined in Chapter 4. The porous carbon cathodes were fabricated by slurrying a mixture of carbon and PTFE (10% w/w, ICI Plastics) in propan-1-ol and drying the mixture in an oven at 100°C. After powdering, the mixture was pressed to form cathodes. The carbon/PTFE loading was 20 mg/cm^2. This was twice as great as for the thickest cathodes employed previously (Chapter 8), thus being well in excess of the 'penetration depth'.

For most of these experiments the carbon used was Shawinigan acetylene black, although some of the work used Ketchenblack EC, a high surface area carbon black found to give a superior performance with 1.8M $LiAlCl_4$ [71]. A glassy carbon disc (area 1.77 cm^2, le Carbone), was also used as a cathode for some of the cells discharged at low rates, in order to study electrolyte effects at a planar surface.

Experiments using cells containing a small lithium reference electrode showed that the potential between the anode and cathode was almost identical to that between the cathode and reference electrode. The lithium anode overpotential remained both low and approximately constant during the cathode reaction. Therefore for most of this work, a reference electrode was not employed.

9.3 Results and Discussion

(a) Cell discharge in acid electrolyte

Figure 9.1 shows the improvement in Li-$SOCl_2$ cell performance which is possible using free Lewis acid electrolyte. A cell containing 1.0M $LiAlCl_4$ + 2.0M $AlCl_3$ gives a higher load voltage and greater reaction time than one containing neutral 1.8M $LiAlCl_4$. Figure 9.1 also shows that a low concentration of $AlCl_3$ (1.0M) with no LiCl initially present is not a viable strength of electrolyte salt. This work has shown that overall concentrations of electrolytes

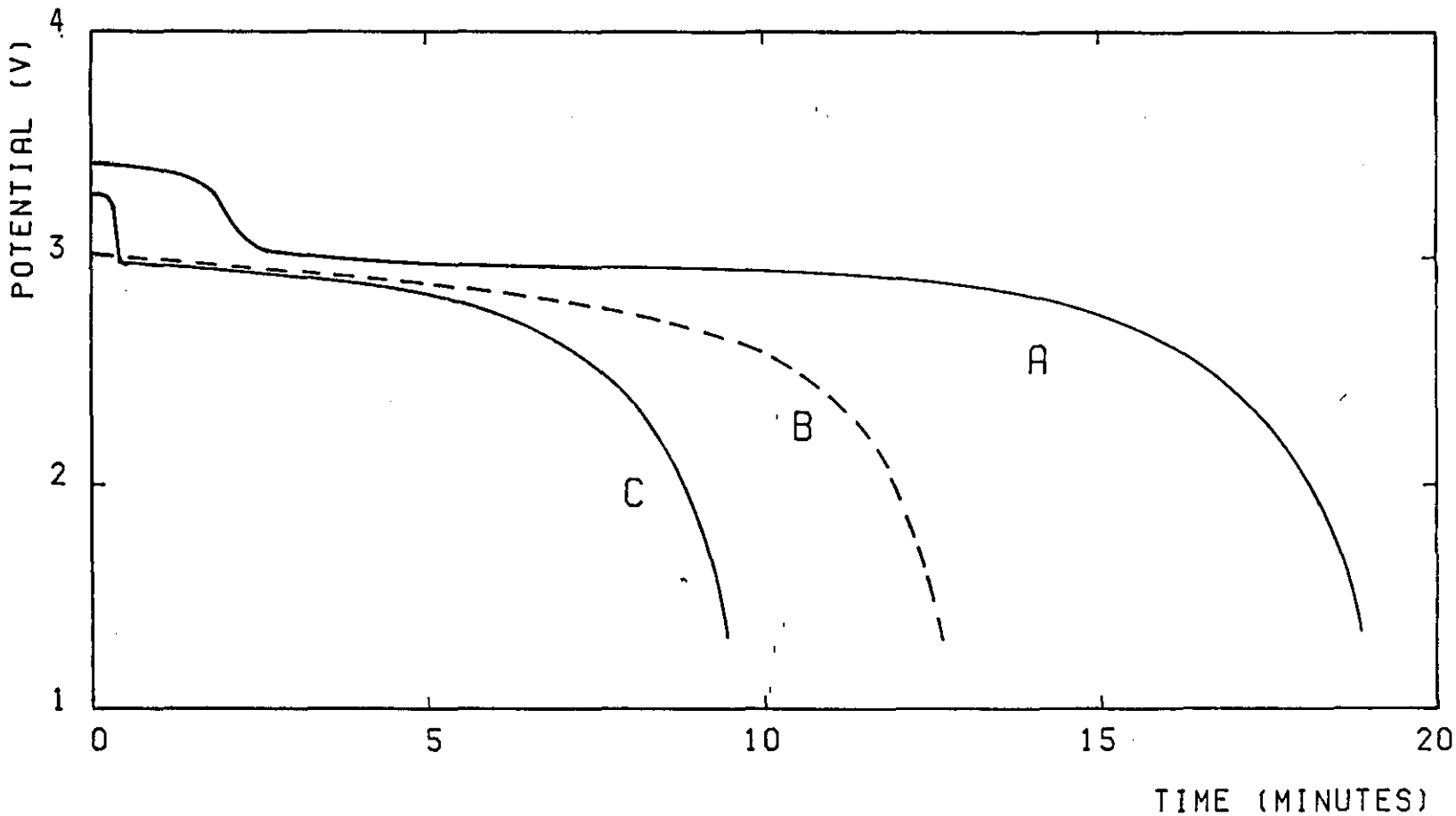

FIG 9.1 DISCHARGE PROFILES FOR Li-$SOCl_2$ CELLS AT 50 mA cm^{-2}: (A)-1.0M $LiAlCl_4$ + 2.0M $AlCl_3$: (B)-1.8M $LiAlCl_4$: (C)-1.0M $AlCl_3$.

(acid or neutral) which are much less than 1.8M yield less favourable performance in high rate Li-$SOCl_2$ cells.

The general shape of the transient obtained for acid electrolyte is similar to the one corresponding to the neutral electrolyte, except for the early stages where there is a clearly visible step, reportedly [77] due to the participation of $AlCl_3$ in the electrode process for lithium dissolution:

$$4Li + 2SOCl_2 \xrightarrow{AlCl_3} LiAlCl_4 + S + SO_2 \qquad (9.2)$$

Although the duration of this step was usually between 90 and 120 seconds, the improvement in cell lifetime possible by using the electrolyte was greater than five minutes, at 50 mA/cm^2. It would therefore appear that this additional acid reaction is by itself insufficient to totally account for the increased capacity. Halving the volume of acid electrolyte used in the cells did not significantly affect the cell performance. Therefore the electrolyte volume is adequate for the reaction and not all of the free $AlCl_3$ is neutralized by LiCl produced during the discharge. This confirms theoretical calculations based on the results which show the cell lifetime could be extended further, should all of the free $AlCl_3$ present react as in equation (9.2). It must be borne in mind however that anode corrosion during discharge and the difficulty of exactly balancing (neutralizing) the electrolyte solution will complicate such calculations.

(b) Optimisation of the electrolyte

Free Lewis acid electrolytes for Li-$SOCl_2$ cells are usually made from $AlCl_3$ which is partly neutralized by added LiCl. It was considered of interest to study the cell performance for a range of free $AlCl_3$ additions to a 1.0M $LiAlCl_4$-$SOCl_2$ solution (Fig. 9.2); and then to examine the effect of various amounts of LiCl initially present in an electrolyte containing 3.0M $AlCl_3$ (Figs. 9.3a and 9.3b).

Figure 9.2 shows that there is an improvement in cell reaction times as the amount of free $AlCl_3$ present increases, up to a maximum at about 2.0M $AlCl_3$(+1.0M $LiAlCl_4$). Clearly this increase is due to more free acid being available to delay cathode passivation by LiCl insulation, also the effects of lithium corrosion neutralizing $AlCl_3$ become less significant at higher acid strengths.

Increasing the free Lewis acid concentration beyond this maximum

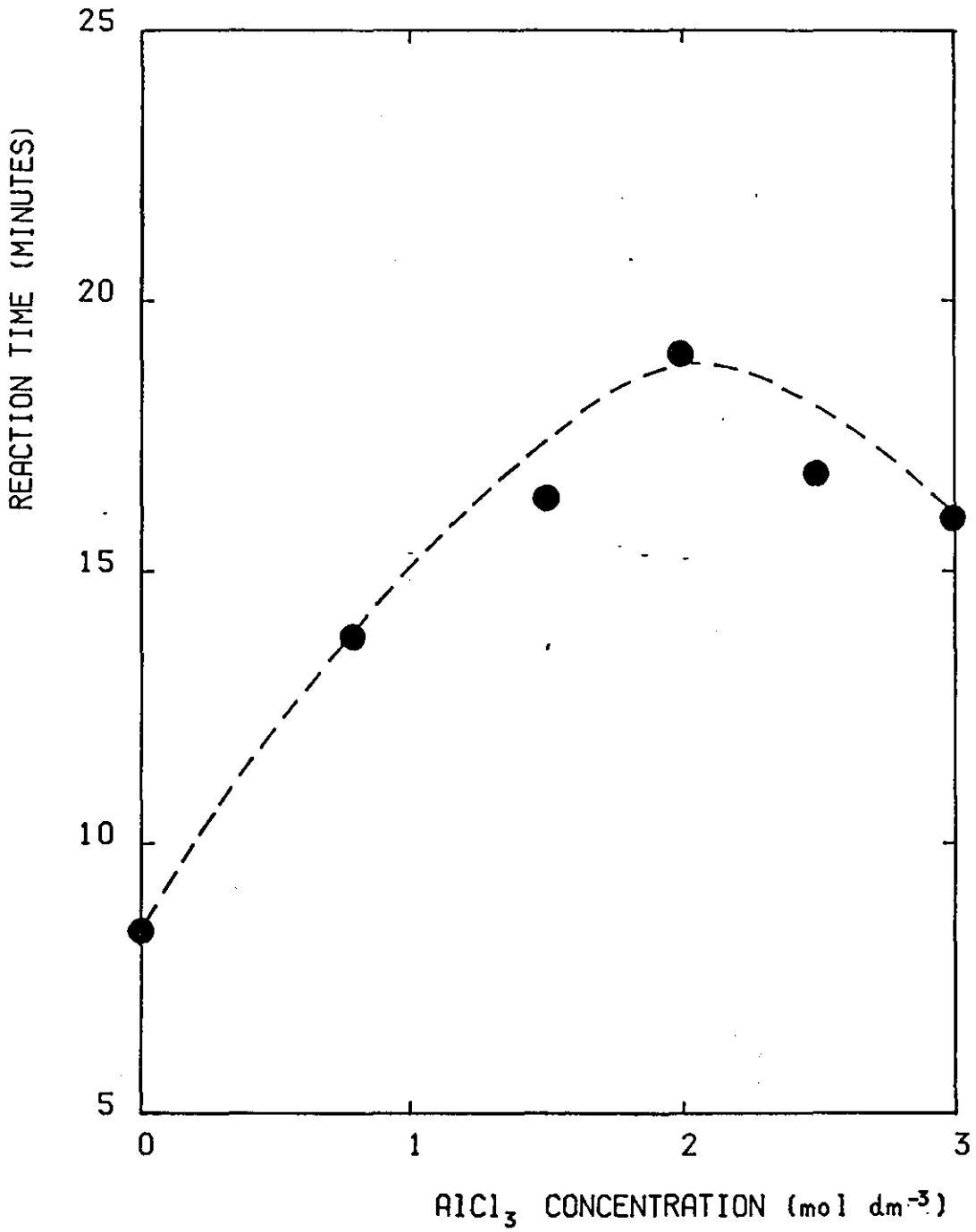

FIG 9.2 DISCHARGE TIME VERSUS CONCENTRATION FOR A $SOCl_2$ SOLUTION CONTAINING 1.0M $LiAlCl_4$. CURRENT DENSITY=50 mA cm^{-2}.

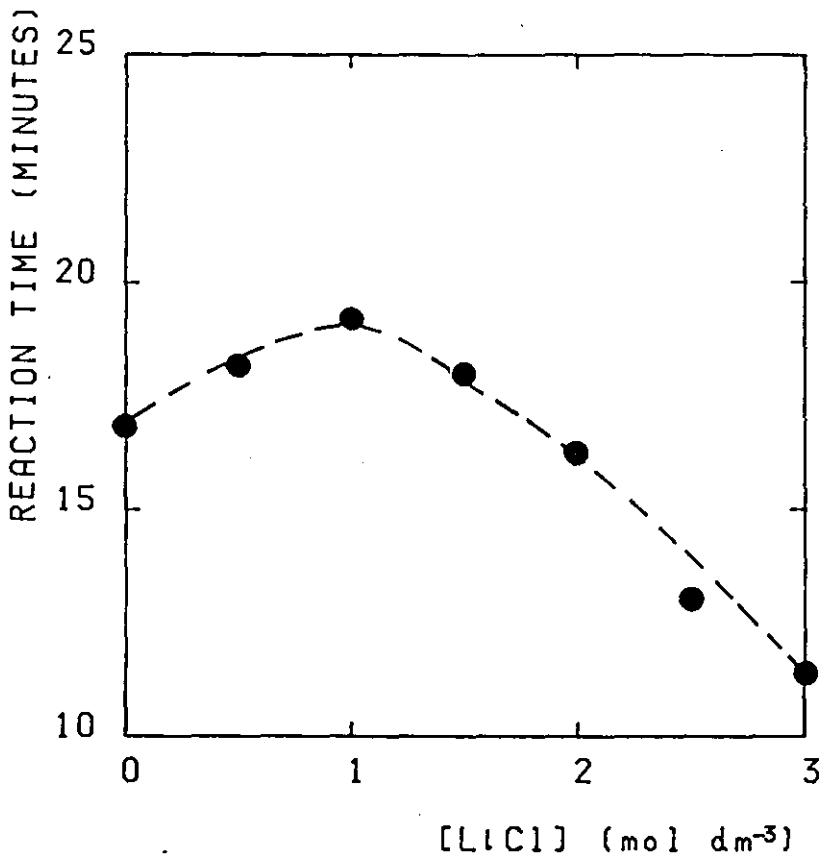

FIG 9.3(a) DISCHARGE TIME AS A FUNCTION OF LiCl FOR A SOLUTION BASED ON 3.0M $AlCl_3$-$SOCl_2$. CURRENT DENSITY=50 mA cm^{-2}.

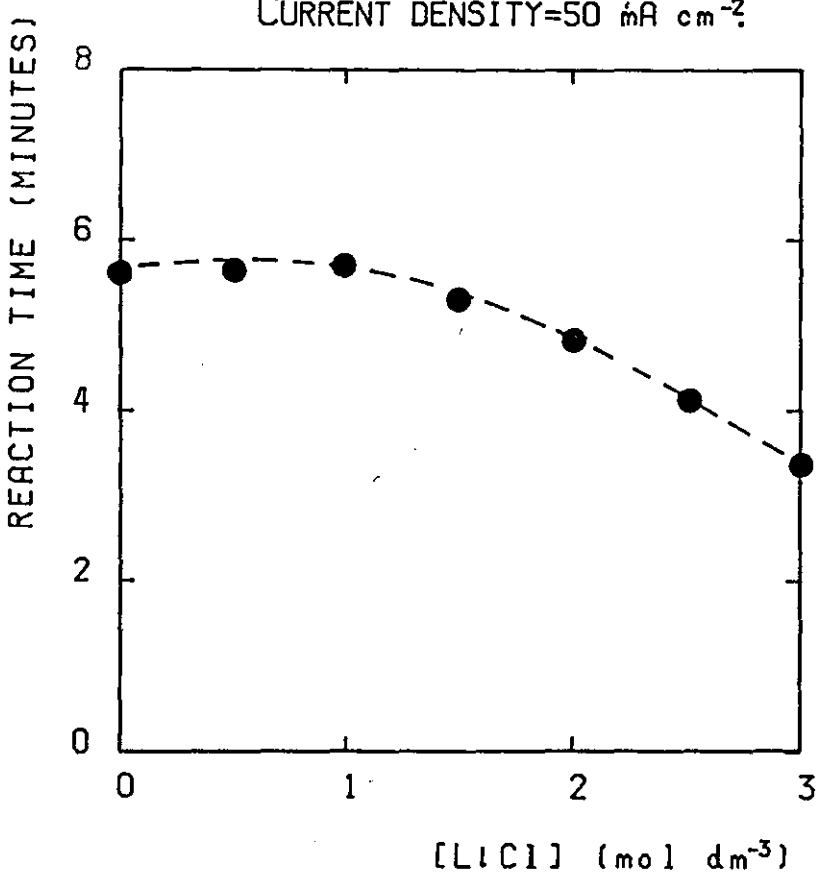

FIG 9.3(b) AS ABOVE BUT AT 100 mA cm^{-2}.

must somehow hinder the discharge process. Cells containing more than 4.0M of Al^{3+} ions were often unable to sustain discharge. Thus for example it was impossible to discharge such cells at 100 mA/cm^2, attempts to do so resulted in rapid cell failure.

Such poor performance is a likely result of increased viscosity and reduced conductivity of $LiAlCl_4$-$SOCl_2$ solutions as $AlCl_3$ is added [77, 104]. This is probably due to the formation of ion pairs and triple ions such as $Al_2Cl_7^-$ and $Al_3Cl_{10}^-$ as well as more complex aggregates [104]. Such effects will hinder the diffusion of lithium ions through the solution.

The optimum electrolyte composition identified by this present work is similar to that suggested for commercial use [83, 116].

Figure 9.3a and 9.3b show the effect of increasing amounts of LiCl initially present in the electrolyte solutions, based on 3.0M $AlCl_3$. The influence of these solutions on cell performance at 50 mA/cm^2 and 100 mA/cm^2 are displayed. Pure acid electrolyte (3.0M $AlCl_3$) was able to function well as an electrolyte as has been noted elsewhere [77, 95]. That it can sustain any discharge current at all, is by virtue of anode corrosion which takes place prior to discharge to produce sufficient Li^+ and $AlCl_4^-$ ions to suitably raise the solution conductivity. The initial presence of up to 1.0M LiCl in a 3.0M $AlCl_3$-$SOCl_2$ based electrolyte does however extend the cell life, particularly at the lower of the two current densities investigated. Initial additions of LiCl to $AlCl_3$-$SOCl_2$ solutions rapidly increase the solution conductivity to give an optimum level for cell performance [187]. The conductivity of $AlCl_3$ by itself in $SOCl_2$ is two orders of magnitude below the conductivity of the corresponding lithium salt solution. This difference in dissociation has been explained in terms of the ionic size, the acid cations $SOCl^+$ are smaller than the solvated lithium ions $[Li(SOCl_2)_n]^+$[5]. Because of this the acid solutions consist mainly of associated ion pairs, $SOCl^+$ and $AlCl_4^-$, which when neutralized by LiCl result in conductive solutions of dissociated ions:

$$LiCl + SOCl_2{:}AlCl_3 + (n\text{-}1)SOCl_2 \rightleftharpoons [Li(SOCl_2)_n]^+ + AlCl_4^- \qquad (9.3)$$

However, further additions of LiCl reduce the effectiveness of the acid electrolyte. The likely reason for these observations include the reduction of free $AlCl_3$ in the electrolyte and an increase

in the viscosity resulting in a hindrance of the electrode reduction process. Experimental data have shown the viscosity of a 3.0M $AlCl_3$-$SOCl_2$ solution increasing 2.5 times as 3.0M LiCl is added [103].

(c) The effect of free Lewis acid on glassy carbon electrodes

Although glassy carbon is not a practical electrode material for high rate Li-$SOCl_2$ cells, it was considered of interest to examine the effects of free Lewis acid electrolytes for cells containing such cathodes. Figure 9.4 compares the discharge characteristics for cells containing glassy carbon cathodes with neutral and acid electrolyte. The improvement in cell discharge time and average load voltage using acid electrolyte is spectacular particularly when compared with Figure 9.1 where porous carbon was used. This improvement is due to LiCl from the cell discharge being accommodated in the acid electrolyte.

At such low current densities (3 mA/cm^2), the rate of LiCl formation will be relatively low, thus the solution capacity to accommodate this product becomes significant. LiCl accommodation occurs either by precipitation on the surface followed by dissolution in the electrolyte, or by LiCl immediately reacting with the electrolyte solution to produce $LiAlCl_4$ as in equation (9.1). Redissolution of LiCl was shown to previously occur in Chapter 8 when a passivated glassy carbon cathode, left on open circuit 'rest' for half an hour, recovered some of its capacity for $SOCl_2$ reduction in 1.8M $LiAlCl_4$. However such redissolution is less likely to take place in a polarized cell, making the process given by equation (9.1) more probable [168]. Faradaic charge calculations show that 5.85 mg of LiCl per cm^2 of glassy carbon cathode are produced during the discharge process in acid electrolyte, with 0.31 mg in neutral electrolyte. Thus in acid electrolyte about 5.54 mg of LiCl, per cm^2 of cathode is accommodated into the solution before the onset of passivation. This amount is much less than the maximum quantity of LiCl which is required to neutralize the $AlCl_3$ present. Considering the situation for a porous carbon cathode discharged at 50 mA/cm^2, 25 mg of LiCl per cm^2 of cathode is produced, in acid electrolyte, with 17.5 mg in neutral electolyte. Clearly in this case most of the LiCl produced in the cell reaction is accommodated in the pores of the cathode, making the enhancement due to free $AlCl_3$ proportionately less.

(d) Free Lewis effects for high surface area carbon cathodes

So far for the cells employing porous carbon cathodes, the widely used type of amorphous carbon, Shawinigan Acetylene Black (SAB) has

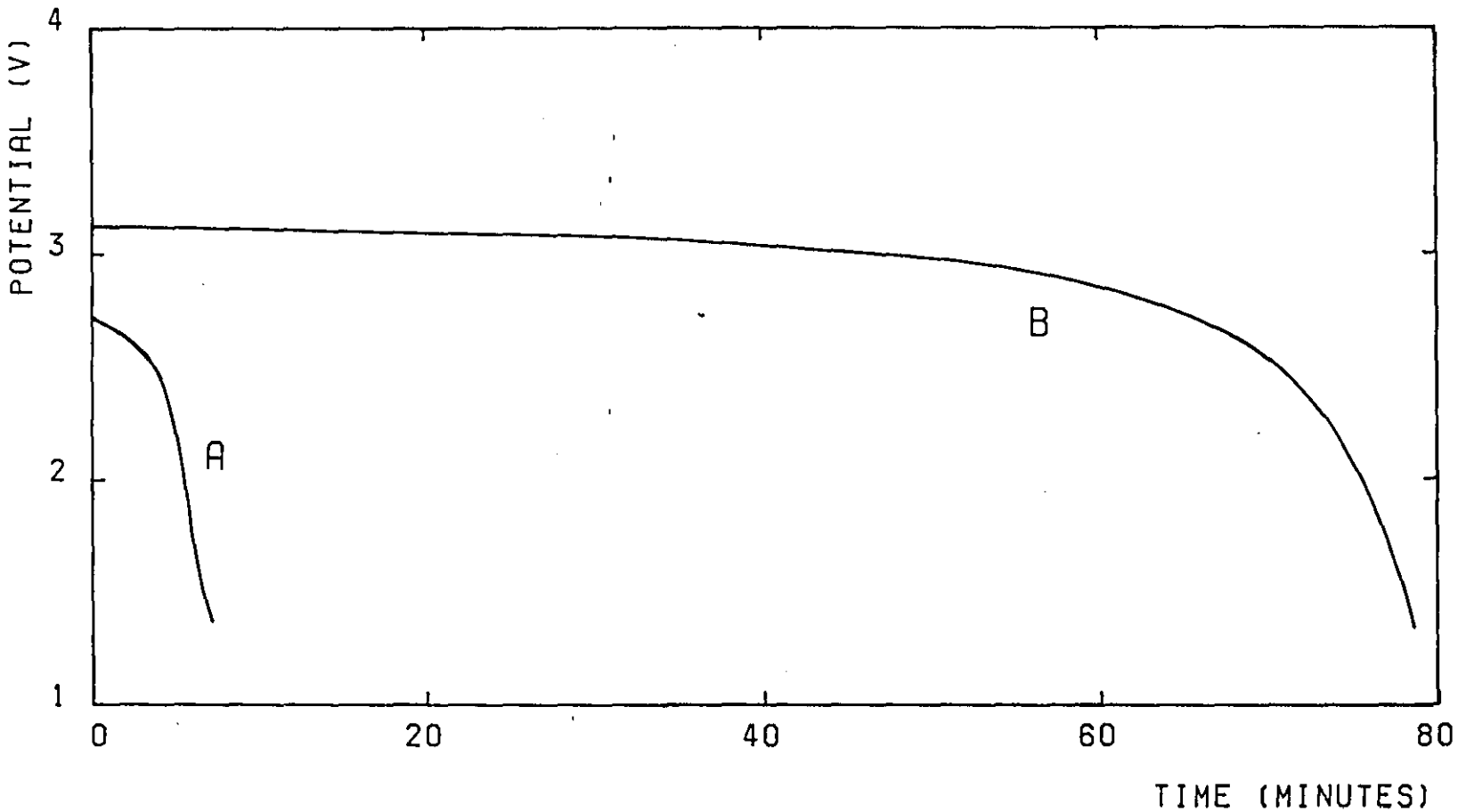

FIG 9.4 DISCHARGE PROFILES FOR CELLS CONTAINING GLASSY CARBON CATHODES COMPARING 1.8M $LiAlCl_4$ (A) AND 1.0M $LiAlCl_4$ + 2.0M $AlCl_3$ (B). CURRENT DENSITY =3mA cm^{-2}.

been employed. However, other carbon blacks are also used, in battery manufacture, one such being Ketchenblack EC (KEC). This particular carbon has a greater specific surface area and porosity than SAB and improves cell performance [67]. Figure 9.5 shows discharge curves for cells containing KEC cathodes in acid and neutral electrolyte. Clearly in neutral electrolyte, cells with KEC cathodes are superior in performance to those with SAB cathodes, exhibiting an increase in both cell voltage and active reaction time. This improvement is particularly significant at elevated temperature [71]. However there is little further enhancement of capacity by using acid electrolyte in conjunction with KEC cathodes. Thus the free Lewis acid is not able to improve the performance in an identical manner to that for cells containing SAB cathodes.

The nature of the 'acid step' differs also. Discharge curves for cells containing SAB cathodes show distinct plateaux around 3.3 V for about 90 seconds before the potential falls rapidly over a period of around 30 seconds to about 3.0V. For KEC cathodes the step is more like a voltage ramp between 3.55 and 3.2 V which lasts for about four minutes. This suggests that the process of equation (9.2) and the normal cell discharge process occur simultaneously during this period, the latter reaction becoming increasingly dominant.

Previous workers have found poor performances using acid electrolyte in cells containing catalysed carbon cathodes [83]. A 20% addition of iron to a SAB cathode was found to greatly increase cell capacity for cells containing neutral electrolyte. In acid electrolyte however the cell capacity was in fact less for the same cell containing neutral solution.

9.4 Conclusions

(1) The well established improvement in Li-$SOCl_2$ cell performance obtained by the use of free Lewis acid electrolytes has been confirmed. The optimum concentration of Al^{3+} ion present in an electrolyte was found to be 3.0 M. For low concentrations of Al^{3+}, cathode passivation due to LiCl precipitation is favoured and lithium corrosion is enhanced. If concentrations of Al^{3+} much higher than 3.0M are present, the reaction is hindered by excessive concentrations of large complex $AlCl_4^-$ based species.

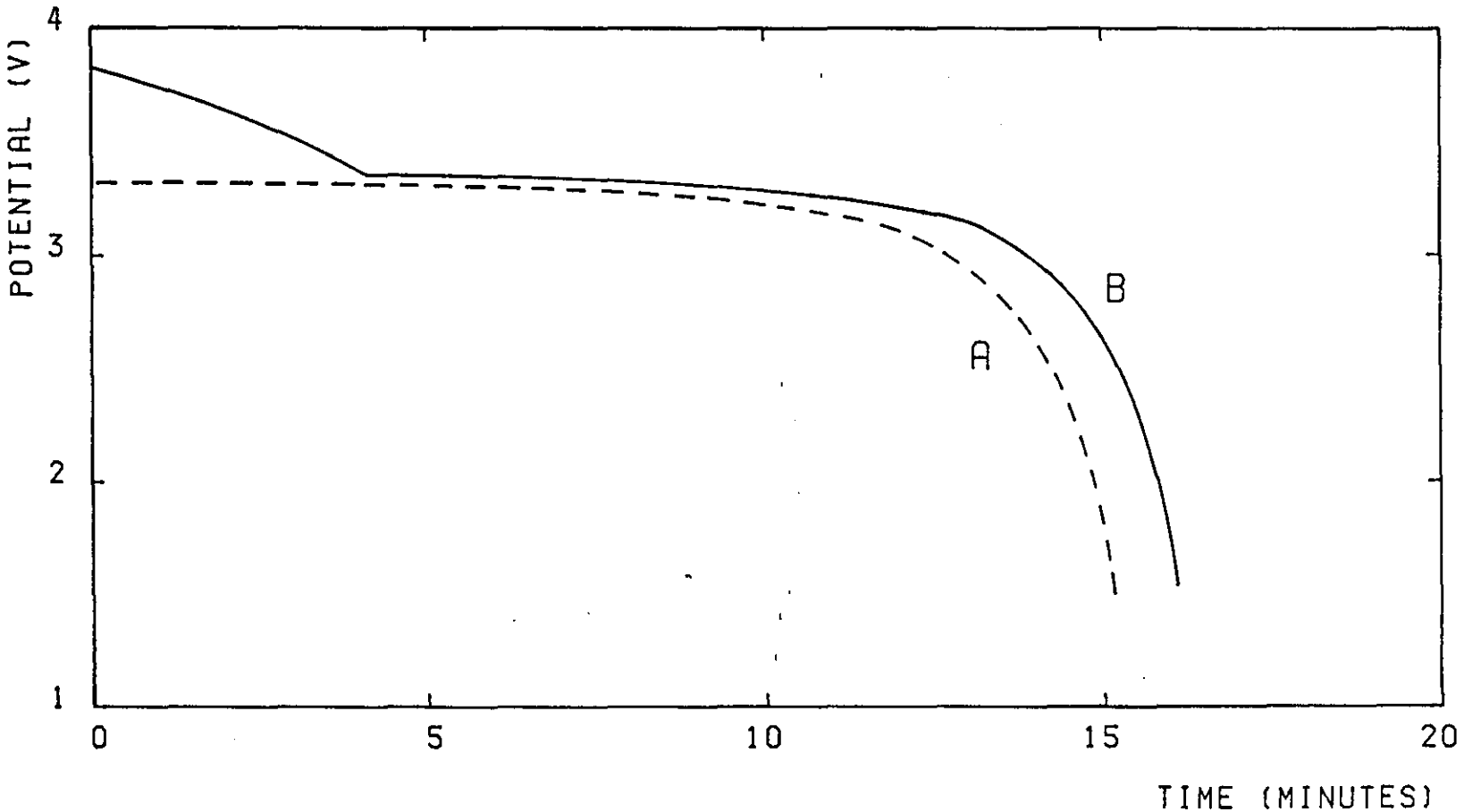

FIG 9.5 DISCHARGE PROFILES FOR CELLS CONTAINING CATHODES MADE FROM KETCHENBLACK CARBON: 1.8M $LiAlCl_4$ (A) AND 1.0M $LiAlCl_4$ + 2.0M $AlCl_3$ (B). CURRENT DENSITY =50 mA cm^{-2}.

(2) For an electrolyte solution based on 3.0M $AlCl_3$, the initial presence of LiCl enhances cell performances, due to an increase in solution conductance. The optimum initial concentration of LiCl under these conditions was found to be 1.0M, increasing quantities of LiCl were found to decrease the cell performance.

(3) The duration of the 'acid step' at the start of the cell discharge does not wholly account for the additional capacity obtained by using acid electrolyte.

(4) With low specific area carbons (glassy carbon in the limit) the beneficial effect of the free acid in the electrolyte is greatest. High specific surface carbons derive less benefit from free Lewis acid additions.

CHAPTER 10

DEPTH PROFILE ANALYSIS OF POROUS CARBON CATHODES

10.1 Introduction

Although the major emphasis of this chapter involves a study of LiCl product distribution throughout discharged porous carbon cathodes, two other aspects of Li-$SOCl_2$ cells are also discussed. A brief examination of the nature of impurities in lithium samples was carried out, after it was found that cells containing anodes from different sources, but similar in every other way gave different performances. Additionally, the effect of the cathode additive iron phthalocyanine on the cell performance was evaluated.

It was considered of interest to undertake a depth profile analysis of carbon cathodes from cells which had been discharged under various conditions. Such an investigation is useful since a knowledge of the way in which LiCl is distributed throughout discharged cathodes yields valuable information relating to the extent of utilization, and the mode of cathode failure. This is particularly relevant since the eventual blocking of this electrode by cell reaction products is generally regarded as the major reason for cell failure. As discussed in previous chapters a lot of Li-$SOCl_2$ cell research has centred on improving the performance of this positive electrode. Attempts have been made to increase the amount of LiCl which can be accommodated within the cathode matrix. Such methods include using high surface area and porosity carbon blacks [67], allowing the cathodes to swell during discharge [72, 73] and the use of poreformers [67].

An analysis of cathode reaction profiles has been undertaken previously by Dey and Bro [76] for low rate (2.4-4.9 mA/cm^2) cells. It was concluded by these workers that mass transport of the electrolyte through the porous carbon cathodes was the limiting factor, the cathode remaining under utilized at higher current densities. This work employed a technique for performing depth profile analyses of porous carbon cathodes from high rate cells (50-100 mA/cm^2). Much of the credit for the development of this technique must go to Martin Hayes and Leslie Teale, who initiated this study at the G.E.C. (Hirst) Research Centre.

10.2 Experimental

Electrode and electrolyte preparation are described in Chapter 4, the cathodes were prepared by pressing the carbon/PTFE mixture. The design of the PTFE electrolytic cell and the nickel stud current collector enabled easy recovery of an intact cathode for subsequent analysis.

After discharge at ambient temperature (20°C), the cell was dismantled and the cathode on its nickel stud mounting was removed. For some of the experiments the solute $LiAlCl_4$ was removed by immersion in $SOCl_2$ for 12 hours, then replaced, in fresh solvent for a further 12 hours. The carbon electrodes were allowed to stand in an argon filled dry box for 48 hours, in order to remove the solvent $SOCl_2$. All experiments so far described were carried out in an argon atmosphere.

The studs were then bolted to a stainless steel block which was mounted on a microtome. The alignment of the knife edge to the cathode was achieved by first using a plain nickel stud.

The carbon layer was then sectioned into 20 μm slices which were collected and washed with distilled water to dissolve the LiCl. The solution was subsequently filtered and analyses for lithium and aluminium ions were carried out. The lithium ion concentration was determined by atomic absorption spectroscopy, which was found to be the most satisfactory procedure. A colorimetric method was used to determine the aluminium ion concentration. For neutral electrolyte, the molar concentration of Al^{3+} ions is equal to that of the LiCl associated with the electrolyte. Therefore knowing the total concentrations of Li^+ and Al^{3+} ions, the quantity of LiCl produced from the cell reaction could be determined. A careful check was made during the calibration procedure for both analyses to ensure that neither the aluminium or the lithium ion interfered. This precaution was particularly important for lithium ion determination since it was demonstrated [188] using atomic emission spectroscopy that a high concentration of aluminium interferes with the determination of lithium ions. No such interference could be observed for this work however, probably because the concentration of Al^{3+} in the test samples was less than the concentration of Li^+, and because atomic absorption is a more selective technique than atomic emission.

The major errors in these experiments concerned the physical sectioning of the electrode and subsequent collection of all the material of interest. There was a reasonable degree of variance between the weights of successive slices of equal thickness. Because

of this it was necessary to combine some of the slices. There was also some uncertainty regarding the exact location of the first few slices.

Uniform current distribution radially across the electrode was demonstrated by removing small area sections from the centre and edges of the discharged cathode. This was achieved using a narrow cylindrical 'borer' to collect samples of reproducible size. After analysing each sample for Li^+ and Al^{3+}, no consistent variation in product distribution between samples from the edge and those from the centre of the electrode was observed. Any difference in values of ion concentrations between the samples for a given electrode were likely to arise from the non-uniform thickness of the layer across the stud.

Analyses of lithium samples were carried out by atomic emission spectroscopy (Section 4.5). Samples of lithium foil from two sources were exposed to a normal laboratory atmosphere until they became white and brittle, then were crushed into small pieces and left again until all of the lithium metal had hydrolysed. A weighed quantity of each sample was then dissolved in dilute hydrochloric acid, yielding a stock solution for the subsequent determination.

10.3 Results and Discussion

(a) Analysis of lithium samples

Discharge experiments on Li-$SOCl_2$ cells have shown that some lithium foil samples have proved unsuitable for battery manufacture due to reduced discharge times of up to 50% [71]. The impurity level of one such 'poor' sample was compared with a sample of lithium normally used in this work, from Lithco (the Lithium Corporation of America). The results showed that the amounts of calcium and potassium in each sample were approximately equal, however there was about five times as much sodium in the poor sample as in the Lithco sample, i.e. 0.023% in the poor sample compared to 0.0045% in the Lithco sample. The detrimental effect of this impurity has been confirmed by Hagan et al[71] who doped relatively pure lithium anodes with sodium. When discharged in high rate Li-$SOCl_2$ cells, increased sodium levels in the anode led to a corresponding drop in cell capacity. The way in which the sodium impurity limits the cell performance is not certain, although it is possible that sodium concentrates on the lithium surface during discharge and forms some sort of passivating film. Iron has been found to behave in this way [48]. Alternatively it may behave in a similar manner to calcium in

lithium sulphuryl chloride cells, which becomes complexed as $Ca(AlCl_4)_2$. This complex forms on the cathode where it is effective in blocking the active carbon surface [65]. An in depth study of the effect of the impurity level on anode passivation is currently being undertaken by Hagan [189].

(b) Depth profile analysis of discharged cathodes

Voltage profiles for cells discharged during this study are shown in figure 10.1. The results of subsequent depth profile analyses are shown in figures 10.2-10.5. The electrode depth is expressed as the distance from the electrode-electrolyte interface. These histograms are typical of many such profiles obtained during this study.

The results at 50 mA/cm^2 (Fig. 10.2) show that for a cathode discharged in neutral electrolyte there is a gradual decrease of LiCl in each cathode section on progressing from the front to the rear of the electrode. At 100 mA/cm^2 (Fig. 10.3) the decline in LiCl concentration towards the interior of the cathode is much sharper. The electrode is clearly not so well utilised at this higher current density. Anomalously low LiCl content in the first few slices, is likely to be due to these slices being incomplete. Additionally, some of the LiCl from the front face of the cathode may re-dissolve in the electrolyte solution, after the cell discharge.

The utilisations at these current densities confirm findings from previous work [190], which showed that the penetration depth of porous carbon cathodes decreases with increasing current density. This is in accordance with the theoretical predictions of de Levie [158]. Hayes and Teale [190, 191] carried out initial work, prior to this study under similar conditions; the results shown in figures 10.2 and 10.3 confirm their preliminary findings. For low rate cells [76] a similar relationship exists between current density and utilization, although the penetration depths are greater.

Pollard and co-workers [79,80] using a mathematical model calculated reaction distributions in the positive electrode of Li-$SOCl_2$ cells containing both neutral and acid electrolytes. The model, was essentially based on Ohms Law and the polarization kinetics for an electrochemical reaction, diffusion control was not considered. The contribution to the current control of the diffusion effects within the pore were therefore not considered. The interplay of the polarization due to current density decrease as the reaction penetrates the pores, was shown with an eventual enhancement of the current due

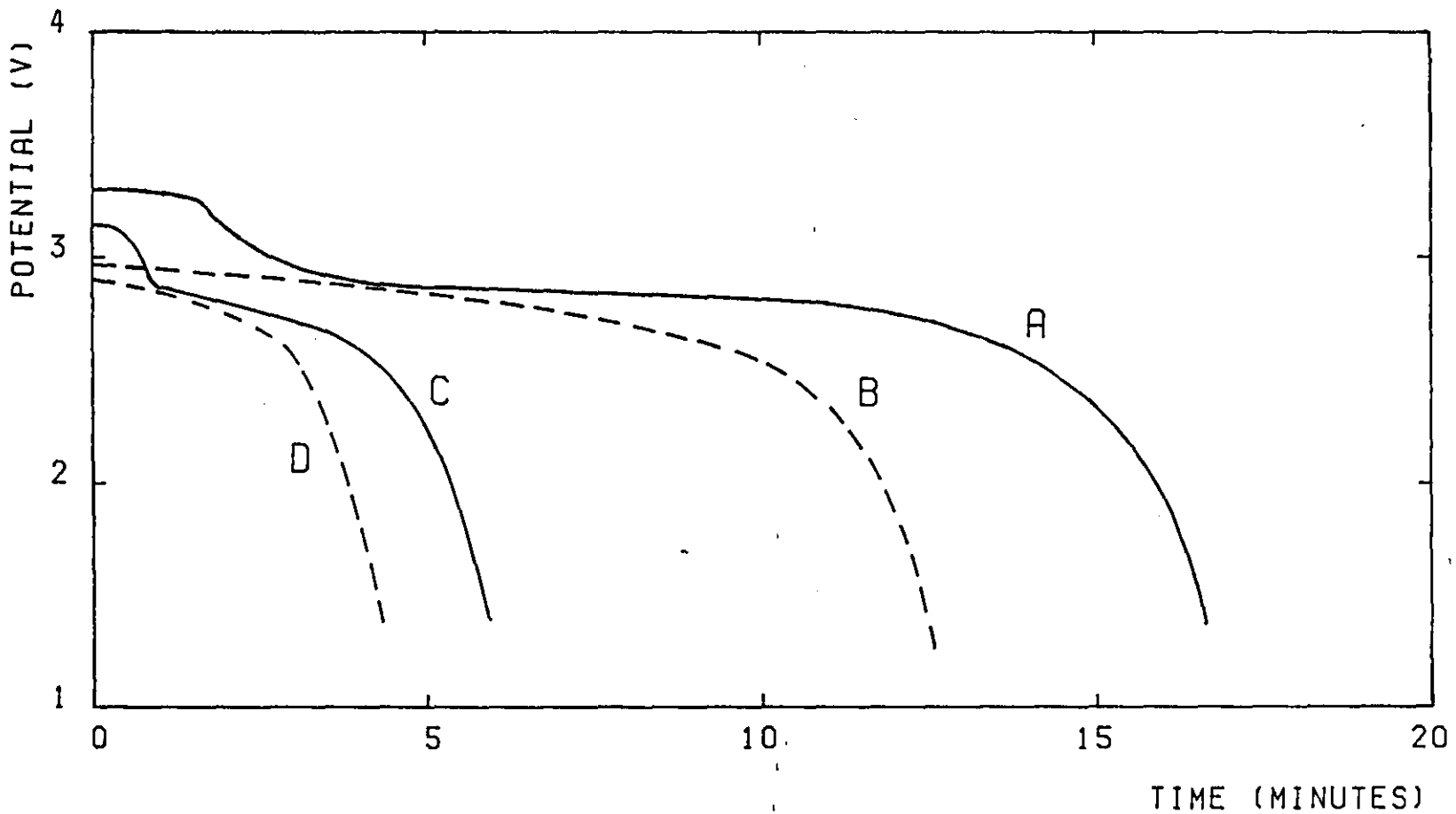

FIG 10.1 $Li-SOCl_2$ CELL DISCHARGES. (A) AT 50 mA cm^{-2} WITH 3.0M $AlCl_3$. (B) AT 50 mA cm^{-2} WITH 1.8M $LiAlCl_4$. (C) AT 100 mA cm^{-2} WITH 3.0M $AlCl_3$. (D) AT 100 mA cm^{-2} WITH 1.8M $LiAlCl_4$.

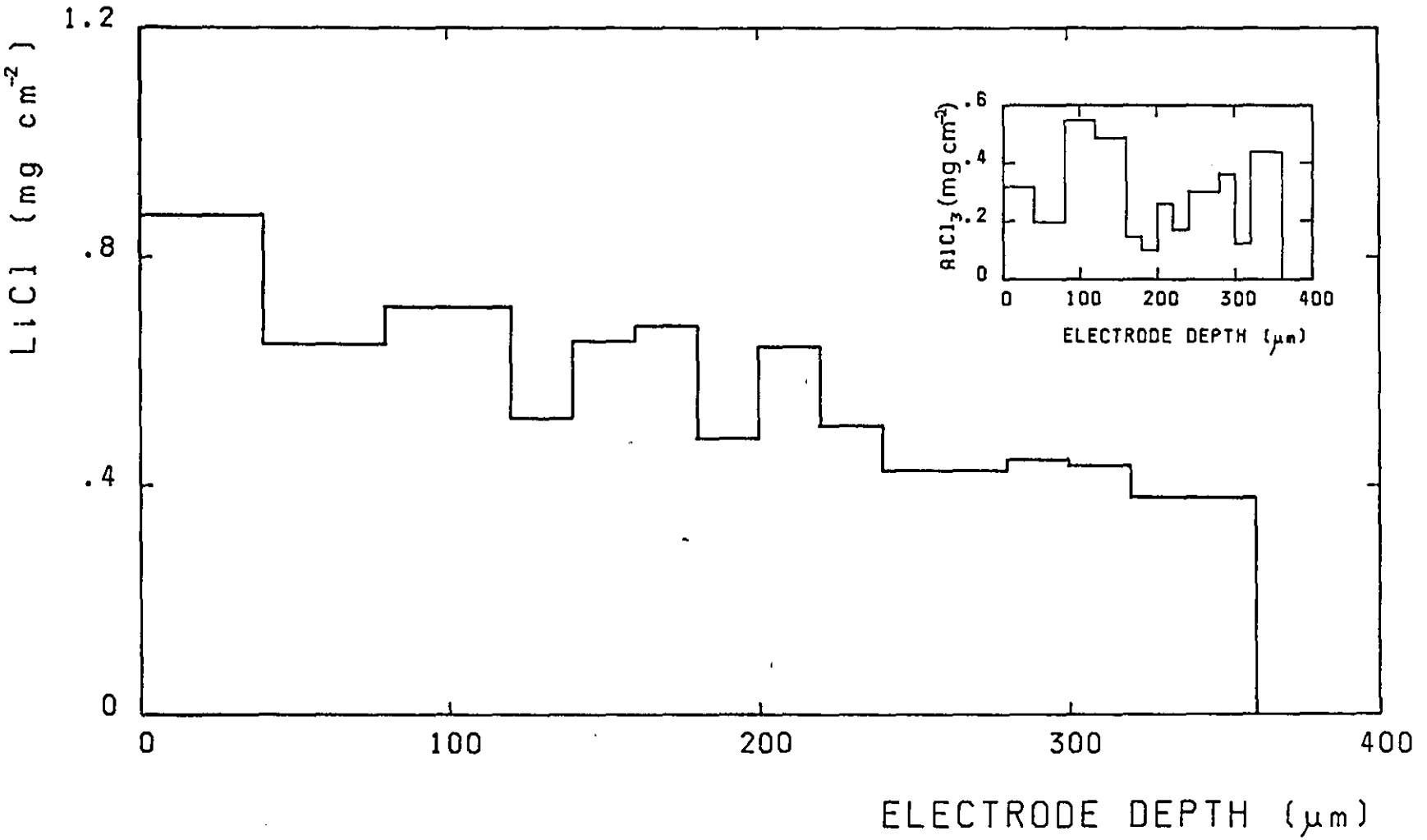

FIG 10.2 REACTION PROFILE. SHOWING LiCl DISTRIBUTION IN A CATHODE FROM A CELL DISCHARGED AT 50 mA cm^{-2} IN 1.8M $LiAlCl_4$. INSET SHOWS THE ALUMINIUM DISTRIBUTION.

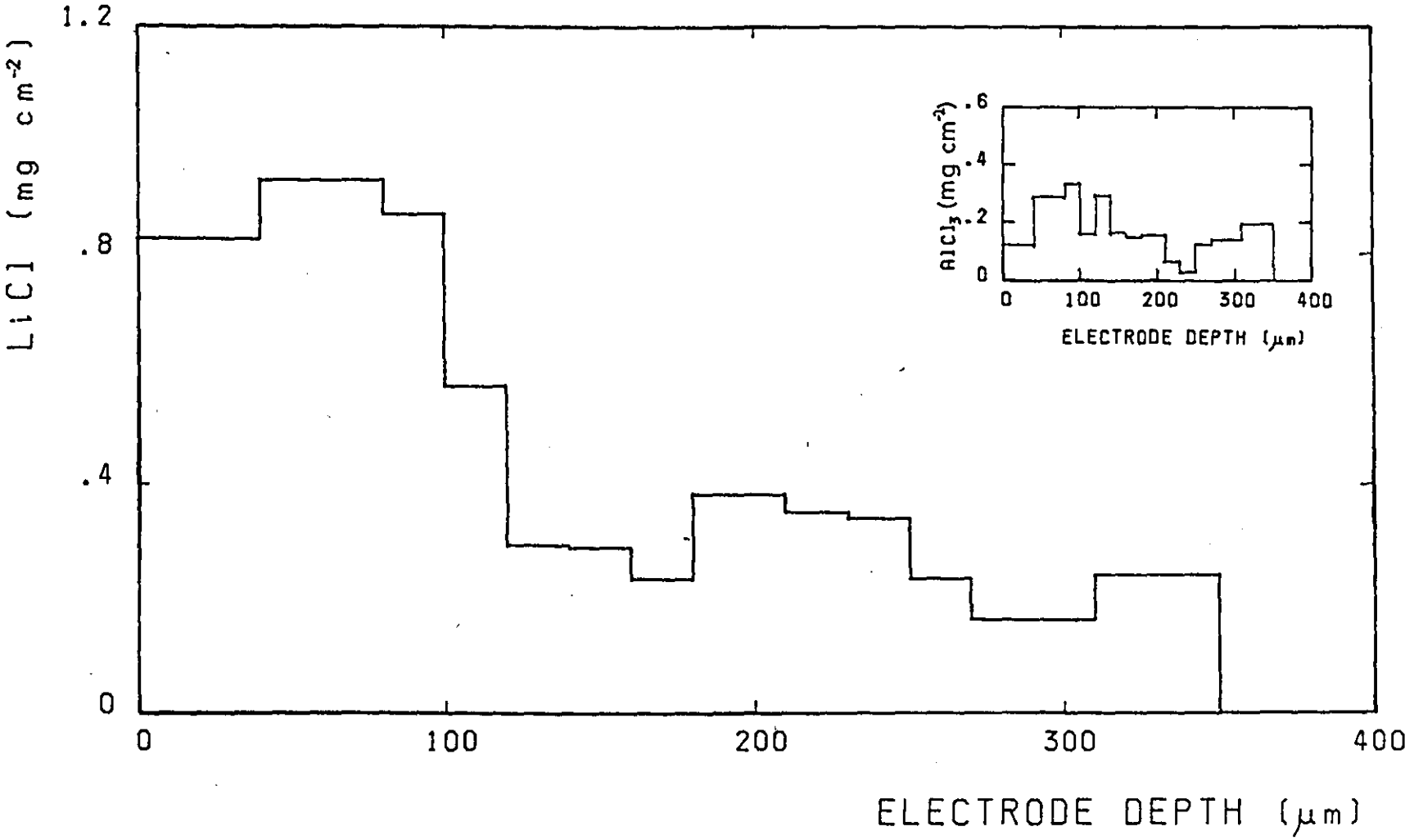

FIG 10.3 AS FIG 10.2 BUT AT 100 mA cm^{-2}.

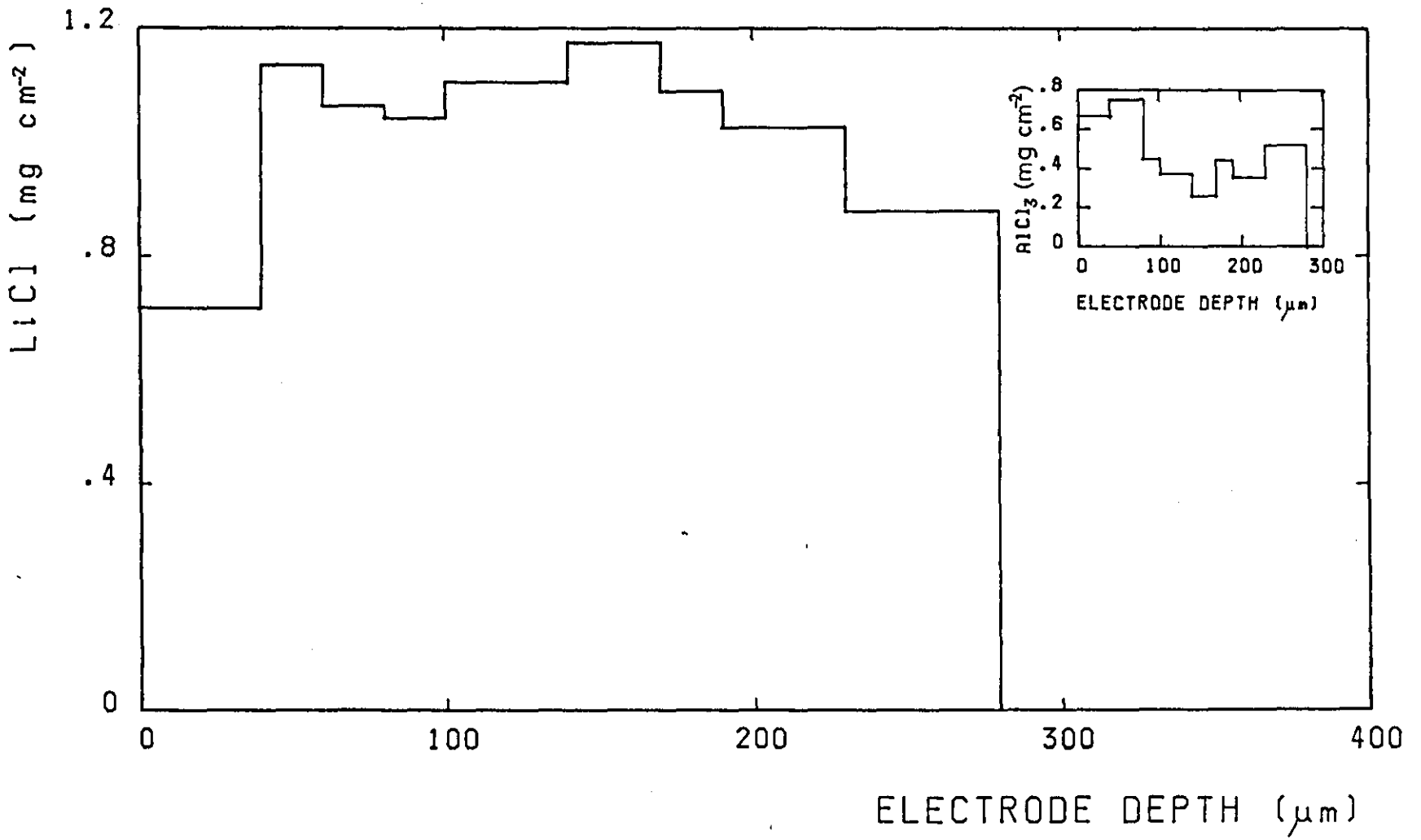

FIG 10.4 REACTION PROFILE, SHOWING LiCl DISTRIBUTION IN A CATHODE FROM A CELL DISCHARGED AT 50 mA cm^{-2} IN 3.0M $AlCl_3$. INSET SHOWS THE ALUMINIUM DISTRIBUTION.

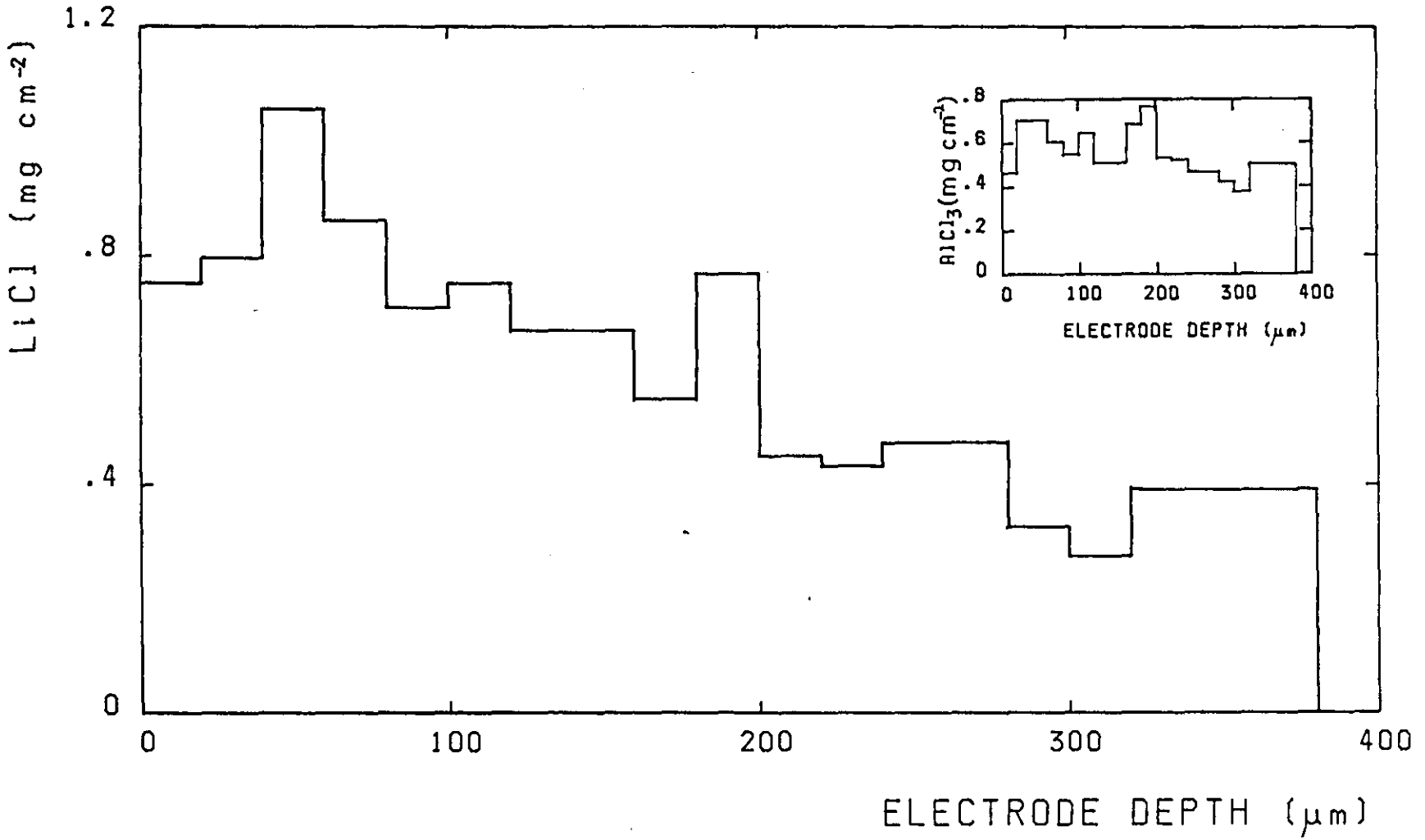

FIG 10.5 As FIG 10.4 BUT AT 100 mA cm^{-2}.

to reduced ohmic resistance near the inner current take off. The simulated current density was 80 mA/cm^2. The theoretical predictions were to some extent confirmed by EDAX analysis [72, 73]. The results presented in this section are largely in accordance with this mathematical analysis.

The results of the depth profile analyses for cathodes in cells containing 3.0 M $AlCl_3$-$SOCl_2$ electrolyte are shown in figures 10.4 and 10.5. It was difficult to distinguish between Li^+ ions from the LiCl product and Li^+ ions from the $LiAlCl_4$ which is produced as the $AlCl_3$ is neutralized. The histograms therefore show the total Li^+ ion resulting from the experiments, subtraction of the Li^+ ion associated with the Al^{3+} present may give misleading results, since it is unlikely that all of the $AlCl_3$ in the cell is neutralized by LiCl. However it was demonstrated that the profiles for such "corrected" Li^+ ion distribution were very similar in form to figures 10.4 and 10.5.

The results at 50 mA/cm^2 show great similarity to those obtained from cathodes discharged in neutral electrolyte, i.e. cathode utilisation at this current density is good, the interior of the positive electrode being well utilised. At 100 mA/cm^2 cathode utilisation is not as good as at 50 mA/cm^2 which agrees with theory [158] and past experience. Repeated results however have clearly shown that in acid electrolyte the utilisation of the interior of the cathode is greater than for 1.8 M $LiAlCl_4$ at the same current density. For neutral electrolyte, the initially high level of Li^+ ion at the front of the cathode falls off rapidly after the frist few slices. In acid electrolyte this decline in Li^+ concentration from the front to the rear of the cathode is more gradual.

Lithium ions are thought to be transported through the electrolyte by a 'hopping' type mechanism [104]. Therefore Li^+ ion transport in the neutral electrolyte is likely to be greater than in acid electrolyte because of the higher initial concentration of Li^+ ions. Taking only this factor and the greater conductivity of the neutral solution into consideration [103-105] one would expect the utilization in neutral electrolyte to be greater. This is because the lithium ions are more likely to be precipitated sooner in a solution which does not encourage their movement. In this instance however the poor ion transport in acid electrolyte is more than compensated for by the greater solubility of LiCl in a Lewis acid solution. This affinity for LiCl means that Li^+ ions are carried to the rear of the electrode where they are able to penetrate more effectively. Delay in the precipitation of LiCl means that Li^+ ions have the opportunity to accumulate within the

cathode pores, driven to the rear of the electrode by migration and the electrochemical reaction. The difference in utilisation between these electrolytes is further illustrated in figure 10.6 which shows how the ratio of LiCl to $AlCl_3$ varies with electrode depth for two of the cathodes studied. For 1.8M $LiAlCl_4$ there is a rapid fall in the magnitude of this ratio, for 3.0M $AlCl_3$ there is a gradual decline.

These results clearly indicate that for SAB cathodes the increased cell discharge time with acid electrolyte is not due to the delay in LiCl precipitation alone. Another major factor in the improvement is the increase in LiCl accommodation within the cathode matrix.

Charge calculations have shown that the amount of LiCl produced during the reaction was slightly less than the amount calculated. Although it is likely that this is due to the experimental errors inherent in such a determination, LiCl which becomes solubilised in the electrolyte [26, 94] may contribute to the difficiency.

The inserts in figures 10.2 to 10.5 show the distribution of Al^{3+} throughout the cathode. Although it is difficult to draw any clear conclusions from the results, it does appear that there is some direct correlation between the quantity of Li^+ ion and Al^{3+} ion in each slice. However further experiments are required to confirm this. One possible explanation for such a correlation is that sections of the cathode which contain large amounts of LiCl, will be depleted in $SOCl_2$. Since the volume of products of the Li-$SOCl_2$ cell are less than the reactant volume [26], these regions of $SOCl_2$ depletion will therefore have a higher concentration of Al^{3+}.

(c) Enhancement of cell performance by iron phthalocyanine

It was considered of interest to examine the effect of iron phthalocyanine (FePc) additions to the cathode. Figure 10.7 shows the improvement in cell performance attainable from FePc additions. Even as little as 0.5% w/w of FePc is sufficient to greatly enhance the cell capacity, as demonstrated in figure 10.8. The optimum FePc addition appears to be 1%, which is less than the amount used by other workers [74]. Figure 10.9 shows how the cell load voltage varies with iron phthalocyanine content. The highest load voltage is achieved by using a 5% addition. These results show that, even though iron phthalocyanine is very expensive compared to the cost of carbon blacks, the dramatic improvement in Li-$SOCl_2$ cell discharge due to relatively small additions, indicate that this compound may be an economically viable catalyst. It must be remembered that these experiments were carried out at ambient temperature, at 70°C the beneficial effect of

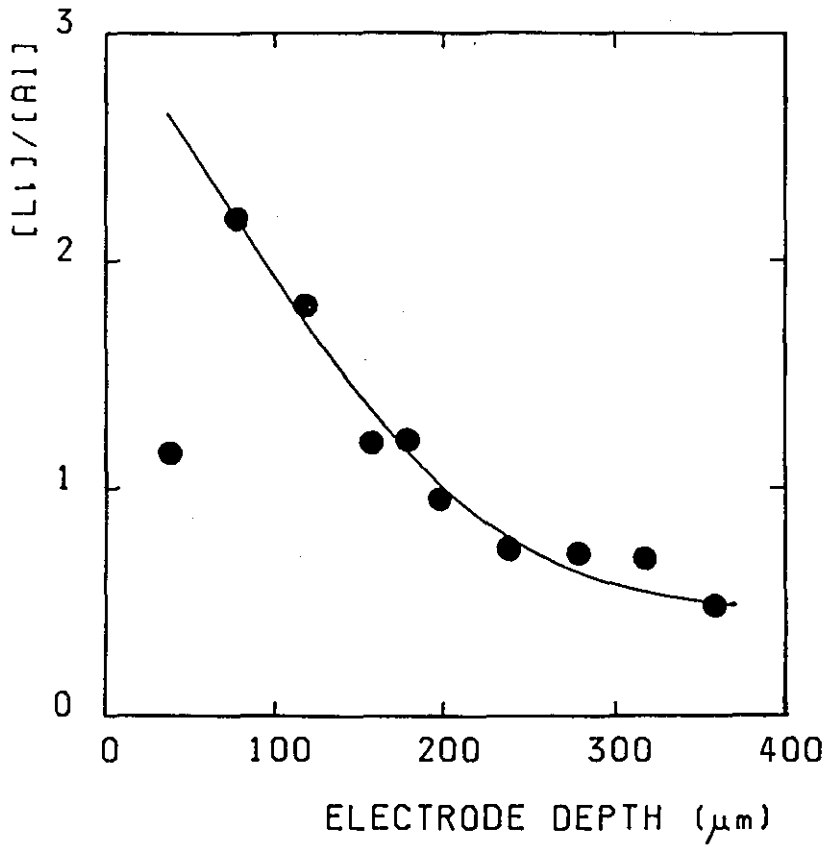

FIG 10.6(a) VARIATION OF THE RATIO Li^+/Al^{3+} WITH ELECTRODE DEPTH FOR A CATHODE DISCHARGED AT 100 mA cm^{-2}. IN 1.8M $LiAlCl_4$.

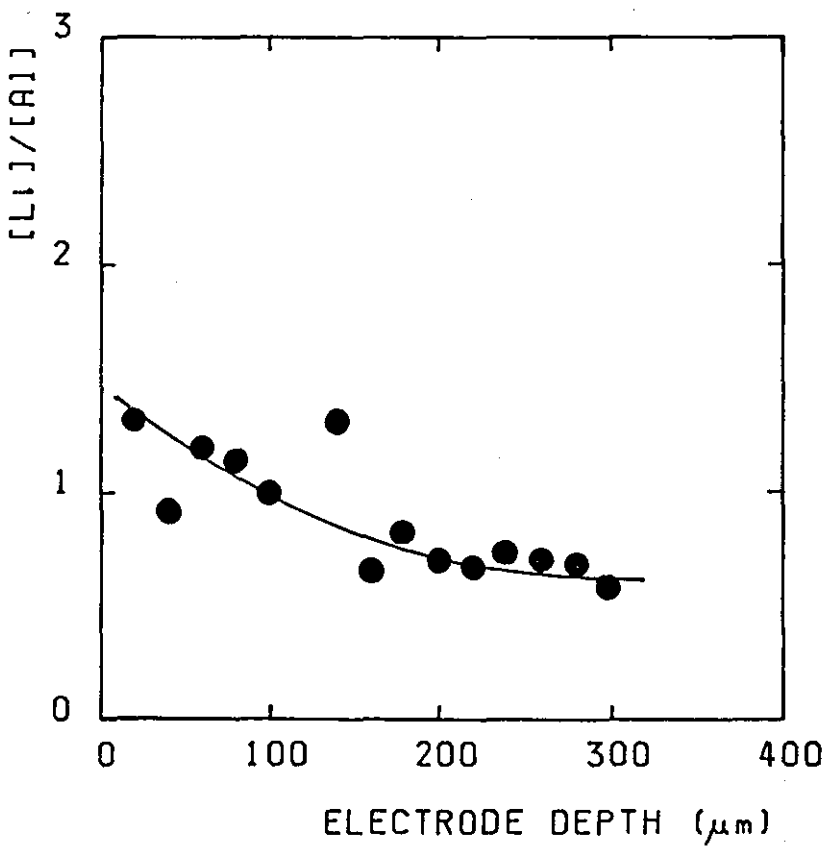

FIG 10.6(b) AS ABOVE BUT IN 3.0M $AlCl_3$.

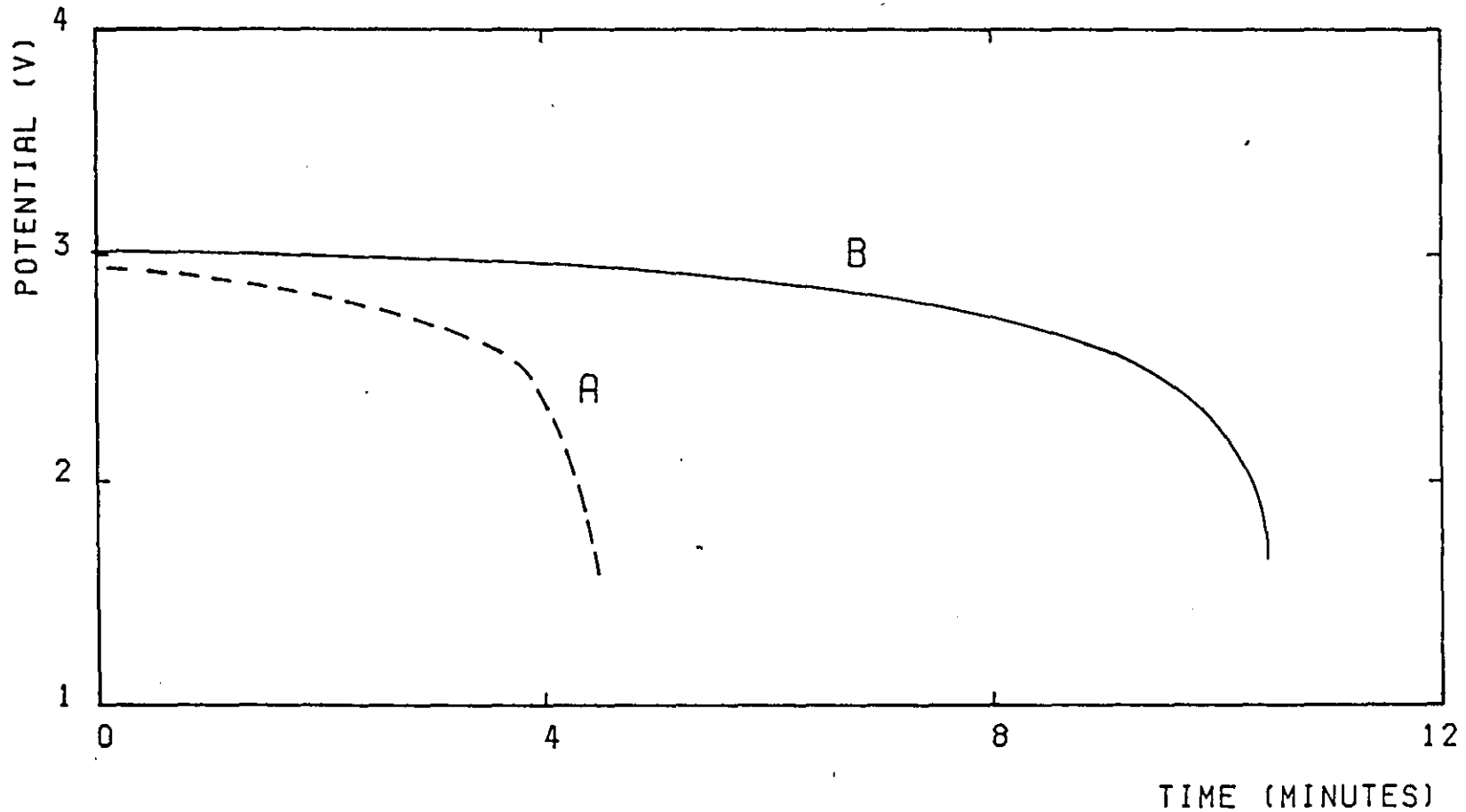

FIG 10.7 DISCHARGE CHARACTARISTICS OF Li-$SOCl_2$ CELLS AT 100 mA cm^{-2}. (A) IS FOR A CELL CONTAINING AN UNCATALYSED CATHODE. (B) CONTAINS A CATHODE ENRICHED WITH 1% IRON PHTHALOCYANINE.

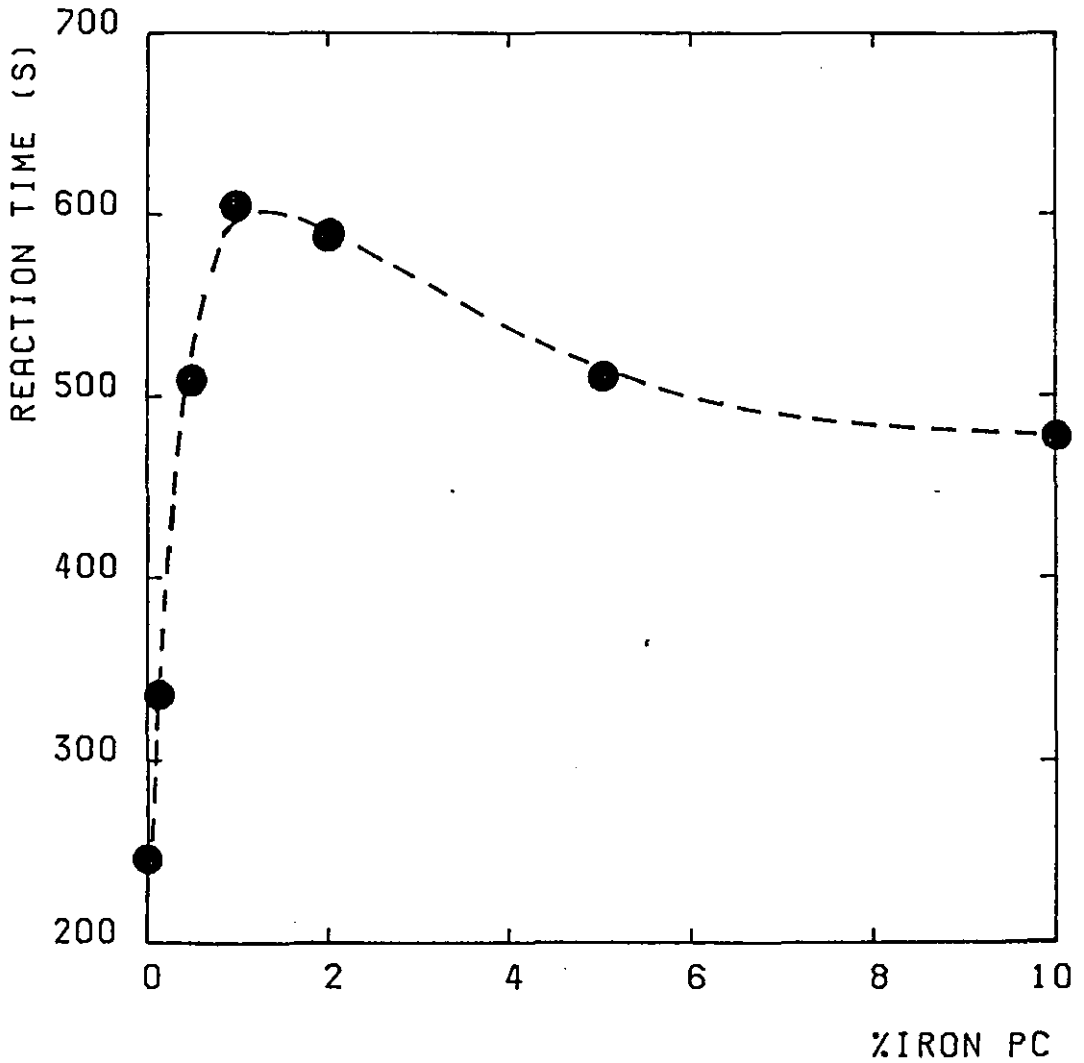

FIG 10.8 VARIATION OF CELL DISCHARGE TIME WITH AMOUNT OF IRON PHTHALOCYANINE (W/W) ADDED TO THE CATHODE.

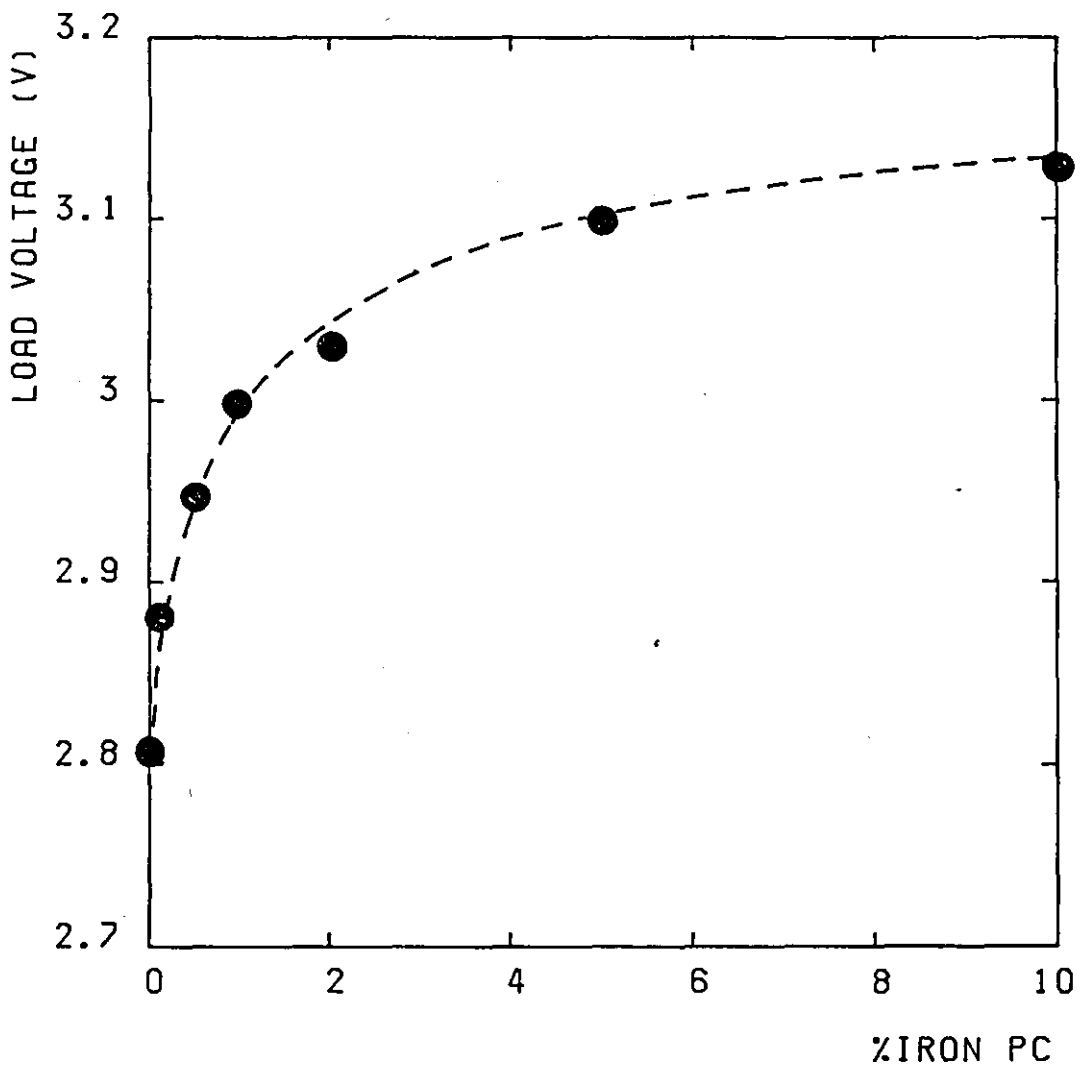

FIG 10.9 VARIATION OF CELL (INITIAL) LOAD VOLTAGE WITH AMOUNT OF IRON PHTHALOCYANINE (W/W) ADDED TO THE CATHODE.

this catalyst has been demonstrated to be greatly reduced [71]. Therefore FePc may not be a viable catalyst for high rate cells where a great deal of heat is generated.

It proved experimentally impossible to section the cathode as previously, the FePc seemed to alter the physical properties of the cathode making it more brittle and less adhesive to the nickel stud. Analysis of the Li^+ ion produced in the cathode as a whole showed good agreement with that predicted from charge calculations. However it is thought that not all of the Li^+ ion produced forms LiCl [86]. It was proposed that the mechanism was somehow altered, lithium dithionite being produced.

10.4 Conclusions

(1) Although the cathode is usually regarded as the performance limiting electrode, purity of the anode is important. Results show that lithium from one source giving poor performances in Li-$SOCl_2$ cells, contained a relatively high amount of sodium.

(2) Depth profile analyses of carbon cathodes from discharged Li-$SOCl_2$ cells have shown that utilisation is greater for current densities of 50 mA/cm^2 than for 100 mA/cm^2. This is consistent with the theory of de Levie. It also confirms the importance of selecting cathodes of suitable thickness, for a particular application.

(3) The cathode utilisation at high current density (100 mA/cm^2) is improved by using an electrolyte containing free Lewis acid. This is in accordance with the results of Chapter 9 which show that cell capacity increase using acid electrolyte is not due to LiCl complexation alone.

(4) An optimum concentration of the cathode additive iron phthalocyanine has been identified. For cells discharged at high rate a 1% addition was sufficient to greatly improve the on load voltage and capacity of the cell.

CHAPTER 11

FINAL DISCUSSION

11.1 Impedance Studies

From the results of Chapters 5-7, it has been demonstrated that the electrochemical behaviour of lithium and glassy carbon electrodes in $LiAlCl_4$-$SOCl_2$ solutions are influenced by the presence of a LiCl film. In Chapter 5 it was shown that the magnitude of the impedance of a lithium electrode in neutral electrolyte increased with storage time, indicating a film whose thickness increases continuously with time. The film also affects the shape of the impedance locus, yielding a flattened semi-circle usually characteristic of a porous electrode. In practice this film leads to voltage delay problems in lithium battery systems, which is discussed in detail in Chapter 2. Impedance spectra of a lithium electrode in a Lewis acid $AlCl_3$-$SOCl_2$ solution however, yielded near perfect semi-circles, which confirm that the free Lewis acid is able to remove the LiCl layer on the electrode. However, the initial presence of LiCl in the electrolyte appeared to allow some degree of film growth. Further work using scanning electron microscopy could be carried out to confirm these results.

In spite of this filming however it was still possible to obtain kinetic data for the Li^+/Li exchange in a 1.8 M $LiAlCl_4$-$SOCl_2$ solution (Chapter 5). This was achieved by analysing a series of impedance spectra, for the same electrode under various applied potentials. The data, after matching to a Randles equivalent circuit yielded values for various impedance parameters, including θ, the charge-transfer resistance. The influence of the film, which may alter the effective electrode area between experiments, was mitigated by including values of C_{dl}, the apparent double layer capacitance. The variation of C_{dl} was thought to give a reasonable indication of the way in which the electrode area varied. A value for α, the charge-transfer coefficient of 0.59 was obtained. From a similar study in 3.0 M $AlCl_3$-$SOCl_2$ solutions α was found to be 0.46. The difference in the extent of filming on the lithium electrode in neutral and acid electrolytes were reflected in values of i_o, the exchange current. These were

respectively 0.48 mA/cm^2 and 45 mA/cm^2 in neutral and acid electrolyte. This study could be extended further in order to examine the Li^+/Li exchange in other lithium battery solvents, in order that kinetic constants obtained can be compared.

Impedance studies on glassy carbon were less revealing although again the data was influenced by LiCl filming on the electrode, particularly during the cathodic process. It was clear that $SOCl_2$ reduction and oxidation reactions at glassy carbon electrodes are complex and do not easily yield kinetic data.

11.2 Cathode Studies

Chapters 8-10 are largely concerned with the carbon electrode and in particular with its passivation by a build up of LiCl within the pores. Because this is the main reason for cell failure it is of importance to understand how this cathode blocking process occurs so that eventually cell lifetime can be extended. The anode however can influence cell failure, in Chapter 10 it was shown that lithium electrodes yielding poor performances in Li-$SOCl_2$ cells contained relatively high levels of sodium impurity. In Chapter 10, the way in which LiCl is deposited within the cathode was determined using depth profile analysis. This study was particularly revealing since it confirmed and extended further the findings of Chapters 8 and 9.

One clear observation to emerge from Chapter 8 was that a limiting thickness of carbon cathode is reached, beyond which further increases yield little improvement in reaction time. This limiting value, which corresponds to the penetration depth was found to be $\sim$400 μm. This penetration depth does however vary according to the current density used. This was clearly demonstrated by the depth profile analyses of Chapter 10 which showed that for a cathode discharged at 100 mA/cm^2, the distribution of LiCl is largely towards the side of the electrode which faces the anode. At 50 mA/cm^2 however the distribution was more uniform, with a lesser decline in LiCl precipitation from the front face to the interior of the cathode. Electron micrographs of cathode interiors could also be used to qualitatively indicate the extent of cathode utilization. This is a possibility for further investigation.

The reaction product, LiCl is not entirely insoluble in the electrolyte however, as demonstrated by the ability of a passivated glassy carbon cathode to recover much of its capacity for $SOCl_2$ reduction, on standing in neutral electrolyte. This factor along with the observed linear $\tau^{-\frac{1}{2}}$ vs i, Sand equation behaviour suggested that

the cathode reduction process is largely controlled by diffusion of LiCl away from the cathode. Passivation of a carbon surface occurs as the solution capacity for LiCl immediately surrounding it is exceeded and so LiCl is precipitated. When the whole electrode is passivated in this way, cell failure occurs. Further work involving potential step measurements at carbon surfaces may yield additional information about the cathode failure mechanism.

In Chapter 9 the previously observed benefits of free Lewis acid in the electrolyte were confirmed. An optimum electrolyte composition was obtained for this work, which contained 3.0 M $AlCl_3$ and 1.0 M LiCl. In such a solution the effects of solution conductivity, viscosity and LiCl accommodation by free Lewis acid were balanced to optimise the electrolyte. The results of Chapter 9 along with depth profile analyses of discharged cathodes (Chapter 10) showed that $AlCl_3$ in the electrolyte improved cell lifetime not only by accommodating more LiCl in the solution, but actually increased the cathode utilization, allowing more LiCl to be precipitated in the cathode. In view of this it would be interesting to see whether a greater limiting thickness of cathode is possible with acid electrolyte, than was for neutral electrolyte (Chapter 10). Free $AlCl_3$ in the electrolyte was found to be more effective for carbon blacks with lower BET surface areas. This was dramatically illustrated in the extreme case of a glassy carbon cathode whose lifetime was increased over 20 fold when a Lewis acid electrolyte was employed.

Two methods of cathode fabrication were employed during this work. For some experiments a carbon-PTFE-solvent mixture was sprayed onto nickel studs, for others the more usual method of dry pressing was used. Comparisons of cells containing cathodes prepared by these two methods show that gravimetric energy densities are the same, but in terms of volumetric capacity (Ah cm^{-3}) pressed cathodes yielded superior performances. From a technological view point however, spraying cathodes may have advantages for mass production.

The effects of iron phthalocyanine additions to the cathodes were briefly evaluated in Chapter 10. It was found that as little as 0.5% significantly increased the cell performance. It would be interesting to carry out further work in order to reveal the nature and extent of the blocking deposits under these conditions.

APPENDIX 1

Numerical Analysis of Impedance Data

Using a mainframe computer it is possible to analyse data from impedance spectra of electrochemical systems. The impedance of such a system can usually be represented by a network of resistors and capacitors, from which electrochemical parameters of interest can be obtained (Section 3.6). A relatively straightforward analogue is the Randles equivalent circuit (fig. 3.6.2) for which the overall impedance may be written as:-

$$Z = R_{\Omega} + \frac{1}{j\omega C_{dl} + \left[\frac{1}{\theta + \sigma\omega^{-\frac{1}{2}} - j\omega^{-\frac{1}{2}}}\right]} \qquad (A.1.1)$$

The symbols above are all as defined in Section 3.6.

The task is to calculate, in this case, R_{Ω}, θ, σ and C_{dl} from the impedance data. Firstly approximations to these values must be made such that

$$R_{\Omega} = R_{\Omega}' + \Delta R_{\Omega} \quad (i) \qquad (A.1.2)$$

$$C_{dl} = C_{dl}' + \Delta C_{dl} \quad (ii)$$

$$\theta = \theta' + \Delta\theta \quad (iii)$$

$$\sigma = \sigma' + \Delta\sigma \quad (iv)$$

where x' values refer to approximations and Δx to the difference between the approximations and the real values.

The objective of this analysis is to reduce the Δx values as much as possible by successive iteration.

Using Taylors theorem and only the first order terms, we can say:

$$Z_{cell} = Z'_{cell} + \left(\frac{\delta Z_{cell}}{\delta R_\Omega}\right)' \Delta R_\Omega + \left(\frac{\delta Z_{cell}}{\delta \theta}\right)' \Delta\theta + \left(\frac{\delta Z_{cell}}{\delta \theta}\right)' \Delta C_{dl} + \left(\frac{\delta Z_{cell}}{\delta \sigma}\right)' \Delta\sigma \qquad (A.1.3)$$

Where Z'_{cell} is a value for the impedance using the estimated values of the impedance parameters. The dashes indicate that the value of the derivative is to be taken at the approximate value of the parameter.

(A.1.3) is linear for Δx values and can thus be solved. However, due to neglect of second and higher order terms of the Taylor expansion the Δx values will be incorrect. The new values for the impedance parameters must be treated as new approximations and the procedure repeated.

Let us consider a general case as opposed to a Randles circuit, since an electrode analogue may consist of a number of resistances and capacitances, possibly including a roughness factor.

Consider a circuit with n impedance parameters $(P_1, \ldots . P_i)$

$$\text{let then: } D_1 = \left(\frac{\delta Z_{cell}}{\delta P_1}\right)', \quad D_2 = \left(\frac{\delta Z_{cell}}{\delta P_2}\right)', \quad D_i = \left(\frac{\delta Z_{cell}}{\delta P_i}\right)' \qquad (A.1.4)$$

$$Z'_{cell} - Z_{cell} + D_1\Delta P_1 + D_2\Delta P_2 + \ldots + D_n\Delta P_n = 0 \qquad (A.1.5)$$

or

$$Z'_{cell} - Z_{cell} + \sum_{i=1}^{n} D_i\Delta P_i = Z'_{cell} - Z_{cell} + \Delta Z = 0 \qquad (A.1.6)$$

If N represents the number of data points where N>>n, a least square type regression can be performed. For any particular frequency

$$Z_{cell} - Z'_{cell} - \Delta Z = E \qquad (A.1.7)$$

where E represents the error.

The best fit for N number of points is obtained when (E^2) is at a minimum. From the least squares method:

$$E^2 = (Z_{cell} - Z'_{cell})^2 - 2(Z_{cell} - Z'_{cell})\Delta Z + (\Delta Z)^2 \qquad (A.1.8)$$

For ΣE^2 to be a minimum:

$$\frac{\delta \Sigma E^2}{\delta \Delta Pi} = 0 \qquad (A.1.9)$$

Or by expanding equation (A.1.8):

$$\frac{\delta \sum_{k=1}^{N} E^2}{\delta \Delta Pi} = 2 \sum_{k=1}^{N} [D_{i,k}\{\Delta P_i + \sum_{j=1}^{n} D_{j,k} \Delta P_j \delta_{i,j} - (Z_{cell} - Z'_{cell})_k\}] = 0 \qquad (A.1.10)$$

where $\delta_{ij} = 0$ when i=j and is 1 otherwise. Thus n simultaneous equations are obtained with $P_i, P_2 \ldots$ Pn as unknowns.

These are called normal equations and are general to the N data points. To obtain the ΔP_i quantities these normal equations are solved using a method of matrix inversion. Thus new values of P_i are obtained. These may be substituted back into the equations and the process is repeated, until the value of ΣE^2 becomes constant, resulting in an accurate value of P_i.

Initially in the process, if the approximations were poor the ΔP_i values will oscillate badly about zero and may if too large keep increasing, so causing the program to crash. To prevent this it is possible to use only a fraction of this ΔP_i value for the initial few interactions, increasing this fraction as the results converge.

The main program used for this work calls a subroutine which contains an expression for the impedance of the particular analogue circuit used. For a new electrode analogue therefore it is necessary to write a new subroutine.

APPENDIX 2

Controlling the F.R.A. through the I.E.E.E.

With the development of the microprocessor, came a quick and effective means of data acquisition and analysis. Digital control of electrochemical experiments provides precision and stability, the data obtained is readily available for easy analysis and presentation.

For these experiments a NEC PC-8001B microcomputer was used, this was connected to disc drives and a PC-8011B expansion unit. The latter unit contains the IEEE-488 interface bus used to communicate or 'talk' with the FRA.

The technique employed for data transmission is known as 'polling'. Using a serial poll each bit of information is sent sequentially on a single channel. A parallel poll is one with sufficient wires for all bits in a word to arrive simultaneously at the interface, i.e. eight wires. The IEEE-488 interface can connect up to 10 devices together in a parallel poll. It allows all devices to receive data output on the interface bus, while prohibiting more than one device from sending data at any one time.

The PC-8011B acts as controller, controlling the other devices, also having a talker function to send data over the bus lines and a listener function to receive data. Other devices may act as talkers, listeners or both, the FRA being in the latter class.

All talkers and listeners have addresses by means of which the controller can control the interface bus. The controller will first output an address onto the IEEE bus, indicating the devices between which data is to be transferred, all devices receive this. After completion of this, data transfer takes place between the talker and listener who have just been designated by their addresses.

The IEEE contains 16 signal lines which are divided into three groups as follows:

(1) Data lines [DIO1-DIO8], these are bidirectional data bus lines.

(2) Handshaking lines, which are abbreviated as follow.

DAV - when a low signal is given, data transmitted from any device is valid.

NRFD - a low signal indicates that this device is busy and not ready for data.

NDAC - a low signal indicates that the listener has not completed data reception.

N.B. Handshaking refers to communication between two parts of a system, the receiving end confirms that it has received something. Each line is controlled by a single binary digit, thus transmits 0, a low signal or 1 a high signal.

(3) Management lines:

ATN - a low signal means that the interface bus is in control mode, control signals are also to be sent to the IEEE.

REN - a low signal places each device in a remote state.

IFC - a low signal clears the interface.

SRQ - a low signal indicates that a device is requiring service from the controller; who polls each device in turn in order to discover who sent the signal.

EOI - a low signal indicates a delimiler.

The status of the handshaking and management lines can be stored using a single byte, known as the status byte. This consists of eight bits each indicating whether the line is active (low) or inactive (high). Any of the bits may be 'set' to low or reset to high. A fortran program, 'Fimp' was used to control the FRA by calling a number of assembly language subroutines. These routines actually performed the operations which controlled the FRA. It was important that the software was compatible with other machines in the laboratory which used the CP/M operating system. Assembly language routines have a short response time, which means that the results output from the FRA are received and stored in the computer memory very quickly.

Extensive detail of how the PC-8011B communicates with the FRA would require the reader to be familiar with Z-80 assembly language, however using simple alogrithms it is possible to demonstrate the principles involved.

A routine known as 'talker' is used to enable direct communication between the NEC PC-8011B and the FRA. This routine was called many times during the program, when it was required to transfer data between devices. The term data refers to any information, numerical or otherwise. A flow diagram showing the stages involved in data transmission via this routine, is displayed (Fig. A2.1).

Writing data to and reading data from the FRA data store are as outlined below:

Writing into the Data Store

(1) A message is constructed, for output.
(2) This message is stored, the ATN signal is set.
(3) The NEC talk address and the FRA listen address are placed on the IEEE using 'talker'.
(4) The ATN signal is reset, it is not required for data transmission.
(5) The data to be transmitted (latch store address) is assembled.
(6) The data is transmitted using 'talker'.

Reading the Data Store

(1) Space is reserved for the message which shall be received, the ATN signal is set.
(2) The NEC talk address and FRA listen address are placed on the IEEE using 'talker'.
(3) The ATN signal is reset, the data, telling the FRA which latch store address is required to be read is transmitted.
(4) ATN is again set, the NEC listen address and FRA talk address are transmitted to the IEEE. ATN is reset.
(5) The FRA is told that the NEC is not ready for data, i.e. the NRFD signal is transmitted.
(6) Space previously reserved for data is retrieved, the NRFD signal is reset.
(7) The NDAC signal is set, telling the FRA not to send data until the FRA is ready.
(8) The NEC asks the FRA if the data is available when it is, the data is received.
(9) Once data is received and accepted by the NEC, the FRA will reset the DAV signal indicating that data is no longer available.

(10) If the last data received signifies a line feed, this signals that the FRA talking has finished. [Go to 12]. A carriage return signals that more data is still to come.

(11) The data is stored. [Go to 6].

(12) The data is retrieved by the computer and converted into decimal format.

The procedures outlined previously represent the basis of interfacing the FRA with the microprocessor.

FIGURE A.2.1 DATA TRANSFER VIA THE IEEE

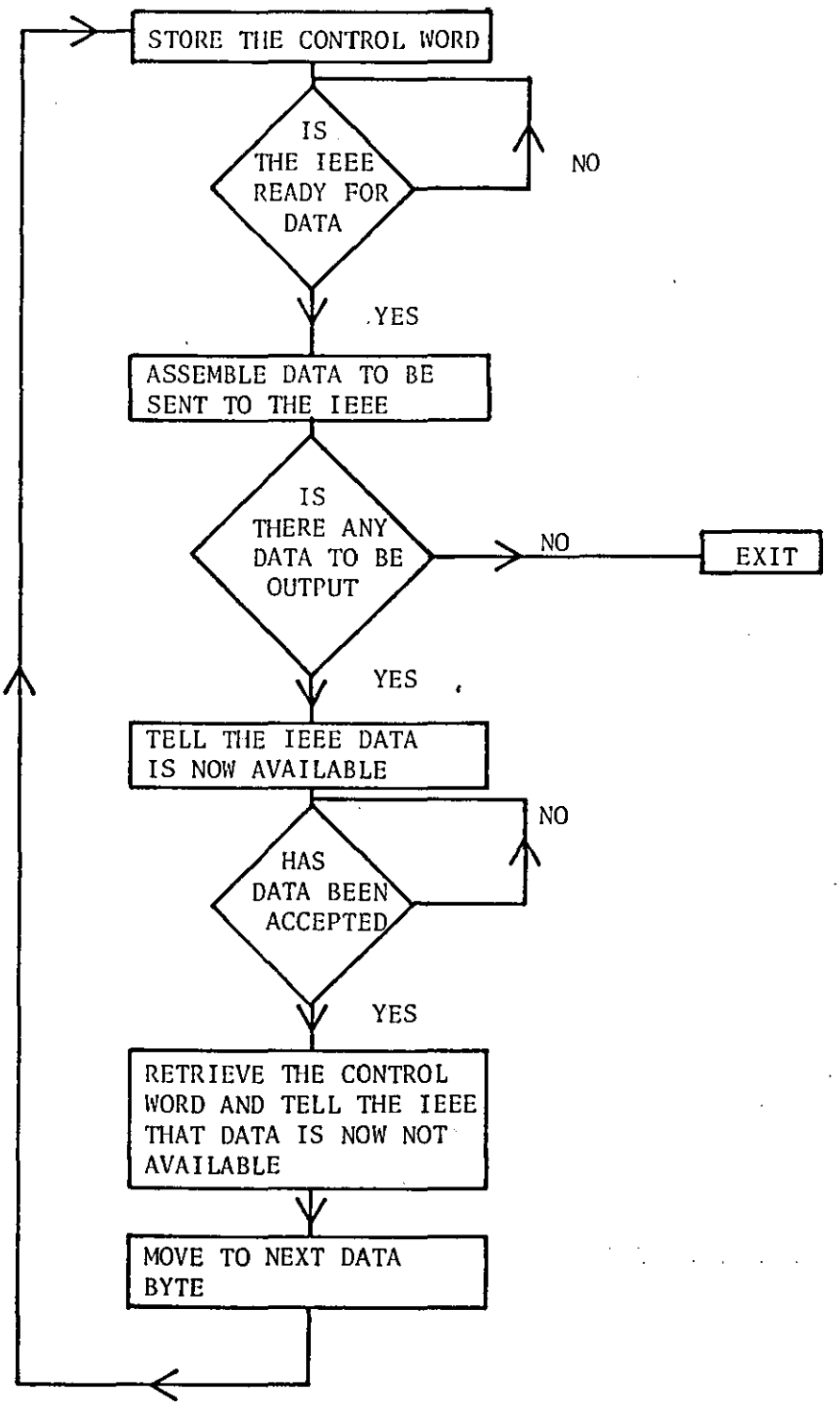

REFERENCES

[1] M. Hughes, N.A. Hampson and S.A.G.R. Karunathilaka, J. Power Sources, 12, (1984), 83.

[2] C.R. Schlaikjer in "Lithium Batteries", J.P. Gabano (ed.), Academic Press, London (1983), 303.

[3] J.P. Gabano, French Pats., 1, 583, 804(1969); 2,079, 744 (1971).

[4] G.E. Blomgren and M.L. Kronenberg, German Pat., 2,262, 256 (1972).

[5] J.J. Auborn, K.W. French, S.I. Lieberman, V.K. Shah and A. Heller, J. Electrochem. Soc., 120, (1973),1613.

[6] W.K. Behl, J.A. Christopulos, M. Ramirez and S. Gilman, J. Electrochem. Soc., 120, (1973) 1619.

[7] H. Spandau, A. Beyer and F. Preugsehat, Z. Anorg. Algem. Chem., 306, (1960), 13.

[8] J.R. Driscoll, G.L. Holleck and D.E. Tolland, Proc. 27th Power Sources Symposium, Atlantic City, New Jersey, (1976), 28.

[9] A.N. Dey and C.R. Schlaikjer, Proc. '26th Power Sources Symposium, Atlantic City, New Jersey, (1974), 47.

[10] L.A. Beketaeva, 28th International Society of Electrochemistry meeting, Varna, Bulgaria, Paper 150, Vol. 2, (1977), 643.

[11] A.N. Dey, J. Electrochem. Soc., 123, (1976), 1262.

[12] N. Marincic, Power Sources 6, D.H. Collins ed., Academic Press, London (1977), 506.

[13] C.R. Schlaikjer, F. Goebel and N. Marincic, J. Electrochem Soc., 126, (1979) 513.

[14] J.C. Bailey and J.P. Kohut, Power Sources 8 (J. Thompson ed.), Academic Press, London and New York, (1981), 17.

[15] W.K. Behl, J. Electroanal. Chem., 101, (1979), 267.

[16] H.V. Venkatasetty, J. Electrochem. Soc., 127, (1980), 2531.

[17] W.L. Bowden and A.N. Dey, ibid., 127, (1980), 1419.

[18] N.K. Istone and R.J. Brodd, ibid., 129, (1982), 1853; 131, (1984) 2467.

[19] W.K. Behl, ibid., 127, (1980), 1444.

[20] M.J. Madou and S. Szpak, ibid., 131, (1984), 2471.

[21] H.V. Venkatasetty and D.J. Saathoff, ibid., 128, (1981), 773.

[22] G.E. Blomgren, V.Z. Leger, T.A. Kalnoki-Kis, M.L. Kronenberg and R.J. Brodd, Power Sources 7, J. Thompson ed., Academic Press, London and New York (1979), 583.

[23] R. Williams, F.D. Tsay, S. Kim, M. Evans, Q. Kim, A. Rodriguez, B.J. Carter and H. Frank, Proc. Symp. Lithium Batteries, A.N. Dey ed., publication 84-1 (1984), 60.

[24] B.J. Carter, R.M. Williams, F.D. Tsay, A. Rodriguez, S. Kim, M. Evans and H. Frank, J. Electrochem. Soc., 132, (1985), 525.

[25] V.A. Mozalevskaya, V.P. Ponkratov, N.V. Shavrin and V.N. Dam'e, Soviet Electrochem., 21, (1985), 327.

[26] N. Marincic, in Modern Aspects of Electrochemistry, Vol. 15, ed. by R.E. White, J. O'M. Bockris and B.E. Conway, Plenum Press, New York and London (1983), 167.

[27] A.N. Dey and P. Bro, Power Sources 6, D.H. Collins ed., Academic Press, London and New York, (1977), 493.

[28] A.N. Dey, Electrochem. Acta., 21, (1976), 855.

[29] S.D. James, J. Power Sources, 10, (1983), 105.

[30] S.D. James, Proc. Symp. Lithium Batteries, A.N. Dey ed., Publication 84-1, (1984), 18.

[31] K.M. Abraham, P.G. Gudrais, G.L. Holleck and S.B. Brummer, Proc. 28th Power Sources Symposium, Atlantic City, New Jersey, (1978), 255.

[32] A.N. Dey, Thin Solid Films, 43, (1977), 131.

[33] E. Peled in "Lithium Batteries", J.P. Gabano ed., Academic Press, London, (1983), 43.

[34] E. Peled, J. Power Sources, 9, (1983), 253.

[35] R. Moshtev, Y. Geronov and B. Puresheva, J. Electrochem. Soc., 128, (1981), 1851.

[36] A.N. Dey, Electrochim. Acta, 21, (1976), 377.

[37] A. Leef and A. Gilmour, J. Applied Electrochem., 9, (1979), 663.

[38] E. Peled and H. Straze, J. Electrochem. Soc., 124, (1977), 1030.

[39] E. Peled and H. Yamin, Proc. 28th Power Sources Symposium, Atlantic City, New Jersey, (1978), 237.

[40] A.J. Hills, N.A. Hampson and M. Hayes, J. Electroanal. Chem., 209, (1986), 351.

[41] F. Alessandrini, B. Scrosati, F. Croce, M. Lazzari and F. Bonio, J. Power Sources, 9, (1983), 289.

[42] M. Mogensen, Proc. 9th Scandinavian Corrosion Congress, Copenhagan, (1983), 669.

[43] M. Mogensen, J. Power Sources, 14, (1985), 123.

[44] E. Peled, J. Electrochem. Soc., 126, (1979), 2047.

[45] M. Babai and J. Bineth, J. Power Sources, 9, (1983), 295.

[46] J. Thevenin, J. Power Sources, 14, (1985), 45.

[47] G.L. Holleck and K.D. Brady, Proc. Symp. Lithium Batteries, A.N. Dey, ed., Publication 84-1, (1984), 48.

[48] J.W. Boyd, J. Electrochem. Soc., 134, (1987), 18.

[49] J.R. Driscoll, U.S. Patent, 4,093, 478, (1978).

[50] D.L. Chua, W.C. Merz and W.S. Bishop, Proc. 27th Power Sources Symposium, Atlantic City, New Jersey, The Electrochem. Soc. Inc., (1976), 33.

[51] T. Iwamaru and Y. Uetani, Prog. Batteries and Solar Cells, (Japanese Electrochem. Soc. Press Inc.) 5, (1984), 36.

[52] T. Kalnoki-Kis, U.S. Patents, 3,933, 301, (1976); 4,277, 545, (1981); 4,278, 741, (1981).

[53] N.A. Fleischer, J.R. Thomas and R.J. Ekern, Proc. 30th Power Sources Symposium, Atlantic City, New Jersey, The Electrochem. Soc. Inc., (1982), 172.

[54] C.R. Schlaikjer, Proc. 28th Power Sources Symposium, Atlantic City, New Jersey, The Electrochem. Soc. Inc., (1978), 241.

[55] C.R. Schlaikjer, U.S. Patent, 4,020, 240, (1977).

[56] C.R. Schlaikjer and C. Young, Proc. 29th Power Sources Conference, Atlantic City, New Jersey, The Electrochem. Soc. Inc. (1980), 129.

[57] A.N. Dey and J. Miller, U.S. Patent, 4,071, 667, (1977).

[58] idem., J. Electrochem. Soc., 126, (1979), 1445.

[59] J.P. Gabano and G. Gelin, Power Sources 8, J. Thompson, ed., Academic Press, London and New York, (1981), 3.

[60] J.P. Gabano and J.Y. Grassien, German Patent, 2,902, 526, (1979).

[61] A.N. Dey, J. Electrochem. Soc., 126, (1979), 2502.

[62] R.J. Brodd, Proc. Workshop on the Electrochemistry of Carbon, the Electrochem. Soc. Inc., (1983), 1.

[63] K. Kordesh, J. McBreen, H. Olender, S. Srinvasan and R. Tomantschger, Proc. Symp. Corrosion in Batteries and Fuel Cells, The Electrochem. Soc. Inc., Publication 83-1, (1983), 159.

[64] R. Cristopolus and S. Gilman, Proc. 10th IECE Conference (1975), 437.

[65] C.W. Walker, M. Binder, W.I. Wade and S. Gilman, J. Electrochem. Soc., 132, (1985), 1536.

[66] W. Wade, C. Walker, M. Binder and S. Gilman, Proc. Workshop on the Electrochemistry of Carbon, the Electrochem. Soc. Inc., (1983), 479.

[67] K.A. Klinedinst, J. Electrochem. Soc., 132, (1985), 2044.

[68] T.M. Watson, Power Sources, 11, L.J. Pearce ed., Taylor and Francis Ltd., Basingstoke (1987), 403.

[69] S. Gilman and W. Wade, J. Electrochem. Soc., 132, (1985), 2044.

[70] V. Danel, J.P. Descroix and A. Petit, Proc. Symp. Lithium Batteries, A.N. Dey ed., Publication 84-1, (1984), 136.

[71] W.P. Hagan, N.A. Hampson and K. Packer, Power Sources, 11, L.J. Pearce ed., Taylor and Francis Ltd., Basingstoke, (1987), 413.

[72] S. Szpak and J.R. Driscoll, Proc. 30th Power Sources Symposium, Atlantic City, New Jersey, the Electrochem. Soc. Inc., (1982), 166.

[73] S. Szpak and J.R. Driscoll, J. Power Sources, 10, (1983), 343.

[74] S. Szpak and H.V. Venkatasetty in Power Sources 9, J. Thompson ed., Academic Press, London (1983), 403.

[75] S. Subba Rao, S.P.S. Yen, B.J. Carter, M.M. Evans and R. Somoano, Electrochem. Soc., Extended Abstracts Publication, 84-2, (1984), 198.

[76] A.N. Dey and P. Bro, J. Electrochem. Soc., 125, (1978), 1574.

[77] K.A. Klinedinst and M.J. Domeniconi, J. Electrochem. Soc., 127, (1980), 539.

[78] K.A. Klinedinst, ibid., 128, (1981), 2507.

[79] J.R. Driscoll, R.J. Pollard, J.J. Smith and S.Szpak, in Power Sources 10, L. Pearce ed., Academic Press, London, (1985), 145.

[80] K.C. Tsaur and R.J. Pollard, J. Electrochem. Soc., 131, (1984), 975.

[81] L.R. Giattino, U.S. Patent, 4,262,065, (1981).

[82] W.K. Behl, J. Electrochem. Soc., 128, (1981), 939.

[83] T.W. Beck, H.J. Orman and M. Hayes, French Patent, 2,539,250, (1984); British Patent 2,134,697, (1984).

[84] C.Y. Oh, Y.Y. Wang and C.C. Wan, J. Power Sources, 16, (1985), 233.

[85] N. Doddapaneni, Electrochem. Soc. Extended Abstracts, Publication 81-4, No. 83, (1981), 218.

[86] N. Doddapaneni, Proc. 30th Power Sources Symposium, Atlantic City, New Jersey, the Electrochem. Soc. Inc., (1982), 169.

[87] H. Jahnke, M. Schonborn and G. Zimmermann, Topics in Current Chemistry, 61, (1976), 135.

[88] P.W. Krehl and C.C. Laing, J. Applied Electrochem., 13, (1983), 451.

[89] C.C. Liang, M.E. Bolster and R.M. Murphy, J. Electrochem. Soc., 128, (1981), 1613.

[90] D.L. Chua, J.O. Crabbe and S.L. Despanche, Proc. 28th Power Sources Symposium, Atlantic City, New Jersey, the Electrochem. Soc. Inc., (1978), 247.

[91] N. Marincic, J. Epstein and F. Goebel, Proc. 26th Power Sources Symposium, Atlantic City, New Jersey, the Electrochem Soc. Inc., (1974), 51.

[92] J.J. Auborn and N. Marincic in Power Sources 5, D.H. Collins ed., Academic Press, London, (1975), 683.

[93] A.N. Dey, J. Power Sources, 5, (1980), 57.

[94] W.P. Hagan, N.A. Hampson and K. Packer, Electrochim. Acta., 31, (1986), 699.

[95] M. Domeniconi and K.A. Klinedinst, Proc. 28th Power Sources Symposium, Atlantic City, New Jersey, the Electrochem. Soc. Inc., (1978), 262.

[96] J.C. Hall, Proc. 30th Power Sources Symposium (1982), 204.

[97] R.A. Brown and L.R. Erisman, ibid., (1982), 204.

[98] N.A. Fleischer, S.M. Manske and R.J. Ekren, J. Electrochem. Soc., 131, (1984), 1733.

[99] J.J. Auborn, U.S. Patent, 4,177,329, (1980).

[100] W.L. Bowden, J.S. Miller, D. Cubbison and A.N. Dey, Proc. Symp. Lithium Batteries, A.N. Dey ed., publication 84-4, (1983), 80.

[101] L. Friedman and W. Wetter, J. Chem. Soc., A, (1967), 36.

[102] H.V. Venkatasetty and W.B. Ebner, Proc. 29th Power Sources Symposium, Atlantic City, New Jersey, the Electrochem. Soc. Inc., (1980), 22.

[103] H.V. Venkatasetty and S. Szpak, J.Chem. Eng. Data, 28, (1983), 47.

[104] S. Szpak and H.V. Venkatasetty, J. Electrochem. Soc., 131, (1984), 961.

[105] H.V. Venkatasetty, Lithium Battery Technology, John Wiley and Sons, (1984)

[106] M.J. Harney and S. Brown, Proc. Symp. Power Sources for Biomed. Imp., Publication 80-4, the Electrochem. Soc. Inc. (1980), 102.

[107] D. Morley and R.J. Solar, Proc. 28th Power Sources Symposium, Atlantic City, New Jersey, the Electrochem. Soc. Inc., (1978), 232.

[108] N. Marincic, J. Applied Electrochem., 5, (1975), 313.

[109] N. Marincic, ibid., 6, (1976), 51; 263.

[110] N. Marincic and F. Goebel, ibid., 8, (1978), 11.

[111] A.N. Dey and N. Hamilton, in Power Sources 8, D.H. Collins ed., Academic Press, London and New York, (1980), 41.

[112] J.F. McCartney, W.H. Shipman and C.R. Gundersen, Proc. 27th Power Sources Symposium, Atlantic City, New Jersey, the Electrochem. Soc. Inc., (1976), 45.

[113] F. Goebel, R.C. McDonald and N. Marincic, Proc. 29th Power Sources Conference, (1980), 168.

[114] K.F. Garoutte and D.L. Chua, ibid., (1980), 153.

[115] J.F. McCartney, W.H. Shipman and C.R. Gundersen, Proc. 11th IECE Conference, (1976), 457.

[116] N. Doddapaneni, D.L. Chua and J.T. Nelson, Proc. 30th Power Sources Symposium (1982), 201.

[117] W.L. Eppley and R.J. Horning, Proc. 28th Power Sources Symposium, (1978), 257.

[118] M. Babai, U. Meishar and B. Ravid, Proc. 29th Power Sources Conference, (1980), 140.

[119] R. Hiller and J.R. Driscoll, Proc. 30th Power Sources Symposium, (1982), 198.

[120] P. Bro, J.Electrochem. Soc., 125, (1978), 674.

[121] P. Bro, Power Sources 7, J. Thompson ed., Academic Press, London, (1979), 571.

[122] N. Marincic, Proc. 30th Power Sources Symposium, Atlantic City, New Jersey, The Electrochem. Soc. Inc., (1982), 208.

[123] J. Phillips and H.F. Gibbard, Electrochem. Soc. Extended Abstracts, Publication 80-2, (1980), 165.

[124] F.C. Hall, H.F. Gibbard and L.W. Wiechmann, ibid., Publication 80-2, (1980), 142.

[125] A.N. Dey, Proc. 27th Power Sources Symposium, Atlantic City, New Jersey, The Electrochem. Soc. Inc., (1976), 42.

[126] K.Y. Kim and D.L. Chua, Proc. 29th Power Sources Symposium, (1980), 125.

[127] V. Danel, J.P. Descroix, F. Moisson and J. Jacquelin, Power Sources 11, L.J. Pearce ed., Taylor and Francis Ltd., Basingstoke, (1987), 473.

[128] Y.I. Cho, J. Electrochem. Soc., 134, (1987), 773.

[129] A.N. Dey, U.S. Patent, 4,115,629, (1978).

[130] L.J. Johnson and A.H. Willis, Proc. 29th Power Sources Conference, Atlantic City, New Jersey, The Electrochem. Soc. Inc., (1980), 138.

[131] K.M. Abraham and R.M. Mank, ibid., (1980), 135.

[132] R.L. Zupancic, L.F. Urry and U.S. Alberto, ibid., (1980), 137.

[133] N. Doddapaneni and G.L. Hoff, Proc. Symp. Lithium Batteries, A.N. Dey ed., Publication 81-4, (1984), 146.

[134] J.C. Hall and L.W. Wiechmann, Electrochem. Soc. Inc. Extended Abstracts, Publication 81-1, (1981), 117.

[135] K.M. Abraham, L. Pitts and W.P. Kilroy. J. Electrochem. Soc., 132, (1985), 2301.

[136] D.H. Johnson, A.D. Ayres, R.L. Zupancic, U.S. Alberto and J.C. Bailey, J. Power Sources, 12, (1984), 61.

[137] N. Doddapaneni and D.L. Chua, U.S. Patent, 4,598,029, (1986).

[138] J.F. McCartney, A.H. Willis and N.J. Sturgen, Proc. 30th Power Sources Symposium, Atlantic City, New Jersey, The Electrochem. Soc. Inc., (1980), 159.

[139] "The Chemistry of Non-Aqueous Solvents", Vol. VB, Chapter 4, ed. by J. Lagowski, (1985), Academic Press, New York.

[140] H. Helmholtz, Wied. Ann., 7, (1879), 377.

[141] G. Gouy, J. Phys. Chem., 9. (1910), 457.
[142] D.L. Chapman, Phil. Mag., 25, (1913), 475.
[143] O. Stern, Z. Elektrochem., 30, (1924), 508.
[144] G.N. Lewis, J. Franklin Inst., 226, (1938), 293.
[145] R.G. Pearson, J. Am. Chem. Soc., 85, (1963), 3533.
[146] J.A.V. Butler, Trans. Faraday Soc., 19, (1924), 729; 734.
[147] T. Erdey-Gruz and M. Volmer, Z. Physik. Chem., 150A, (1930), 203.
[148] J. Tafel, ibid., 50, (1905), 641.
[149] M. Sluyters-Rehbach and J.H. Sluyters, Electroanalytical Chemistry, Vol. 4, ed. A.J. Bard, Marcel Dekker, New York, (1970).
[150] E. Warburg, Ann. Physik., 67, (1899), 493.
[151] J.E.B. Randles, Disc. Faraday Soc., 1, (1947), 11.
[152] H. Ershler, ibid., 1, (1947), 269.
[153] H. Gerischer, Z. Physik. Chem., 198, (1951), 286.
[154] J.H. Sluyters, Rec. Trav. Chim., 79, (1960), 1092.
[155] D.C. Grahame, J. Electrochem. Soc., 99, (1952), 360.
[156] H.A. Laitinen and J.E.B. Randles, Trans. Faraday Soc., 51, (1976), 5.
[157] R.D. Armstrong and A.A. Metcalfe, J. Electroanal. Chem., 71, (1976),5.
[158] R. de Levie in P. Delahay ed., Adv. Electrochem. and Electrochem. Eng. Vol. 6, Interscience, New York, (1967), 329.
[159] R. de Levie, Electrochim. Acta, 8, (1963), 751.
[160] R. de Levie, Electrochim. Acta, 9, (1964), 1231.
[161] N.A. Hampson et al, J. Appl. Electrochem., 10, (1980), 357; 603; 709; 11, (1981), 365.
[162] N.A. Hampson, S.A.G.R. Karunathilaka and R. Leek, J. Applied Electrochem., 10, (1980), 3.
[163] Frequency Response Analyser Operating Manual, The Solatron Group Ltd., Farnborough, 1979.
[164] L. Ebdon, An Introduction to Atomic Absorption Spectroscopy, Heydon and son Ltd., (1982).
[165] M. Hughes, N.A. Hampson, S.A.G.R. Karunathilaka and T.J. Sinclair, J. Appl. Electrochem., 12, (1982), 537.
[166] N.F. Harman, N.A. Hampson, S.A.G.R. Karunathilaka and D. Eyre, J. Appl. Electrochem., 14, (1984), 765.
[167] S.A.G.R. Karunathilaka, R.T. Barton, M. Hughes and N.A. Hampson, J. Appl. Electrochem., 15, (1985), 251.
[168] J. Phillips, J.C. Hall and H.F. Gibbard, Proc. Symp. Lithium Batteries, ed. H.V. Venkatasetty, publication 81-4, (1981), 41.
[169] S.A.G.R. Karunathilaka, N.A. Hampson, T.P. Haas, R. Leek and T.J. Sinclair, J. Applied Electrochem., 11, (1981), 573.

[170] K.B. Oldham and L.E. Tapol, J. Phys. Chem., 71, (1967), 3007; 73, (1969), 1455; 1462.

[171] S.A.G.R. Karunathilaka, N.A. Hampson, R.Leek and T.J. Sinclair, J. Applied Electrochem., 10, (1980), 357.

[172] W. Lorenz, Z. Elektrochem., 58, (1954), 917.

[173] R. Tamamushi, Supplement to Electrochim. Acta, 9, (1964), 963, 1972.

[174] P.W. Schenk and H. Triebel, Z. Anorg. Allg. Chem., 229, (1936), 305.

[175] P.W. Schenk and H. Platz, ibid., 215, (1933), 113.

[176] Yu M. Povarov, T.D. Nikolaeva and V.S. Bagotskii, Soviet Electrochem., 14, (1978), 732.

[177] F.M. Delnick, C.D. Jaeger and S.C. Levy, Chem. Eng. Commun., 35, (1985), 23.

[178] J. Phillips and H.F. Gibbard, Proc. Symp. Lithium Batteries, H.V. Venkatasetty ed., Publication 81-4 (1981), 51.

[179] W.K. Behl, Proc. 27th Power Sources Symposium, Atlantic City, New Jersey, The Electrochem. Soc. Inc., (1976), 30.

[180] K.M. Abraham and R.M. Mank, J. Electrochem. Soc., 127, (1980), 2091.

[181] N.A. Hampson and M.J. Tarbox, J. Electrochem. Soc., 110, (1963), 95.

[182] R.N. Elsdale, N.A. Hampson, P.C. Jones and A.N. Strachan, J. Applied Electrochem., 1, (1971), 213.

[183] H.J.S. Sand, Phil. Mag., 1, (1901), 45.

[184] A.N. Frumkin, Zh. Fiz. Khim., 23, (1949), 1447.

[185] P.J. Hilson, Trans. Faraday Soc., 56, (1954), 138.

[186] J. Sullivan, D. Hansen and R. Keller, J. Electrochem. Soc., 117, (1970), 779.

[187] H.V. Venkatasetty and S. Szpak, Electrochem. Soc. Extended Abstracts, Publication 81-2, (1981), 188.

[188] Z. Li-Xing and H. Shi-Fu, International Laboratory, May (1986), 28.

[189] W.P. Hagan, Private Communication.

[190] M. Hayes, Chemistry in Britain, 22, (1986), 1101.

[191] M. Hayes and L. Teale, G.E.C. Research, Internal Report.